THE EFFICIENCY OF METHIONINE AS A RADIOPROTECTANT OF *BACILLUS ANTHRACIS* FOR CELL VIABILITY AND OUTGROWTH TIME AFTER UVC AND GAMMA IRRADIATION

THESIS

Cameron N. Harris

AFIT-ENP-MS-15-M-105

DEPARTMENT OF THE AIR FORCE
AIR UNIVERSITY

AIR FORCE INSTITUTE OF TECHNOLOGY

Wright-Patterson Air Force Base, Ohio

DISTRIBUTION STATEMENT A.
APPROVED FOR PUBLIC RELEASE; DISTRIBUTION UNLIMITED.

AFIT-ENP-MS-15-M-105

THE EFFICIENCY OF METHIONINE AS A RADIOPROTECTANT OF *BACILLUS ANTHRACIS* FOR CELL VIABILITY AND OUTGROWTH TIME AFTER UVC AND GAMMA IRRADIATION

THESIS

Presented to the Faculty

Department of Engineering Physics

Graduate School of Engineering and Management

Air Force Institute of Technology

Air University

Air Education and Training Command

In Partial Fulfillment of the Requirements for the

Degree of Master of Science in Material Science

Cameron N. Harris, BS

March 2015

AFIT-ENP-MS-15-M-105

THE EFFICIENCY OF METHIONINE AS A RADIOPROTECTANT OF *BACILLUS ANTHRACIS* FOR CELL VIABILITY AND OUTGROWTH TIME AFTER UVC AND GAMMA IRRADIATION

Cameron N. Harris, BS
Second Lieutenant, USAF

Committee Membership:

Dr. Larry W. Burggraf
Chairman

Dr. Yun Xing
Member

Dr. Willie F. Harper
Member

Dr. Roland Saldanha
Member

Abstract

Samples containing approximately 10^7 spores of *Bacillus anthracis* (Ba) Sterne in water were irradiated with 267 nm UVC light using small LEDs and, for comparison, by gammas produced from a Cs-137 source. Spores were exposed to methionine and DP1 in different settings. L-methionine and D-methionine were introduced to Ba during sporulation and adherence to the spore was verified using circular dichroism spectrometry. Before irradiation, 1 mM L-Met, D-Met, and DP1 were added to solution and remained in solution through germination. Following UV irradiation, minimal media was added and the spores were incubated for various times. Spore viability was quantified as time to outgrowth of the spore using SYTO 16 photoluminescence. Fluorescence counts were compared between irradiated and unirradiated experiments, demonstrating a delay in outgrowth time for irradiated samples. D-Met samples showed increased damage repair compared to control spores, while L-Met spores expressed delayed outgrowth for unirradiated and correspondingly irradiated spores. Colony forming units were collected after gamma irradiation for 1000 gray (Gy) increments between 0 and 8000 gray. The gamma doses corresponding to 1-$\log_{10}$ inactivation for the four types of Ba spores were: ~5000 Gy for wild type and D-methionine; >8000 Gy for DP1 spores; inconclusive for L-methionine. DP1 doped spores showed a significant resistance to damage, while D-Met spores showed minimal change in cell viability. L-Met spores clumped readily and produced unsatisfactory results. The average dose for 1-$\log_{10}$ inactivation for the control is approximately twice the value previously reported; this illustrates the importance of dose rate in radiation effects.

Acknowledgments

I owe my greatest thanks to my advisor, Dr. Larry Burggraf, and my committee members Dr. Roland Saldanha, Dr. Yun Xing, and Dr. Willie Harper. Without them or my extended committee, Army Lieutenant Colonel Douglas Lewis and Dr. Thomas Lamkin, this research would not have come to fruition. I thank them for their patience, understanding, and continued advice.

Additional thanks go to Mrs. Chelsea Marcum, who taught and guided me to attempt the success which she so gracefully achieved. Her level of effort in bettering my comprehension of the research was prodigious. Further appreciation is extended to Ms. Kandace Bailey, on whom I consistently relied for laboratory experience. Thank you as well to Air Force Captain Michael Spencer for your assistance in fabricating my reactor circuit board. Significant gratitude also goes to Mr. Jeffrey Bailey from the Cincinnati Children's Hospital Medical Center; your continuous assistance in sample radiation made my research and life much simpler.

For all of the help I received, I can do no more than to wish you the best of luck in your careers, lives, and futures; it is much deserved.

Cameron N. Harris

"If you try to change it, you will ruin it. Try to hold it, and you will lose it."

Tao Teh Ching, 6th Century BCE

Table of Contents

List of Figures

List of Tables

Page

THE EFFICIENCY OF METHIONINE AS A RADIOPROTECTANT OF *BACILLUS ANTHRACIS* FOR CELL VIABILITY AND OUTGROWTH TIME AFTER UVC AND GAMMA IRRADIATION

I. Introduction

Research Statement

The primary objective of this research is to show whether or not methionine, a sulfur-containing amino acid, sporulated in *Bacillus anthracis* (Ba) Sterne, has similar radiation protection efficiency as Ba spores in solution of DP1, a decapeptide containing methionine, from the effects of damage by UVC and gamma irradiation. Ba spores represent an interesting model system to study because the damage to assaults in the spore state can be studied separately from the damage repair in the vegetative state. The effectiveness of methionine as a scavenger of reactive oxygen species (ROS) is expected to show minimal protection against UVC irradiation, but is expected to be substantial for gamma protection based on known mechanisms. Protein transport and regulatory functions would accept methionine more readily than the decapeptide; the bacterium must germinate to allow these molecules to enter the cell and interact with ROS. The metrics for measuring repair efficiency after UV and gamma radiations are outgrowth time and colony forming units of the spores, respectively.

Problem Statement

The purpose of this research is to compare the effectiveness of Ba sporulated with methionine and DEHGTAVMLK, referred to as decapeptide 1 (DP1), in solution of Ba spores as radioprotectants for gamma irradiation. The amino acid and polypeptide were applied to aqueous solutions of *Bacillus anthracis* spores following ultraviolet C (UVC)

radiation at 267 nanometers and gamma (γ) irradiation using a cesium-137 source. The metrics used to quantify the radioprotection efficiency were spore survival curves and germination outgrowth time. Studying the complexes of methionine and decapeptides including methionine and their effect on cell viability post-irradiation is fundamentally important in radiation damage. Air Force Research Lab's (AFRL) branch at the 711th Human Performance Wing has empirically shown that DP1 is a radioprotectant for enzymes and has argued, alongside Daly that proteins are the primary concern in radiation damage, more important than damage to DNA, in opposition to interpretation of evidence obtained by most radiation biologists [1][2]. DP1 and similar polypeptides have provided protection in an enzyme, beta-galactosidase, from gamma irradiation [3]. The use of *Bacillus anthracis* as a model system to evaluate radiation damage from ionizing (γ) and non-ionizing (UVC) irradiation provides an opportunity to: test the possibility of augmenting its already potent radiation resistance; test if the ability of small molecules to confer protection can be generalized to other bacteria; and obtain supplemental data to aid in discovering the protection mechanisms of proteins containing sulfur. Damage and repair to DNA in spores can be more easily investigated in space and time than in vegetative cells.

Performing experiments on *Bacillus anthracis* (Ba) spores are useful because of the bacterium's resistance to radiation. Ba is a hardy bacterium and inactivation of the spore form of the bacteria is well studied and integrally related to damage and repair mechanisms [4][5]. Unlike *anthracis* vegetative cells, the spore has no metabolic activity. With no repair occurring during this phase, damage incurred by radiation increases in proportion with dose. When germination is conducted in a low radiation

background, there is a distinct separation between time of damage and time of repair. Delay in outgrowth, the transition from spore form to the vegetative cell, directly correlates to the damage of DNA and enzymes within the cell. There is also a spatial separation of bio-active DNA and enzymes in the core of a spore from the external environment outside the spore.

The effects from the introduction of an additional repair or protection mechanism will provide insight into the effectiveness of that mechanism. Results from irradiation with γ and UVC will provide a comparison on doses used and cell susceptibility to different types of radiation damage. Completion of experiment matrices that include L-methionine, D-methionine and DP1 provides a view of each molecule's consequence on *Bacillus anthracis*. With these results and an analytical comparison of their chemistry, the effectiveness of methionine and DP1 as radioprotectants can be gauged more accurately.

Motivation

Though the range of damage mechanisms on the cell are known for UV and ionizing radiation (IR), the degree to which the mechanisms are applied is an unanswered and oft researched problem; more so for UV radiation than ionizing radiation. Methionine and DP1 have been shown to increase protection when applied before irradiation: methionine in human and other mammalian cells [6] and DP1 in glutamine synthetase and mouse methionine sulfoxide reductase A [1]; but a comparison in efficiency and the degree to which damage is inhibited has not been analyzed. Application of effective radioprotectants to humans is well sought for medical,

occupational and combat purposes, e.g. oncology, acute radiation syndrome, etc. Conversely, understanding resistance mechanisms that are hitherto unexplored may allow design of countermeasures that sensitize the bacterium to irradiation and thus facilitate decontamination applications.

The use of Ba to resolve this inquiry stems from the mechanistic foundations of the bacterium. Before germination, the cell remains in a dormant state, the spore, where it is most resistant to extreme environments [7][8]. This dormant state is the single focus of this research, due to the impressive defensive mechanisms integrated in the spore system and the separation of time between damage and repair.

Research Focus

Current research at AFRL's Human Effectiveness directorate is designed to explore the crucial elements of cell death via radiation damage on DNA and enzymes. Research that has been conducted with the bacterium *Deinococcus radiodurans* as the primary motivation. The bacterium's ability to withstand over 17,000 gray, or 1.7 megarads, through its robust repair mechanisms is the forefront of research in radiation biophysics. The mechanisms of repair for such high doses are still uncertain, but a combination of peptides within the bacterium's robust structure suggests an avenue for paralleled work with other bacteria and enzymes.

Previous research at the Air Force Institute of Technology (AFIT) has focused on the efficient inactivation of spores by methods such as: thermal inactivation, pulsed UV inactivation and continuous UV inactivation [9][10][11][12]. Contrarily, this research

focuses on combining the robust elements of *D. radiodurans* and *B. anthracis* to augment the number of repair mechanisms and damage-preventing mechanisms.

UV irradiation on Ba is studied more often than ionizing radiation because of the ease of accessibility, reduced cost, better understood mechanisms and relevance to public health and understanding. Although multiple data sources exist for Ba gamma irradiation [13][14] and Ba UVC irradiation [15] [16][17], a comparison of the two is seldom accomplished in *bacilli*, or any spore forming genera [4]. The inclusion of proteins into both systems and a consequent comparison to analyze the mechanistic effects is novel.

Additional focus of this research is the inclusion of dextrorotary methionine (D-Met) and levorotary methionine (L-Met) during sporulation of *B. anthracis* and the anticipated adherence of each of the chiral molecules to the spore. The two chiral amino acids interact differently with chiral surfaces; these interactions determine molecular recognition. The characterization of amino acid adsorption to bacteria by circular dichroism spectroscopy appears to be new to the field.

Approach

Acquiring the necessary data to review the research statement requires many procedural steps. This research will focus on growing *Bacillus anthracis* Sterne spores in the same manner as previous AFIT students, for purposes of comparability and continuation. A duplicate of the previously used UV irradiation setup will be analyzed via chemical actinometry to assess the radiation efficiency of the UV LEDs and reactor. The *anthracis* spores are supplemented with methionine and DP1 prior to irradiation. Colony forming units will provide a metric for comparing methionine and DP1 protection

from gamma irradiation and germination outgrowth time will measure methionine's effect on DNA repair after UVC irradiation. This research approach will be outlined in detail in Chapter III.

Assumptions

Assumptions made throughout this research include: Cell death was considered to be the inability to outgrow a viable colony of daughter cells; all plotted data was modeled by a Gaussian distribution; each photon produced by the LEDs during actinometry is absorbed by potassium iodate. The wavelength of the LEDs, 267 nm, is considered to be monochromatic since the full width at half maximum is narrow, 11 nm.

Document Structure

This document is partitioned into 5 chapters, each with respective sections and subsections. Chapter I introduces the purpose of the research and discusses the general outline of the processes taken to resolve the research objective. Chapter II covers the science and theory behind the topic of the research. This chapter serves as the analytical backbone of the project and includes: *Bacillus anthracis* background; Ba damage mechanisms; the two radioprotectants; actinometry; circular dichroism spectrometry; and spectrofluorometry. Chapter III outlines the preparation and subsequent irradiation of the spores to provide empirical data for measuring the test metrics. Chapter IV introduces and analyzes the data. The results of the data will reveal implications on the damage mechanisms. Chapter V will provide an overview of research accomplishments and suggested future work. The appendix contains additional content that supports the methods of the project but is not directly related to the primary research focus.

II. Background & Theory

Chapter Overview

The purpose of this chapter is to provide supplemental information about *Bacillus anthracis*, radiation damage, and radiation protection. Topics covered in this chapter include: *anthracis* background; growth phases; IR damage and repair mechanisms; UV damage and repair mechanisms; methionine protection; DP1 conception and corresponding protection. There is also discussion about the theoretical approach to the experiment, including: circular dichroism spectrometry; actinometry; and spectrofluorometry.

Bacillus anthracis

Bacillus anthracis (Ba) is a non-motile, gram positive, spore forming bacterium, with recorded human awareness reaching to the second millennium B.C.E. [18]. The bacterium is at the center of this research due to its robust defense against extreme environments, compared to other biological or chemical agents, and the characteristics of its dormancy phase. Unlike other bacilli such as *Bacillus subtilis*, which are also hardy bacteria, Ba has a unique ability to cause disease [19]. Ba's survival success is primarily attributed to its dormancy phase as a spore. Inactivation of Ba spores by thermal, chemical, UV and ionizing radiation are of interest for inactivation of biological weapons, for which the bacterium is publicly known [20][21]. Unlike in vegetative cells, DNA damage and repair is more easily investigated in the spore. Damage and inactivation of the spore form was the focus of this research.

Growth Phases.

Bacillus anthracis experiences two very distinct cell morphologies, the dormant spore form and the vegetative cell. The characteristics of the transition between these states are important: timing, morphological change, molecular structure, and DNA changes. The transition back and forth between the two phases is known to be highly complex [22]. These transition traits are important because of the changing susceptibility of the cell to different types of damage.

The vegetative cell transitions to a spore when the environment is typically desiccated and lacks appropriate carbon, nitrogen and phosphate nutrients. The spore form is considered to be the predominant form of *anthracis*. During transition from a metabolically active to dormant phase, the cell dehydrates and compresses its DNA from B-conformation to A-conformation by small, acid-soluble spore proteins (SASPs). The spore is formed within the vegetative cell, and ultimately the membrane is cracked and the spore is released. The spore is dehydrated and metabolically inactive, i.e. dormant. The cell can survive in this fashion for extended periods of time and in space environments [8]. The resistance mechanisms associated with the spore are highly dependent upon the stages of the life cycle, including growth sporulation and germination [7].

The nutrients required for growth of the vegetative cell of *B. anthracis* vary greatly between strains of the bacteria, but consistently require methionine and thiamine [23]. The nutrients used in this research are derived from protocol established by Pandey et al. [24]. The media base is LB MOPS supplemented with germination triggers AGFK, the recipe of which is found in *AGFK Minimal Media Recipe*. AGFK is an acronym for

the ingredients: L-asparagine, glucose, fructose and potassium chloride. The morphology of the vegetative phase consists of square-ended rods, approximately 1 by 5-8 μm, whereas the exponential phase is characterized by long serpentine chains of the rods [25]. The germination phase also results in a decrease in refractility for the spores and become phase-dark under phase-contrast microscopy [26].

The events that occur in the transition from the dormancy phase to outgrowth are displayed in Figure 1. The items in this figure are crucial for understanding the time to outgrowth, a major test metric of this research.

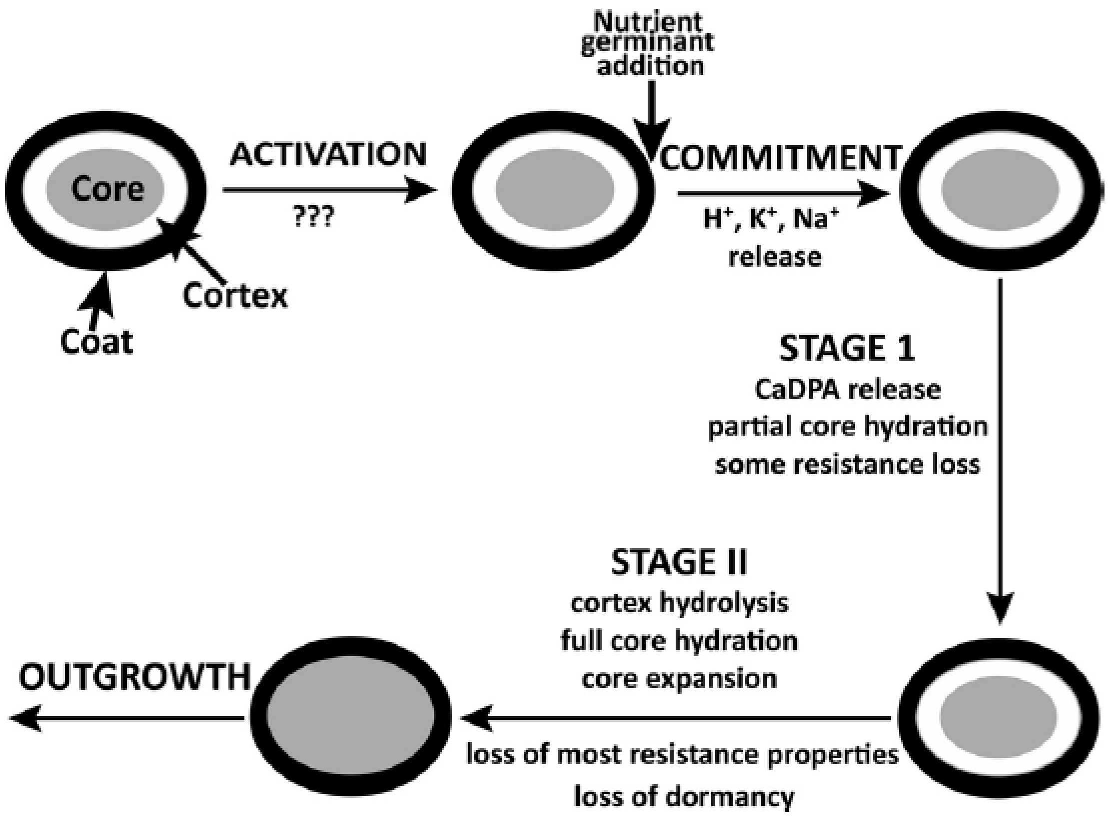

Figure 1. Transition from the dormant spore to outgrowth of the vegetative cell of *Bacillus* species. The structural components of the spore are reviewed in Figure 2. The spore is activated by unknown processes, and the addition of a nutrient germinant begins commitment to germination. Stages I and II are differentiated by the presence of CaDPA. Outgrowth is the final conversion of the germinated spore into a growing cell; this is the point when the cell is most vulnerable. Copyright American Society for Microbiology 2014 [27].

Though germination has been studied excessively, in many settings and with multiple bacteria, there are still many questions about the function, structure, and regulation of proteins that are major actors in spore germination [27]. Beginning with activation, the figure clearly suggests that very little is known about the process. Heat activation has been used effectively to increase spore viability. It is suggested that heat activation changes the tertiary structure of spore macromolecules, thereby making germinant receptors more available to germination nutrients [28].

Once activated, the spore will begin commitment when exposed to germination nutrients. As stated earlier, this research uses LB MOPS with AGFK due to its fast germination time. Germinant receptors are spore specific protein complexes that enable the consumption of germination media. The spore commitment occurs after the media and receptors are bound, and will continue even if the nutrients are removed. Commitment is characterized by the release of monovalent cations such as H^+, K^+, and Na^+, and precedes the release of calcium dipicolinic acid (CaDPA) by a few minutes [29].

The release of CaDPA signifies Stage I of germination and the uptake of core water. This initial hydration is the first loss of resistance of the cell, but is limited; only when the cortex is degraded and the core expands is there a significant increase in damage sensitivity. Core expansion and hydration is completed via cortex-lytic enzymes, which do as the name suggests, and segues into Stage II. Stage II contains full core expansion and hydration, which renders the cell most susceptible and removes it from dormancy. The core content has risen to ~80% of wet weight [27]. At this point, metabolism begins in the cell, thus completing the transition from dormant spore to growing cell. The cell has completed outgrowth and can now grow at an exponential rate.

Anthrax.

The Sterne strain is a non-virulent strain of *Bacillus anthracis*. The virulence factors for certain strains of Ba include two toxins and capsule, which are encoded by the pXO1 and pXO2 plasmids [30]. The capsule on virulent strains of *anthracis* protects the bacterium against consumption by the immune system. Since the Sterne strain does not include the pXO2 plasmid and does not produce a capsule, it is not an etiologic agent of

anthrax. This subsection briefly reviews characteristics of the disease anthrax merely as a reference for prospective AFIT research on *Bacillus anthracis*.

The lethal human disease is present in three forms: cutaneous, inhalational, and gastrointestinal [21]. Of the three forms of anthrax disease, cutaneous form accounts for 95% of cases on record [18]. The inhalational form is the most lethal form and was well-publicized during the 2001 anthrax attacks in the United States. This form is also most likely to be used in a biological weapon due to its lethality. Once ingested in the body, the spore germinates and becomes more susceptible to chemical and radiological attack. The disease is caused by the toxic actions, lethal factor and edema factor, of proteins produced within the human body. Toxin sensitivity is highly variable in humans and effects pathogenicity [20].

***Anthracis* Damage**

Many studies have been completed on the inactivation of Ba by many methods. Researchers have focused on inactivation by radiation, heat and chemical treatments. Each type of treatment focuses on different damage mechanisms and the bacterium has efficient methods of damage repair. Some repair mechanisms are specific to the type of damage while others are applied to all types of damage. Study of non-ionizing radiation damage, such as UV, in the bacterium is more common than ionizing radiation, but recent research has reduced this gap [13] [14] [31].

Structural Mechanisms.

The physical structure of Ba is the first defense against chemical, radiation, and heat damage. When the bacterium is in spore form, many physicochemical attributes

contribute to its success. Figure 2 shows the layers of the spore, some of which significantly contribute to protection from extreme environmental elements.

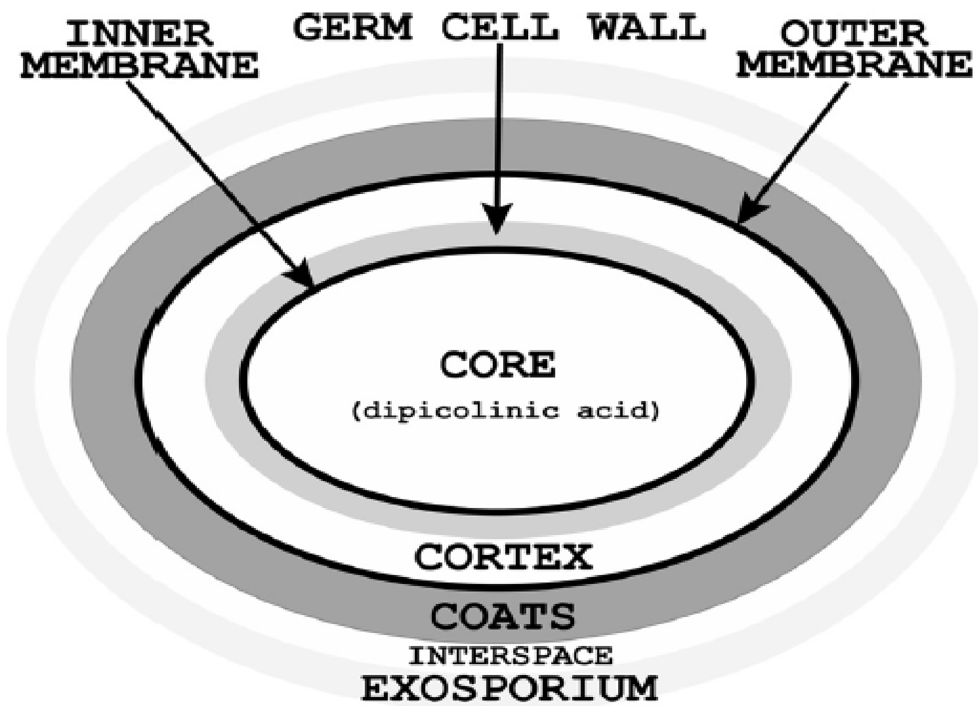

Figure 2. Physical structure of the spore with a focus on layers. The exosporium is present in Ba, but not present within other *bacilli*. The composition and structure of each layer is unique and provide different roles for bacterial processes. Roles of each layer are described in outgrowth, with some mechanisms of germination still unknown. Copyright American Society for Microbiology 2014 [27].

For *Bacillus anthracis*, the spore is approximately 1 μm across, and is oval shaped, similar to the figure. The exosporium, composed of paracrystalline layers of proteins, lipids, and carbohydrates, is not present on other species of *Bacillus* and does not have a clear function in protection against radiation for Ba [32]. The spore coat is composed of spore-specific gene-product proteins [5]. This layer has clear protection against chemical and lytic enzyme attack. Fracturing the spore coat is extremely important in DNA exposure. A breakage can be caused by radiation, thereby making the

DNA more susceptible to damage, or can happen during outgrowth which facilitates staining the DNA, as described in *Spectrofluorometry*.

UV Damage Mechanisms.

Ultraviolet light ranges from 1 nm to 380 nm wavelengths, with health effects subdivided into UVA, UVB and UVC [33]. UVC, also called germicidal UV, ranges from 100-280 nm, and contains the highest energy particles of the three energy ranges; 267 nm was used in this research because of the proximity to the absorption maximum of DPA. UV irradiation of DNA causes absorption of the incident photon (hν) and excites the DNA molecule (Equation 1) [34]. When the target molecule (M) is excited (M*), pyrimidine dimers (products) are formed by covalent bonds between adjacent pyrimidines. Pyrimidines are nucleic bases with a single carbon ring structure; the two bases being thymine and cytosine.

$$M + h\nu \rightarrow M^{*} \rightarrow products \tag{1}$$

Thymine is the more sensitive base and therefore commonly produces thymine dimers after UV irradiation. Other than Ba spores, the two most common photoproducts are cyclobutane pyrimidine dimers (CPDs) and (6-4)-photoproducts (64PPs) [35]. In addition to these dimers, the spore produces a specific DNA lesion found only in spores: 5-(α-thyminyl)-5,6-dihydrothymine), the spore photoproduct (SP) [16]. This lesion, seen in Figure 3, is attributed to the rare DNA conformation found in Ba spores, A-DNA. A-DNA is rarely found in nature and though the chemical composition is the same, the structure is different, i.e. more rotations per base pair. This conformation is produced during sporulation. Small acid-soluble spore proteins (SASPs) dehydrate the DNA, transforming it from B-conformation to A-conformation [4]. This unique conformation

increases the production of SPs. Conversely, B-DNA preferentially forms CPDs and 64PPs. SPs account for 95% of the damage incurred by UVC irradiation [36].

UV irradiation can also produce other direct and indirect damage effects, like strand breaks and ROS production, but at a much lower extent than pyrimidine dimers like the spore photoproduct [35]. Strand breaks are more likely to occur from ionizing irradiation due to the higher energy of the incident waves, and will therefore be discussed in *IR Damage.* ROS in water are produced by two-photon excitation, seen in Equation 2, which dissociates into H• and OH• [37]. The ROS production would use the excess methionine in the system for repair, but the contribution to total UV-induced damage repair is minimal.

$$H_2O + h\nu \rightarrow H_2O^* \xrightarrow{dissociation} H\bullet + OH\bullet \tag{2}$$

UV Repair Mechanisms.

Since the spore photoproduct is the primary damage mechanism after UV irradiation, spore photoproduct lyase (SPL) is appropriately the primary repair mechanism. *Anthracis* spores have the unique ability to repair the SP lesion during germination via the SPL, seen in Figure 3.

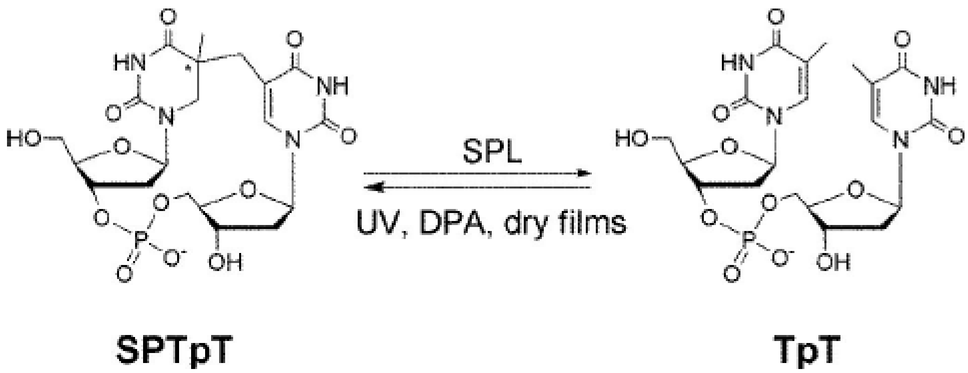

Figure 3. Production and repair of the DNA lesion specific to the spore A-DNA conformation. The repair of the spore photoproduct (SP) by the spore photoproduct lyase (SPL) is the direct reversal of a pyrimidine dimer produced by UV excitation of the nucleobase thymine. TpT is the unmodified dinucleoside monophosphate. Copyright American Society for Biochemistry and Molecular Biology 2008 [38].

SPL is a radical S-adenosyl-methionine (SAM) iron-sulfur enzyme [39]. SAM enzymes are an emerging superfamily of enzymes specializing in repair reactions [16]. As the SPL name suggests, this enzyme specifically repairs the SP but not other thymine dimers. The SPL is initiated by the reduction of the [4Fe-4S] cluster and a subsequent electron transfer occurs [40]. The dimer is directly reversed by cleaving the C5'-S bond and forming a methionine [38]. This process occurs at the early bacterial germination phase, thereby decreasing the time of DNA repair.

Additionally, DNA lesions can be repaired by nucleotide excision repair (NER), base excision repair (BER), and endonuclease enzymes, all of which are present mechanisms not specific to the spore. NER repairs dimers produced by UV excitation. The pathway includes the removal, or excision, of a section of the damaged strand of DNA and fills the gap with a complement strand created by DNA polymerase. Conversely, BER responds to base lesions produced by hydrolysis and reactive oxygen species. DNA glycosylases remove the damaged base, and the apurinic/apyrimidinic

(AP) site is removed by an AP endonuclease or AP lyase, and the broken DNA is ultimately filled by DNA polymerase [35]. UVrA, UVrB, and UVrC endonuclease enzymes are important for damage recognition, and in combination supply damage verification and incision [41]. Lesions not repaired by the aforementioned processes are mutagenic. For the cell to survive, a lesion bypass must occur to eliminate future mutations. Mutations from lack of repair or mutagenic repair contribute to cell death during the transition from the spore to the vegetative cell.

IR Damage.

Ionizing radiation is defined as an incident particle, electromagnetic or matter, that interacts with a molecule with enough energy to extract a charged particle, thereby producing an ion. Gamma radiation is one type of ionizing radiation, in which the electromagnetic particle is produced by the nucleus. Gamma irradiation kills microogranisms by: direct modification of proteins and nucleic acids; and generation of reactive oxygen species. ROS production, an indirect action of IR, is the principal damage mechanism considered in this research.

Indirect action is explicitly defined as “the interaction of solute molecules and the reactive species of solvent molecules formed by the direct action of radiation on the solvent” [42]. Water hydrolysis caused by the ionization of water molecules creates active radical species that readily produce biological damage. The predominant species for reaction with DNA is the hydroxyl radical, OH•. The series of equations in Figure 4 depicts the ROS produced from combination of ionized water, the free electron, and water molecules.

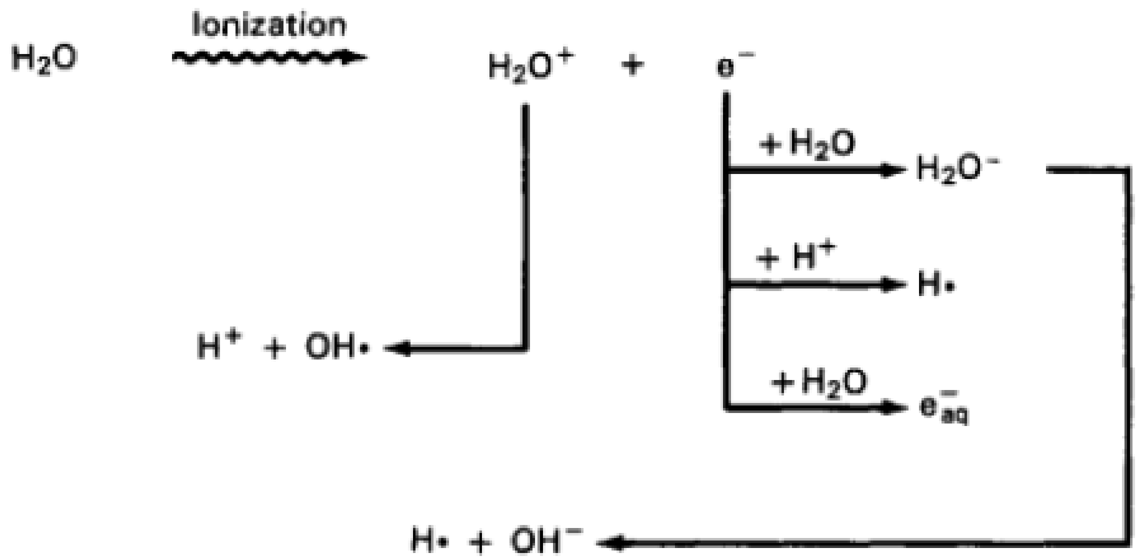

Figure 4. Combination of the immediate products from the ionization of water. The reactive oxygen species are an indirect action created by the irradiation of water and produce the most damage within the spore. OH• is the key reactant in DNA damage. Copyright Elsevier Science & Technology Books 1998 [42].

H•, OH• and e_{aq}^- are formed in the first 10^{-11} seconds and react with water molecules in the immediate vicinity, thereby continuing water radiolysis. The reaction rate constants with DNA are $8x10^7$, $1.4x10^8$ and $3x10^8$ mol/s for H•, e_{aq}^-, and OH•, respectively, which would suggest H• reacts least efficiently and OH• most efficiently with DNA [43]. Diffusion of the molecules is important when considering recombination and restitution. Recombination, the combining of radicals to their previous molecular form, happens on the order of 10^{-11} seconds, while restitution, the chemical restoration of radicals to the original molecular state, occurs in milliseconds. The reaction constants, the number of molecules formed from deposition of 100 eV of energy (G value), and the diffusion of radicals predict the severity of damage in the cell.

The dehydration of DNA by SASPs and an excess of dipicolinic acid (DPA) and calcium DPA (CaDPA) play major roles in protection against ionizing radiation damage.

Production of ROS, an indirect effect of ionizing radiation, is less common in the spore than in the vegetative cell due to reduced water content. Single strand breaks (SSBs) occur from damage to the deoxyribose-phosphate backbone resulting in scission, while double strand breaks (DSBs) are created by the occurrence of two or more SSBs in nearby locations. Strand breaks, particularly DSBs, are thought to be the most critical type of damage caused by the effects of ionizing radiation.

IR Repair Mechanisms.

Bacillus anthracis spores contain many ionizing damage repair mechanisms, including but not limited to: non-homologous end joining (NHEJ), homologous recombination, direct reversal, and excision repair. Since *Bacillus* species spores contain a single chromosome arranged in a toroidal shape, homologous recombination cannot repair DSBs during germination [44]. An alternative to homologous recombination is non-homologous end joining. This process recruits the Ku complex to bind to the two ends of the strand breaks, then a subsequent resection of the ends of the DSB. Finally, a specific DNA ligase directly joins the ends of the strand break and restores the DNA to its previous structure [31].

Nucleotide excision repair and base excision repair, mentioned in UV damage repair, are also common repair mechanisms for ionizing radiation caused by X-rays, gamma rays and heavy charged particles. Additionally, mismatch repair, AP endonucleases, and translesion synthesis can repair spore DNA damage during germination [5].

Methionine

This subsection reviews the mechanisms of methionine that are valuable in radiation protection. This research focuses on both stereoisomers of the amino acid and makes inferences on the biological response of *Bacillus anthracis*, including regulation processes. Methionine is a non-polar amino acid with a sulfur atom at the end of its side chain. The thiol group acts as an ROS scavenger and therefore directly relates to the indirect action on DNA from gamma irradiation.

Protection Mechanisms.

Methionine is a radiation sensitive amino acid due to its sulfur containing side chain. Ionizing radiation causes scission of the SCH_3 group of methionine and subsequent degradation to α-aminobutyric acid, methionine sulfoxide and methionine sulfone [45]. Figure 5 shows the formation of the higher oxidation states of methionine with dose dependence.

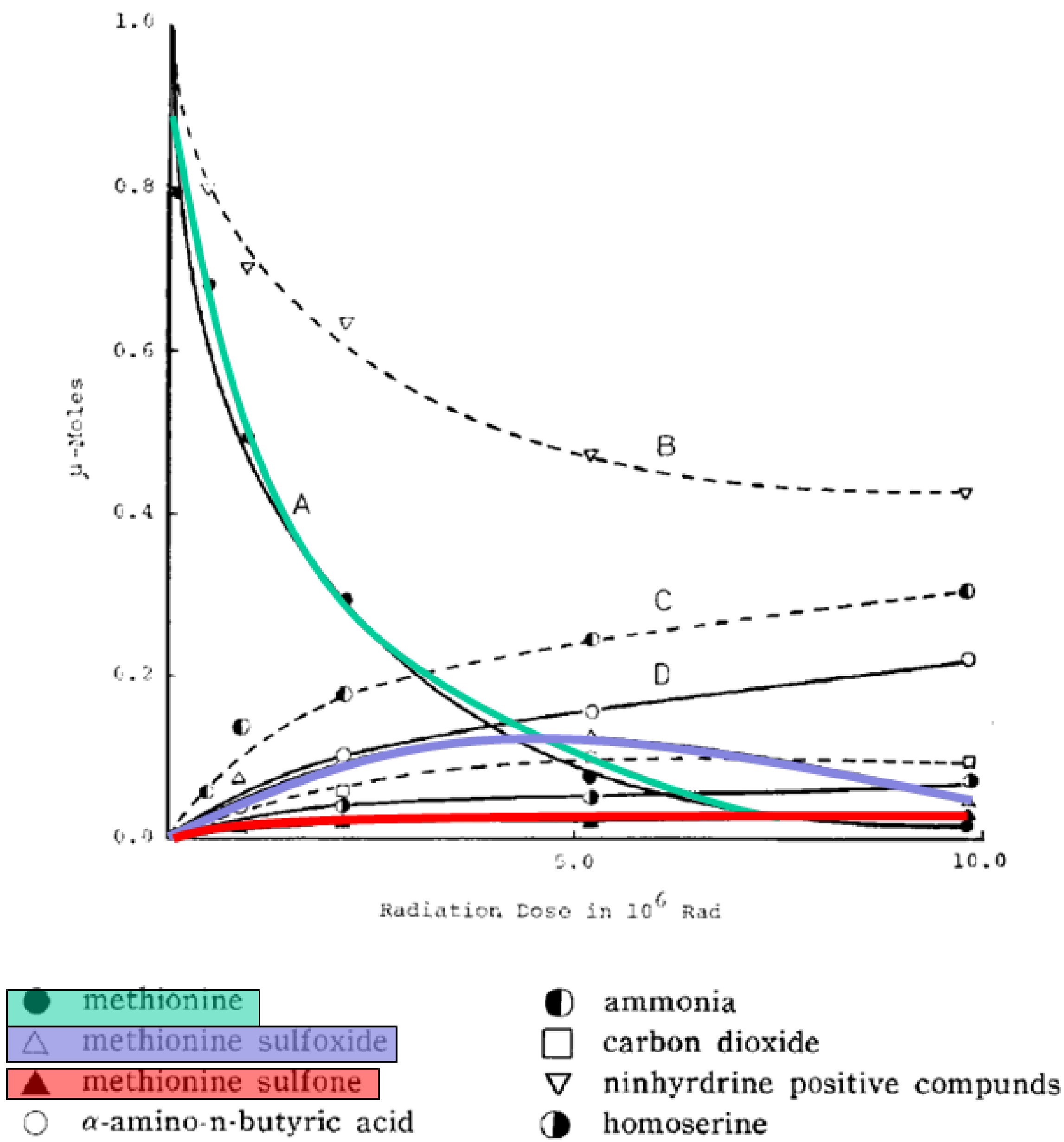

Figure 5. The degradation of methionine due to thiol scission from ionizing radiation. Products of the scission include the higher oxidation states of methionine (green), methionine sulfoxide (purple) and methionine sulfone (red). Further irradiation of these primary products produces similar graphs of additional degradation byproducts. Methionine sulfoxide is reduced to methionine, but the reduction of methionine sulfone is improbable. Copyright Oxford University Press Journals 1966 [46].

These two increased oxidation states of methionine, methionine sulfoxide and methionine sulfone are more stable than methionine, because of its two unshared electrons. Binding

of oxygen atoms to the sulfur atom diminishes the reactivity of the molecule to the free radicals from water [47]. Methionine residues within proteins that have been oxidized disable the protein function and can inactivate repair mechanisms. The methionine sulfoxide can be reduced to methionine by a methionine sulfoxide reductase A or B (MsrA or MsrB) so as to restore protein function [48]. The irreversible oxidation of methionine sulfoxide to methionine sulfone creates a loss of function in the cell that cannot be undone by a reductase.

Biological Processing.

Methionine is crucial in a large range of cellular function, such as methylation and protein synthesis, and is therefore highly regulated in the cell. This subsection discusses the limits of excess methionine in the cell due to these salvage pathways and feedback regulation. Feedback control in the cell regulates the availability of particular proteins within the cell. Methionine is an essential amino acid, so the cell will synthesize its own methionine when needed, but the cell only needs a certain amount, and will remove excess methionine via feedback regulation. Similar processes have been studied in *Bacillus subtilis* with a focus on transport of D- and L-methionine and methionine sulfoxide by the ABC transporter. S-box-controlled genes are involved in methionine biosynthesis and in methionine recycling [49]. The regulated transport of methionine and methionine sulfoxide by YusA, YusB, and YusC in *B. subtilis* suggests that these proteins are good candidates for methionine uptake in the *subtilis* system [50].

Since there are decent uptake and recycling mechanisms in *Bacillus* species, quantifying the amount of methionine absorbed within the cell from this research is

difficult without a radioactive tracer. The use of circular dichroism spectroscopy is a good route to know whether the spores took on some amount of methionine.

DP1

Decapeptide 1 originates from the research conducted by Dr. Thomas Lamkin's research group at Air Force Research Laboratory's Human Effectiveness Directorate (AFRL/RHXBC). The combination of amino acids is inspired by those naturally occurring in *Deinococcus radiodurans* (Drads). This subsection reviews the unique and unparalleled radiation protection mechanisms in Drads, the structure of DP1, and its relation to radiation damage. The implications on the importance of enzymatic proteins in cell damage have created a focus on supplemental proteins as radioprotectants; DP1 is an example of such. The chain of ten amino acids, including methionine, contained in the polypeptide are naturally occurring in Drads.

Deinococcus radiodurans is a very unique and extremely robust microorganism. Discovered in the mid-20th century as a contaminant in radiation-sterilized corned beef cans, this extremely radioresistant organism has been thoroughly studied [51]. Drads research has shown a clear connection between resistance, manganese accumulation and protein protection. Slade et al. suggest that extreme radioresistance can be explained by the protection of proteins in robust bacteria by manganese-dependent antioxidants [52]. Though DNA DSB repair ability has the strongest correlation to radioprotection, protein protection by a mixture of peptides, nucleosides, Mn^{2+} and orthophosphate suggests causation in cellular radioresistance. Mixtures of peptides were determined by chemical

agents identified in bacterial ultrafiltrates; DP1 is composed of ultrafiltrates of *D. radiodurans* [53].

The composition of DP1 is: Aspartic acid, glutamic acid, histidine, glycine, threonine, alanine, valine, methionine, leucine, lysine, or in 1 letter abbreviations DEHGTAVMLK. A linear configuration of the peptide is shown in Figure 6 with an emphasis on the methionine.

DP1
DEHGTAVMLK

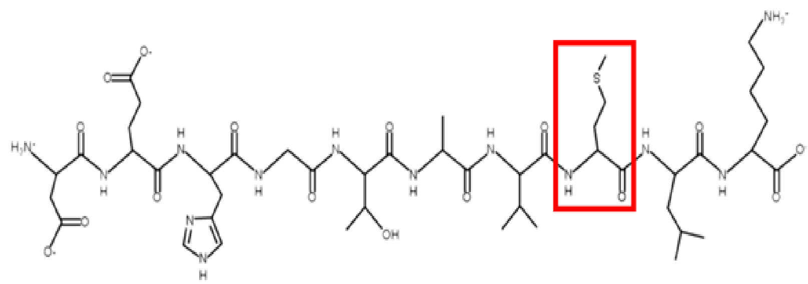

Figure 6. Linear chain of the ten amino acids of the decapeptide DP1. Methionine (red) is the primary focus of this research. The additional amino acids affect the response to radiation, e.g. peptide conformation, peptide folding, hydrophobicity, and electron transfer. Figure was produced using PepDraw software by Tulane University [3].

An additional side chain of interest is the aromatic ring contained in histidine, which confers water solubility. These two sites are the primary source of oxidative damage in the decapeptide due to the radiolability of those amino acids [3].

Numerous versions of the decapeptide have been fabricated and tested by AFRL/RHXBC, but DP1 has shown prominent resistance. Composition rather than sequence of the amino acids has been empirically shown to be of highest importance [1]. The structure of DP1 is important in determining conformation of active sites for ROS interactions. Though many of the amino acids can be modified by reactive oxygen and nitrogen species, as is tabulated by Chondrogianni et al., the methionine and histidine

structural availability is most important for this research and is predicted by the models in Figure 7.

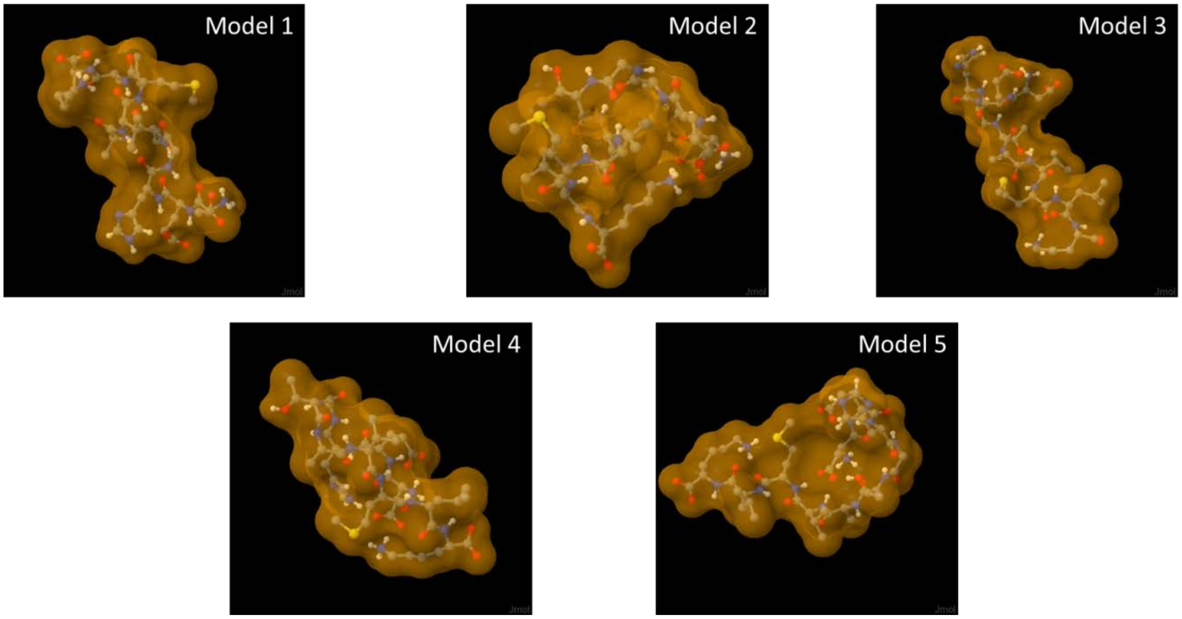

Figure 7. The five most probable structures of the decapeptide, DP1, as modeled from PEP-FOLD server. The availability of the thiol side chain of methionine and the aromatic side chain of histidine to scavenge reactive oxygen species is the key element of these conformational models. The sulfur atom (yellow) is distinguishable from the carbon (grey), nitrogen (blue), oxygen (red) and hydrogen (white). PEP-FOLD models were visualized using Jmol.

Research Techniques

This section reviews the science behind techniques completed to thoroughly view the spore response to irradiation. The techniques include actinometry, circular dichroism and spectrofluorometry.

Actinometry.

An actinometer is a system that determines the number of photons absorbed in a given region of a chemical reaction. This research focuses on a chemical actinometer, specifically the potassium iodide-iodate actinometer. Though not as popular as a

ferrioxalate actinometer, this actinometer is popular for UVC spectra because it is optically transparent for wavelengths above 330 nm and optically opaque for wavelengths below 290 nm [54]. This is significant in ease of fabrication since ambient visible light in the laboratory does not affect the actinometer, while light effective in inactivating bacteria is efficiently absorbed [55]. The application of this chemical actinometer provides the quantum yield of the system: the number of triiodide molecules formed divided by the number of 267 nm photons absorbed [56]. The quantum yield is an established natural value, and the relation of an experimental quantum yield signifies the efficiency of the experimental system to the theoretical or expected value.

Upon exposure to UV, the potassium iodide produces triiodide ions, according to Equation 3 [57].

$$8KI + KIO_3 + 3H_2O + h\nu \longrightarrow 3I_3^- + 6OH^- + 9K^+ \tag{3}$$

The photochemical reaction is explained in Equation 4 [58], which is a stoichiometric variation of Equation 3.

$$8I^- + IO_3^- + 3H_2O + h\nu \longrightarrow 3I_3^- + 6OH^- \tag{4}$$

The triiodide ion has peak absorption at 352 nm. Absorbance (A) is dependent upon optical path length (*l*), the molar absorptivity coefficient (or extinction coefficient) (ε) and the concentration (or molarity) (C) of the solution. The relation of these terms is expressed in Equation 5.

$$A_\lambda = \varepsilon C l \tag{5}$$

The molarity of the solution is used to calculate the number of moles of product, triiodide. To calculate the number of photons absorbed, the denominator of the quantum yield equation, Equation 6 is used [56]:

$$N_{267} = \frac{P(\Psi)(\mathrm{t})(1-10^{-A_{267}})}{hc/\lambda_{267}} \tag{6}$$

This equation incorporates the power of the LEDs (P), the transmittance (Ψ), time of irradiation (t), absorbance at 267 nm (A_{267}), Planck's constant (h), the speed of light (c), and wavelength. The UV transmittance is defined as the percent transmittance in the medium when the path length is one centimeter and the wavelength is 254 nm; the value, 0.975, was calculated with 269 nm emission [59]. The transmittance is used to relate the effect of the LEDs in the actinometer solution and with the addition of spores, since the extinction coefficient in spores is very small and drastically changes absorbance. The $(1-10^{-A_{267}})$ term is approximated as one, since $A_{267} >> 1$ for potassium iodate. Equation 6 can then be transformed to Equation 7 to describe the expected power of the system.

The experimental quantum yield calculated by the chemical actinometer is then compared to the expected quantum yield according to literature. The value for the expected quantum yield at 267 nm ranges between sources. The values vary widely and are reported for a temperature of 23.5°C, and are calculated via actinometry and radiometry. The expected quantum yield used for this research is 0.46. The value is the interpolation of results from: NIST with a reported quantum yield of 0.60 for 264 nm using radiometry [60]; 0.47 as interpolated from table 4 of an iodide-iodate actinometer [54]; 0.65 for 260 nm and 0.51 for 270 nm using BPI radiometry [57], 0.4 interpolated from figure 2 (or table 3) for a ferrioxalate actinometer from Goldstein et al. [55].

Additionally, Bolton expresses dependence in iodide-iodate actinometers on temperature [58]; the regression equation used is for 253.7 nm wavelength, and is therefore not considered for 267 nm, since the approximate difference in quantum yields between the two wavelengths is 54%.

The ratio of the experimental value to the theoretical value represents the efficiency of the reactor system used in this research, and is used to find the corrected fluence from the calculated fluence of the system. To calculate efficiency, the power output of the LEDs measured by an integrating sphere is compared to the power calculated from the slope of the absorbance of triiodide at 352 nm. The method used to calculate power from the slope ($m_{A_{352}}$) is described by Equation 7:

$$P = m_{A_{352}} \frac{hc}{\lambda_{267}} \frac{1}{\phi} \frac{N_A V}{\varepsilon_{I_3^-} \ell} \tag{7}$$

where: $\frac{hc}{\lambda_{267}}$ is the energy per photon at 267 nm; ϕ is the quantum yield; N_A is Avogadro's number; V is the volume of the system; $\varepsilon_{I_3^-}$ is the molar absorptivity coefficient of triiodide at 352 nm; and ℓ is the path length of absorbance.

The equation for calculated fluence as a function of time, H_e, is given below in Equation 8, where Ψ is the ultraviolet transmittance, σ is the cross sectional area in square centimeters of the reactor, t is the time in seconds of irradiation, and P_i is the power in milliwatts for each LED. The units of H_e are millijoules per square centimeter.

$$H_e(t) = \frac{\Psi t \sum_i^n P_i}{\sigma} \tag{8}$$

Circular Dichroism.

Circular dichroism spectroscopy is measured by a spectropolarimeter, which measures the absorbancies of two circularly polarized light pulses. Molecules that produce either left or right handed polarized light are enantiomers, such as the methionine used in this research. The chiral molecule will absorb a particular directional rotation of circularly polarized light, thereby distinguishing the rotary conformation. The magnitude and wavelength of the absorbed light depends on the molecule. Biomolecules have naturally strong CD signals and can even impart chirality to achiral particles [61]. These signal strengths are bringing CD to prominence for understanding protein structure. Sulfur-containing side chains within a protein, such as those found in methionine, have a negative CD band around 228 nm [62]. When viewing independent molecules, methionine exhibits peak absorbance at roughly 220 nm, whereas a chiral sugar molecule peaks around 200 nm.

The sign of the absorbance is dependent upon the handedness and type of molecule. For example, a dextrorotatory amino acid will have negative polarity at peak wavelength while levorotatory would be positive; conversely, dextrorotatory sugars will have positive polarity while levorotatory would be negative.

Spectrofluorometry.

Fluorescence occurs from the transition of an electron in an excited singlet state to the ground state. This transition is allowed, rather than forbidden, and therefore happens quickly and produces a photon. The typical fluorescence lifetime is approximately 10 nanoseconds [63]. The lifetime of a fluorophore, a fluorescent chemical that emits

photons upon excitation, is the average time between the excitation of the chemical and its return to the ground state. The fluorophore used in this research is SYTO® 16 green fluorescent nucleic acid stain, with an excitation of 488 nm and an emission of 518 nm for DNA binding. The spectrofluorometer recorded emission spectra: the wavelength distribution of an emission measured at a single excitation wavelength [63]. For all data recorded, the emission spectra were plotted as wavelength in nanometers against photon counts. The wavelength interval was determined by the slit width and dispersion of the emission laser.

The SYTO fluorophore binds to DNA and RNA and fluoresces at 518 nm for DNA. The photon counts are expressed as relative fluorescence units (RFUs). It is assumed that excess dye, which does not bind to DNA, has fluorescence that cannot be distinguished from background read by the FluoroLog. Conversely, an insufficient dye concentration will not reflect the correct amount of DNA in the sample and be a low estimate of the true value. As the spore begins germination, the DNA becomes exposed as the spore core is opened and the stain can bind to the available DNA. This causes an increase in photon counts and further increase of photon counts tracks the transition to the vegetative cell. As explained in *Growth Phases*., the time between the beginning of germination and the exponential phase is brief, and is expected to be depicted as a sharp increase in photon counts [12].

III. Methodology

Chapter Overview

This chapter details the methods developed and adapted to irradiate *Bacillus anthracis* (Ba) Sterne spores by ionizing radiation produced from a cesium-137 source and by UVC radiation by UV light emitting diodes (LEDs) of 267 nanometer wavelength. The Sterne cells included a pRB373 plasmid with a Turbo-red fluorescent protein (Turbo RFP). These cells were chosen as a continuation from experiments by a previous researcher for continuity purposes [12]. The inactivation curves for these spores were then reproduced to justify continuation. The germinated cells were sporulated under three conditions: control growth, in excess of L-methionine, and in excess of D-methionine. The different spore stocks were irradiated and allowed to germinate for various times. Data for the survival curves was collected by colony forming units (CFUs). Data for the germination outgrowth time was collected as fluorescence measurements from a FluoroLog spectrofluorometer. This chapter also details of the use of: circular dichroism spectrometry for verification of methionine adherence during sporulation; and actinometry experiments to test the efficiency of the LED reactor.

Microbial Technique

The Turbo RFP plasmid was provided by the research group from the 711th Human Performance Wing at Air Force Research Laboratory's Human Effectiveness Directorate (AFRL/RHXBC) [1] and was transformed by the previous researcher, Chelsea Marcum, including: *E. coli* transformation; plasmid isolation; transformation and electroporation in *B. anthracis* [12]. The spore solutions and plate colonies

expressed the same bright pink hue and ampicillin resistance as expected of the pRB373 plasmid.

Spore Preparation

Scale-up Cultures.

The spores used throughout the experiment were prepared from the bacterial stock of Ba cells provided by AFRL. The sporulation procedure was adapted by Dr. Roland Saldanha from Leighton and Doi, found in *Leighton-Doi Media Recipe* [64]. An additional step to the procedure was included for sporulation in excess of D-methionine and L-methionine, and is described in *Sporulation Doping Protocol* in the appendix. 10 μL of the cell stock was added to 20 mL of 2X Difco™ Nutrient Broth in a 250 mL culture flask. The culture was incubated at 37 °C at 180 rpm for 6-12 hours. 2.5 mL of the broth culture was added to 25 mL of nutrient broth in 250 mL culture flasks, and repeated to use all of the original broth culture. The culture was incubated at 37 °C at 200 rpm for 6-12 hours.

Inoculation of Spore Culture.

From the 220 mL of total culture broth, 22 mL culture, 22 mL Leighton-Doi sporulation media, and 198 mL nutrient broth was combined in a 2000 mL culture flask, and repeated seven additional times. The flask is approximately 10-fold larger than the volume of the culture for ample aerobic exchange. The spore culture was incubated at 37 °C at 225 rpm for 6-12 hours. Before harvesting the spores, 10 μL of the spore culture was pipetted to a microscope slide and viewed via phase-contrast microscopy at 63X to

verify sporulation. This step confirmed mostly phase bright spores and no contamination of the culture.

Harvesting Spores.

The confirmed spore culture was moved to 40 mL centrifuge tubes and was centrifuged at 10000 rpm for 15 minutes at 4 °C. The supernatant was removed and the spores were re-suspended in water stored at 4 °C. The spores were pelleted via centrifugation and cold water washes were repeated an additional 5 times. To minimize clumping, the spores were re-suspended in 3 mL of 1X phosphate buffered saline with 0.05% Tween® 20 (PBST) [65].

Inoculation of Methionine Spore Culture.

The method for sporulating Ba cells in excess of methionine was similar to that of the previous spore inoculation. The process for creating spores in excess of L-methionine and D-methionine was the same. The only adaptation to the original sporulation method required that each 2000 mL culture flasks contained 22 mL culture, 22 mL Leighton-Doi sporulation media, 198 mL nutrient broth and 220 mg methionine. 1.0 gram per liter of methionine was chosen as an overestimate of a comparable amount of methionine included in the Difco™ Nutrient Broth, based on the following assumptions: 16 g of an unknown peptide mix per liter of solution; methionine represents 1/20 of the amino acids present in the peptide mix.

Harvesting Methionine Spores.

The method for harvesting the methionine spore culture was modified from the original to include 7 cycles of cold water washes and centrifugation. Any excess

methionine not taken in by the spore needed to be removed from the spore stock for reliable data collection by circular dichroism spectrometry.

Spore Counting.

The final spore concentrations were determined via colony forming units on ampicillin selective tryptic soy agar (TSA) plates and by INCYTO DHC-N01 C-Chip disposable hemocytometers. The ampicillin selective TSA plates additionally verified the presence of the pRB373 plasmid from colony formation expressing the expected pink hue. The plates were counted in triplicate and the initial spore count, N_o, was recorded. The cells within squares of 1/25 square millimeters of the hemocytometer were counted and averaged from 9 repetitions for one-hundredth and one-thousandth dilutions. Cells bordering the top and left walls of the square were not counted. The final spore concentration, N_o, was recorded and compared to the results of the CFUs. The results varied by a factor of two. The spore concentrations for regular spores, L-methionine, and D-methionine were 2.0×10^{10} spores/mL, 1.0×10^{10} spores/mL, and 1.2×10^{10} spores/mL, respectively.

Spore Nomenclature.

So as to prevent confusion: spores containing only the pRB373 are deemed BaC; Ba vegetative cells which were sporulated in an excess of L-methionine will be termed BaLE; Ba vegetative cells which were sporulated in an excess of D-methionine will be termed BaDE; spores supplemented with L-methionine will be termed BaLS; spores supplemented with D-methionine will be termed BaDS; and spores supplemented with DP1 will be termed BaDP1.

Circular Dichroism Spectrometry

This section outlines the procedures used to acquire reliable data from the Jasco J-815 circular dichroism spectrometer. Since CD results are highly dependent on concentration and absorbance of the sample, all preparations were completed with great detail. The samples on which the data were collected were all suspended in water with 5% PBST and included: BaC spores, BaLE, and BaDE. The spores were sporulated, harvested, and suspended as mentioned in the previous section. For optimal spectral readings, each sample was diluted in water in separate Eppendorf tubes containing 1 mL of $2x10^7$ spores/mL and $4x10^7$ spores/mL. The samples were transferred to a 750 μL quartz cuvette and averaged over three repetitive measurements from 200 to 300 nm wavelengths. Between samples, the cuvette was thoroughly washed with bleach and deionized water to minimize residual methionine which would skew results. The BaC spores were measured as the baseline and the BaDE and BaLE samples were measured against the baseline to view the difference in absorbance.

Ultraviolet Irradiation

This section reviews the radiation experiments on *Bacillus anthracis* by ultraviolet LEDs, including reactor setup, LED characterization, and Ba fluorescence curves.

UV Reactor Setup.

This subsection explains the design characteristics of the reactor used to perform UV radiation experiments. The reactor was an adaptation of a design created by Michael Spencer and used by the previous researcher [11]. The reactor, see in Figure 8, was

fabricated from a 3 inch tube of highly polished Type 316 stainless steel. The reactor was further polished and passivated via electrochemical polishing to increase reflectivity of the UV light emitting diodes (LEDs) on the surface of the reactor. The reactor sits upon three aluminum stand offs which were screwed to the incubator and shaker during respective parts of the experiment. The lid of the reactor swiveled open for easy access throughout radiation and germination, and was otherwise tightly fastened with a wing nut. The Thermo Scientific Max-Q 2000 shaker was set for approximately 180 rpm to prevent spores from aggregating to the sides of the reactor and to homogeneously irradiate the solution. The Innova® 42 incubator was set for 37 °C for optimal aerated spore growth and 180 rpm to prevent spore clumping and aggregation [7] [23].

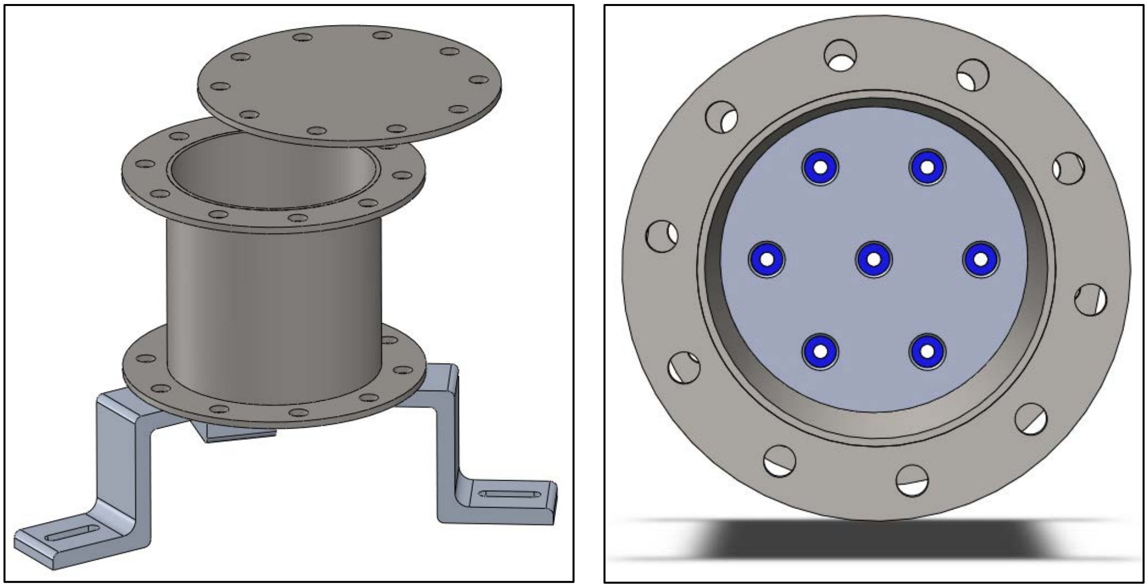

Figure 8. The UV reactor (left) is an adaptation of a design by Michael Spencer, AFIT [11]. The right picture displays the top view of the reactor which houses 7 silicon sealed LEDs (blue) that irradiate from the bottom. Composed of electropolished stainless steel, the reactor allows for a high reflectance. The lid swivels, as shown on the left, for facilitated sample collection. The reactor rested upon three standoffs that are attached to a shaker. The shaker helped to prevent spores from clumping or aggregating to the sides of the reactor. Models were created using SolidWorks software.

LED Characterization.

Seven equidistant LEDs purchased from Sensor Electronic Technology, Inc (SETi) rested at the base of the reactor. The LEDs were sealed to the bottom plate using silicon and were backed by an aluminum plate. This plate distributes heat from the system and prevents the highly sensitive LEDs from burning out. The LEDs were characterized before and after all experiments using a Labsphere® integrating sphere and Illumia®pro operating software. The results were confirmed against the product information for the UVTOP260TO39 LEDs [66]. The values for wavelength, full width at half maximum (FWHM) and total power were averaged from five measurements for each LED. The average power for the 7 LEDs before and after all experimentation was 1.362 and 1.187 milliwatts, which was used for expected fluence and corresponding

doses of the system. The peak wavelength was 267 nm with a FWHM of 11 nm, which corresponds to the data received from SETi [66]. This wavelength was chosen based on research by Wurtele, et al. on UVC irradiation of *Bacillus subtilis* [59]. The UV inactivation kinetics for *B. subtilis* is essentially identical to *B. anthracis* according to Nicholson [67] and can therefore be used as a UV surrogate.

The LEDs were controlled by a circuit board connected to a 10 volt DC source. The LEDs burned out in previous research when the current exceeded 20mA and or if the current became negative. The circuit board was designed with 25 Ω variable resistors at the positive terminals of the LEDs and with diodes at the ground terminals of the LEDs to prevent burn out. With these precautions, which led to facilitated experimental setup, the LEDs could be plugged in to the board before the 10 volt DC source was turned on. More complicated electronics have been used elsewhere and hampered experiments [10] [12].

UV Survival Curves.

The UV experiments focused on the difference in germination outgrowth time and viability for the BaC, BaDS, and BaLS. The primary focus of the experiments was to irradiate all samples at a dose corresponding to 90% kill, or 1-$\log_{10}$ reduction, of 10^7 spores of control *anthracis*. This dose was found by repeating 3 experiments of UV irradiation over a range of times. The times were chosen from the previous research and corresponding radiant exposure values were calculated by Equation 8 [12]. The inactivation experiments were performed by irradiating a 100 mL solution of 10^7 spores in sterile Milli-Q® water. During irradiation, 100 µL aliquots were pipetted at the times listed in Table 1. The aliquots were serially diluted and plated in triplicate. The CFUs

were collected after 18-24 hours of incubation at 37 °C. The data of the three experiments were analyzed and the average of the inactivation experiments was analyzed to obtain the time corresponding to a 1-$\log_{10}$ kill.

Table 1. Times for removal of spore solution from the UV reactor. These times were based off of previous research. The fluence for each time was calculated by Equation 8 from the power of the seven LEDs, recorded by the software for the integrating sphere. These fluence values were used to plot the dependence of spore survival on increasing fluence.

Exposure Time (sec)	Fluence (J/m^2)
0	0
26	58
51	114
77	172
90	201
102	227
115	256
127	283
150	334
178	397
229	510
331	737

UV Outgrowth Time.

To quantify the outgrowth time and lag phase of the *Bacillus anthracis* cells, spectrofluorometry was performed on the cells during germination. 100 mL of water with 10^7 spores was irradiated in the UV reactor, then 100 mL of 2X minimal media was added and incubated for a total of 9 hours. The recipe for the minimal media is found in *AGFK Minimal Media Recipe*. An additional unirradiated solution of 100 mL spores and 100 mL media was placed in the incubator for the same time as a control. 3 mL of both solutions was pipetted at 30 minute time intervals. Each 3 mL sample was partitioned

into 3 Eppendorf tubes and placed into an Eppendorf 5145D benchtop microcentrifuge. The supernatant was removed, replaced with 1 mL of 4 °C water and centrifuged again. This process was repeated 6 times for each time sample and the samples were refrigerated at 4 °C.

Preparations for spectrofluorometry readings were accomplished according to the protocol in *Fluorescence Experiment Protocol* in the appendix. 500 μL of each triplicate sample was transferred to an Eppendorf® UVette® plastic cuvette and prepared in the dark. Irradiated and unirradiated BaC spores were stained with 3 μM SYTO® 16 green fluorescent nucleic acid stain and capped with parafilm. Subsequent irradiated and unirradiated samples of BaLS and BaDS were dyed with 1 μM stain to conserve resources. The cuvettes were vortexed to mix the solution and wrapped in foil to reduce light absorption. The samples incubated at room temperature for approximately an hour. The sample was transported to a HORIBA Scientific FluoroLog®-3-22 spectrofluorometer and 3 readings were averaged for every 30 minute sample. The fluorescence units were collected and associated with time to produce comprehensive outgrowth data. Each experiment was repeated three times for increased statistical power.

Gamma Irradiation

This section reviews the gamma irradiation experiments on *B. anthracis* by a cesium-137 source provided by the Cincinnati Children's Hospital Medical Center. The cesium source provides a dose rate of 6.33 gray (Gy) per minute and was consistently

irradiated overnight to achieve doses on the kilogray scale. The four spore variations irradiated by the Cs-137 source were: BaC, BaLE, BaDE, and BaDP1.

Radiation Preparation and Execution.

The samples for gamma irradiation were prepared according to the protocol found in *Gamma Irradiation* in the appendix. Gamma irradiation saw the addition of DP1 to the matrix as compared to UV experiments. The control samples were reduced from the spore stock of 10^{10} spores/mL to 10^{7} spores in 500 μL of water. The Eppendorf tubes were labeled appropriately with stickers atop the parafilm seal to distinguish between other samples, which were prepared in a similar manner. The tubes were color coded and paired by doses to simplify the irradiation for the operator. The samples were placed in a carousel similar to the model in Figure 9 for more homogeneous dose distribution.

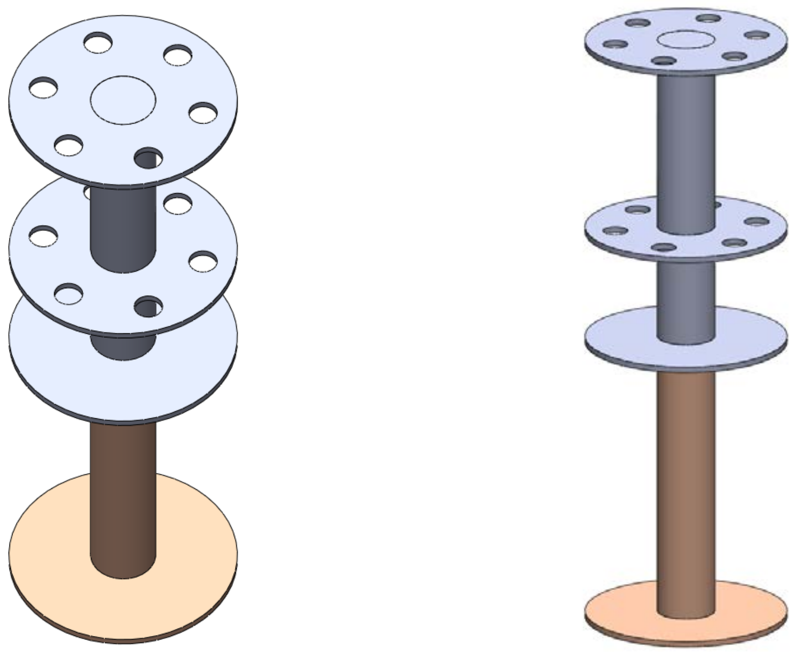

Figure 9. The carousel positioned within the radiation chamber held the 12 pairs of Eppendorf tubes and constantly rotated during irradiations. The two views are an isometric bird's-eye view (left) and a profile (right) of the carousel. The model was created using SolidWorks software.

The samples were retrieved according to irradiation times and were immediately put in a refrigerator at 4 °C to slow radiolysis reactions and early germination within the tubes. Unirradiated control samples were left in the radiation room for the longest radiation time; this quantified the effect of background radiation, variability due to travel, and unplanned germination due to DP1 and methionine in the samples.

The initial dose range was altered after the first experiment to incur more radiation damage. This change is noted in *Gamma Protocol Revision* in the appendix. The dose range used throughout the four replicates of the experiment was from 0 to 8000 gray, with dose increments of 1000 Gy.

Inactivation Curves.

The first set of irradiated samples was retrieved the same day as irradiation. The second, third and fourth repetitions of the experiment were irradiated on three concurrent days and were all retrieved on the third day. All repetitions were placed in a thermally insulated box with cold packs and transported back to the RHXBC laboratory. The samples were prepared following the protocol in *Gamma Irradiation Protocol* in the appendix. Each sample was serially diluted, plated in triplicate on Difco™ Nutrient Agar plates, and incubated at 37 °C for 18 to 24 hours. CFUs were counted and recorded to produce inactivation curves for the four types of spores. The inactivation curves were analyzed to determine the dose relation between the control spores and the supplemented spores.

Actinometry

Chemical actinometry was performed on the UV reactor setup to quantify the fluence of the LED system and rate the efficiency of the LEDs at 267 nm. This research used potassium iodide-iodate actinometry due to its effectiveness in the UV region. Actinometry was performed before any UV experiments were executed and after all experiments were completed. Had there been any change in the LED system, such as loss of an LED, additional actinometry would have been necessary. The actinometer solution was prepared according to the protocol in *Actinometry Protocol* in the appendix. The solution was deposited into the UV reactor and the reactor was turned on. A 3 mL sample was aliquoted every 30 seconds and placed in a plastic cuvette. The cuvette was analyzed by a UV-Vis spectrometer for 200-800 nm wavelengths for a total of 10

minutes. Additionally, a 3 mL cuvette of unirradiated iodide-iodate was analyzed for 10 minutes in the spectrometer to obtain a blank of the system. The calculations performed from the data reflected the actual fluence of the system.

IV. Analysis and Results

Chapter Overview

This chapter discusses the results in context of the research objectives stated in the research statement. The data collected from the methods described in the previous chapter are analyzed and the relevance to the hypothesis is reviewed. Discussion of error is included and the integrity of the research results is examined. A review of these results is covered in the final chapter.

LED Characterization

The seven light emitting diodes used throughout the UV experiments were characterized before all experimentation in October 2014 and were characterized again after all experimentation was completed in February 2015. The collected data are presented in Table 2 for October and Table 3 for February.

Table 2. LED power measurements collected by a Labsphere® integrating sphere in October 2014, before any experiments were performed. The data include the total power, selected power, peak wavelength, and full width at half maximum for each of the 7 LEDs used throughout the research. The data for each LED were averaged from five measurements. The selected power included power between 240 and 300 nm. The total power spanned wavelengths of 200 to 340 nm.

LED	Total Power (mW)	Selected Power (mW)	Peak Wavelength (nm)	FWHM (nm)
1	1.342	1.306	267	11
2	1.389	1.353	267	11
3	1.174	1.138	267	11
4	1.427	1.388	267	11
5	1.425	1.386	267	11
6	1.410	1.370	267	11
7	1.370	1.335	267	11

The data from LED characterization before and after experimentation show that the LEDs lost 13% power over the estimated 2.5 hours of total operation.

Table 3. LED power measurements collected by a Labsphere® integrating sphere in February 2015, after all experimental data were collected. The data include the total power, selected power, peak wavelength, and full width at half maximum for each of the 7 LEDs used throughout the research. The data for each LED were averaged from five measurements. The selected power included power between 240 and 300 nm. The total power spanned wavelengths of 200 to 340 nm.

LED	Total Power (mW)	Selected Power (mW)	Peak Wavelength (nm)	FWHM (nm)
1	1.225	1.194	267	11
2	1.215	1.184	267	11
3	1.238	1.207	267	11
4	1.1424	1.111	267	11
5	1.135	1.104	267	11
6	1.275	1.244	267	11
7	1.080	1.049	267	11

The change in LED power is linear with time, so the value used in actinometry and fluence calculations was the midpoint value in time of the two averages of LED power.

Actinometry

Chemical actinometry was performed on the system prior to and after all UV experiments. An iodide-iodate actinometer was applied to the reactor on 10 October 2014 and 14 February 2015. The efficiency of the system was calculated by first obtaining the absorbance values at 352 nm recorded by the UV-Vis spectrometer. The slope of the absorbance was then applied to Equation 7 from *Actinometry*. The relation

of absorbance, path length, and molar absorptivity to concentration is described by the Beer-Lambert law (Equation 9).

$$A = \varepsilon c \ell \tag{9}$$

For the range of absorbances calculated, the relation of absorbance to time, the slope, is linear. The molar absorptivity coefficient is 2.32×10^4 L/(mole-cm), multiplied by the path length of the cuvette, 1.00 cm, and is in units of liters per mole, or inverse concentration [68]. Once the molarity of the triiodide ion was calculated, the number of moles of triiodide is calculated using Avogardo’s number and a volume of 100 mL. This is the volume contained within the reactor for actinometry and all subsequent UV experiments. With this information, and the quantum yield, 0.46, discussed in *Actinometry,* Equation 7 was used to calculate the power produced by the 7 LEDs in the system, 7.57 mW. The ratio of this power to the power measured by the integrating sphere, 8.92 mW, gave the efficiency of the system: 84.8%. Additionally, the factor of UV transmittance, UVT, approximates the change in absorbance with the addition of spores into the solution. The efficiency and UVT provided the correction to the fluence, which is shown in *Actinometry* in the appendix.

The actinometry performed after all experiments were completed was used to gauge the changes in the system. The final average quantum yield is 29% smaller than the first calculated quantum yield. The average power from the LED characterization was used in the quantum yield calculations that were used to calculate system efficiency. The change in LED power would be a major contributor to a change in system efficiency.

Inactivation Curves

A majority of the research was set up to replicate the conditions used by Chelsea Marcum [12]. Consistency in methodological and analytical processes was necessary to obtain results consistent with the previous research. Growth curves corresponding to a 1-$\log_{10}$ inactivation of the spores were repeated and a comparison to data from the previous researcher was made over the corrected fluence. The method for obtaining corrected fluence is reviewed in *Actinometry*. Figure 10 portrays the spore inactivation at the commencement of this research, averaged over 3 experiments with triplicate samples for each fluence value. Plots of the three separate experiments are included in the appendix in

UV Survival Curves. The error bars on the 4 UV survival curve plots are representative of 3 standard deviations, or 99.7% of the data of a normal distribution.

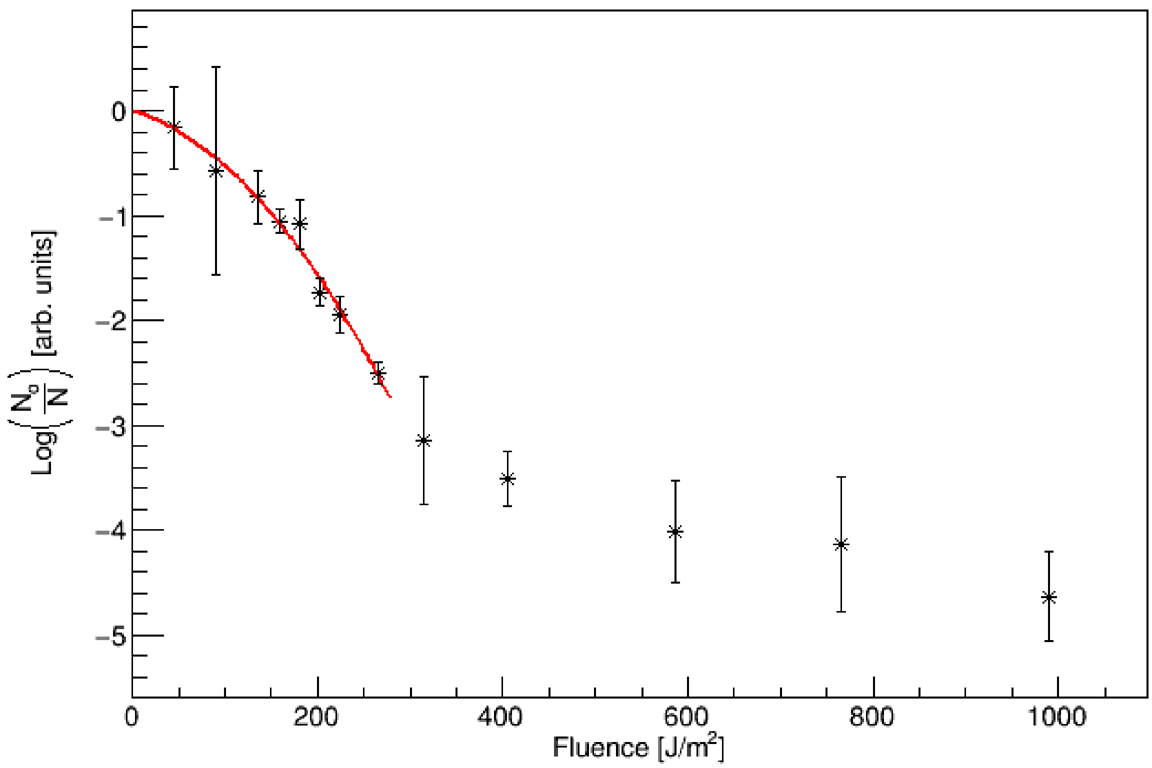

Figure 10. Quadratic fit of inactivation survival data from UVC irradiation of 1.3×10^{7} spores of control *B. anthracis* (BaC). The data represents triplicate samples for each fluence value from 3 repetitive experiments. The regression line (red) is only considered over the shoulder region at low UV fluence and during log-linear inactivation. The points to the right of the red line are part of the tailing portion and are not considered for the regression. The coefficient of determination for the fit is 0.978777.

The regression equation, Equation 10, models the spore response to irradiation. The equation takes a value for fluence (H_e) and returns the common logarithm of the ratio of the original, unirradiated cell count (N_o) to sample cell count (N). The linear coefficient, α, is -2.650×10^{-3} and the quadratic coefficient, β, is -2.59×10^{-5}. Using these values, the fluence corresponding to 1-$\log_{10}$ inactivation was calculated as 152 J/m^2. The irradiation time was then calculated from Equation 8, which equates to an irradiation time of 70 seconds. All UV experiments were programmed for 80 seconds due to an initial regression for the data. This affects the fluorescence data when compared to the previous researcher, since the inactivation is greater than 90%.

$$\log {N_o}/{N} = \alpha H_e + \beta H_e^{\,2} \tag{10}$$

The regression for the system is modeled by Equation 10 and the values in Table 4. The coefficient of determination, or R^2, is 0.97877, where 1.0 would represent a perfect model for the data; R^2 is defined as the total variability accounted for by the regression line. The χ^2 and reduced χ^2 measure the discrepancy between two sets of cell frequencies, where a value of 0 is described as a perfect fit [69].

Table 4. Statistical parameters for data compiled from three repetitions of the UV inactivation experiment. The terms α and β describe the quadratic regression of the data, and the following three terms represent the goodness of fit of the regression to the data.

Combined UV Survival Curve	
α	-0.00265028
β	-0.000025855
X^2	2.05669
Reduced X^2	0.342782
R^2	0.978777

The statistical descriptors of the third and final experiment suggest the best fit of model to data, but the combination of the three survival experiments provides the best statistical power. The values of χ^2, reduced χ^2, and R^2 for the three individual experiments are presented in *UV Survival Curves* in the appendix.

The purpose of choosing a single fluence for all experiments provided simplicity of analysis. The germination times for the three variations of spores, BaC, BaLS, and BaDS, were compared with fewer statistical factors when a single UV fluence was chosen.

CD Spectrometry

The spectrometry experiments produced results that were welcomed yet unexpected. The data shown in Figure 11 through Figure 13 were collected via the procedure described in *Circular Dichroism Spectrometry*. Figure 11 and Figure 12 show the circular polarization of the BaC spores compared to the bacteria sporulated in L-methionine (BaLE) and the bacteria sporulated in D-methionine (BaDE) respectively. The flat slope of the control spores in Figure 11 and Figure 12 shows the subtraction of the baseline, the control spores, from the CD data of BaLE and BaDE.

The DL-methionine has likely been adsorbed on the spore, rather than absorbed beneath the spore coat. This would affect the structural characteristics of the spore, including aggregation with other spores. Methionine is very hydrophobic in water, with a normalized hydrophobicity index of 74, relative to neutral glycine (0 value) [70]. It is suggested that hydrophobic spores can aggregate with each other; spore-spore or spore-Met clumping may arise from the high hydrophobicity of methionine [71]. Physicochemical differences between L-Met and D-Met would explain the difference that arose in BaLE plate counts after gamma irradiation. Though the spores were prepared in the same fashion, the levorotary molecule could bind more preferentially than the dextrorotary molecule to the surface of the other spores, thereby increasing spore hydrophobicity and associated clumping. A racemic mixture, according to this theory, would resolve or prevent the clumping issue, but would negate the ability to compare the exclusive effects of L-Met and D-Met.

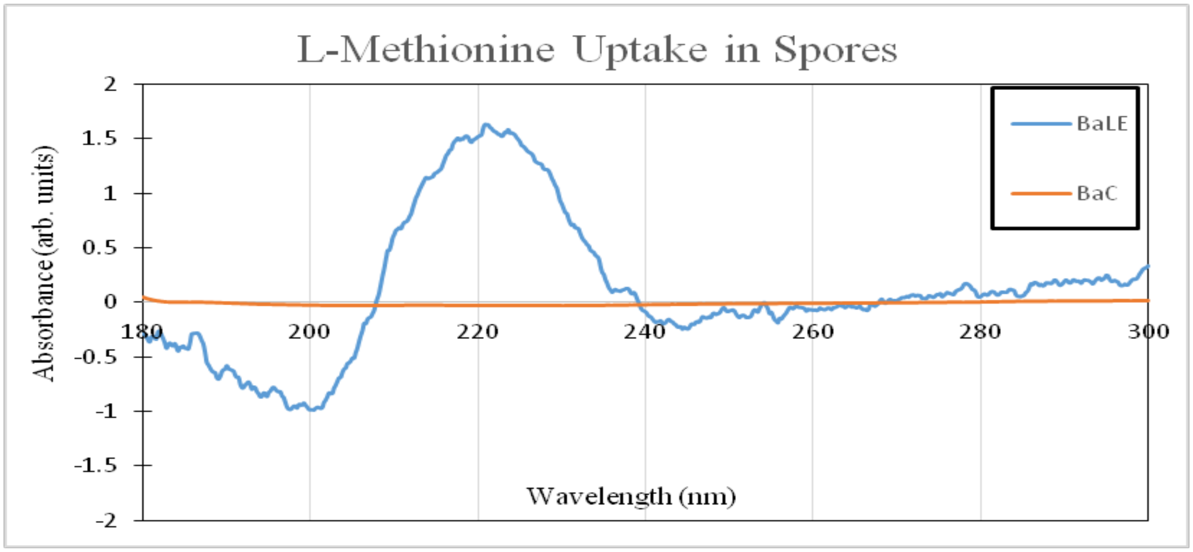

Figure 11. CD spectrometry shows the peaks expected for L-methionine. The comparison between the BaC spore (orange) and the BaLE (blue) shows successful uptake of methionine into the spore. The linear slope indicative of the BaC spores represents the use of BaC as a baseline that was subtracted from all CD measurement.

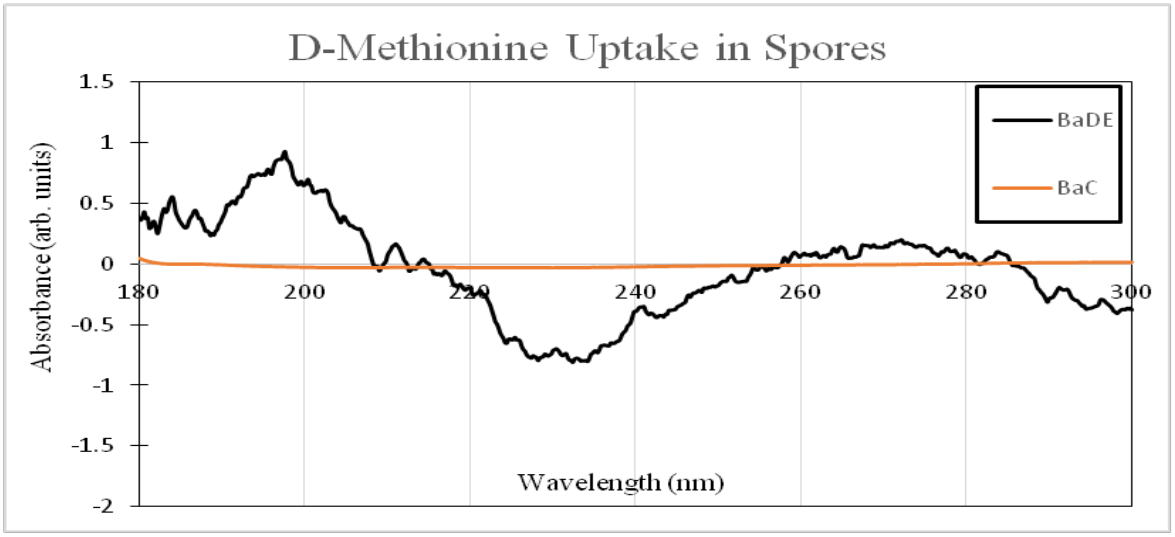

Figure 12. Graph of spores with excess D-Met (BaDE) compared to control spores (BaC). The difference between the lines clearly shows that the BaDE spores did in fact uptake the D-methionine. The absorption value peaks from the CD measurements are at the expected wavelengths. The linear slope indicative of the BaC spores represents the use of BaC as a baseline that was subtracted from all CD measurement.

Figure 13 compares the absorbances of BaLE and BaDE. Theoretically, the peaks should match up at the same wavelength and with the same amplitude, but opposite polarity. It is obvious that L-Met (blue) has a peak of greater magnitude centered over 220 nm while D-Met (black) has a smaller peak centered over 230 nm. Since CD spectroscopy is strongly dependent on concentration of the chiral molecules, small variation between the methionine concentrations would result in large differences on the spectrum. The difference in peaks also suggests that the adherence of methionine in the spore was not consistent for the two enantiomers. The concentrations added during sporulation were the same, but the final concentration was different. Since the L-met peak is larger, it is assumed that the levorotary conformation is preferable for binding to the spore.

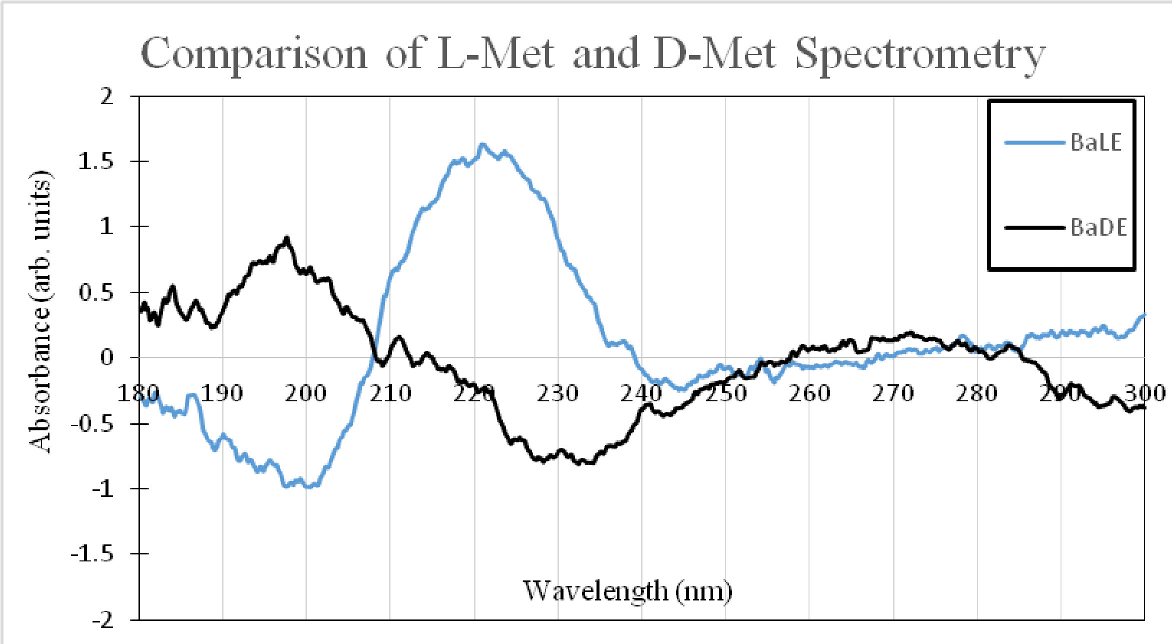

Figure 13. Comparison of BaLE (blue) and BaDE (black) shows the effect of concentration on CD spectrometry. Theoretically, the peaks would be at the same wavelength and amplitude, but with opposite polarity. Rather than a mirror image across the x-axis, the two lines have variation in spectra. This disparity arises from a difference in concentrations for methionine adsorption in the two spore stocks. The same concentration was added to the sporulation media, which implies that the adherence was not consistent between the enantiomers.

Spore Outgrowth Time after UV Irradiation

The fluorescence data collected from the procedure described in *UV Outgrowth Time* represents the time of UV damage repair required before the outgrowth phase of the cell. The amount of damage the spore receives during irradiation directly correlates to the time it takes for the cell to germinate. The lag time, or the difference between the beginning of germination for irradiated and unirradiated spores, is the basis for comparing the three variations of UV irradiated spores: BaC, BaLS, and BaDS. The fluorescence curves compare the irradiated and unirradiated fluorescence values over the 30 minute intervals for each spore variant. Figure 14, Figure 16 and Figure 17 represent the curves for BaC, BaDS, and BaLS, respectively. For all three figures, the data were

averaged over three replicates of each respective experiment. The error bars represent two standard deviations of the data, which accounts for 95% of the data. The standard deviation was calculated as the square root of the photon counts per datum.

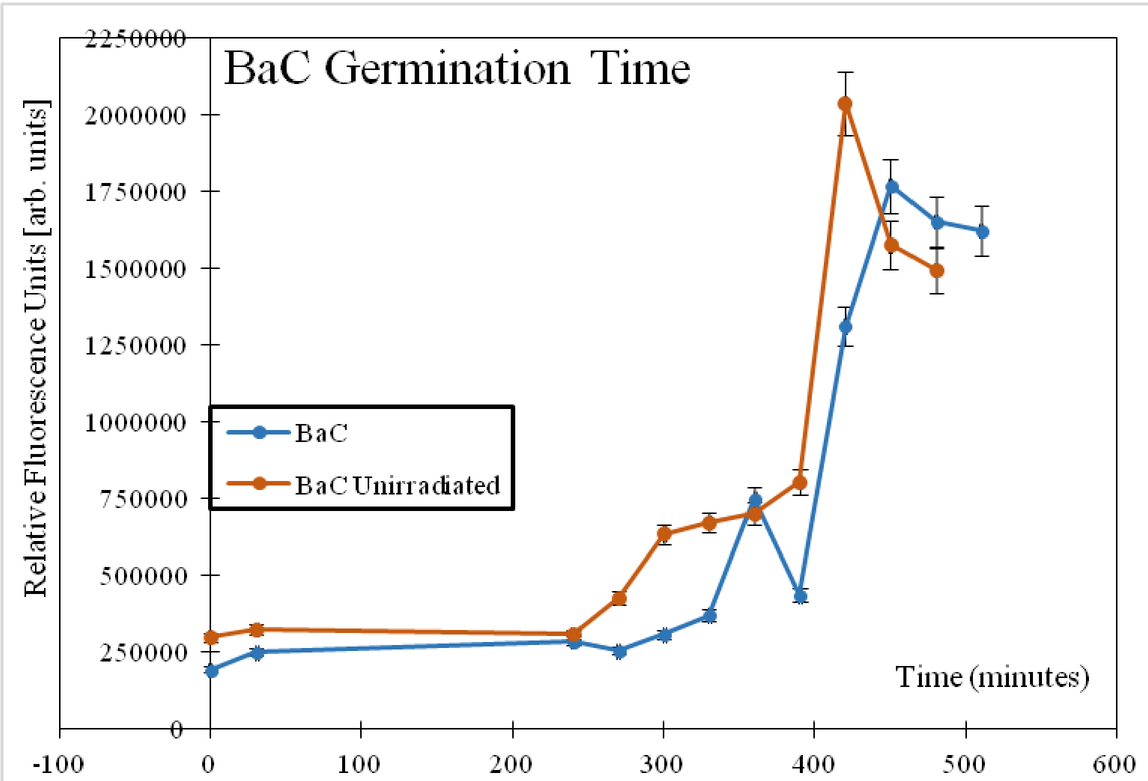

Figure 14. Fluorescence data from UV irradiated and unirradiated *Bacillus anthracis* control spores (BaC). Three 1 mL samples were removed at 30 minute time intervals as the spores incubated in 1X minimal media. The triplicate samples were combined and 1.5 mL was stained with 3 μM SYTO 16 green fluorescent nucleic stain. Each datum was analyzed by a Horiba FluoroLog spectrofluorometer, and relative fluorescence units were recorded. To conserve fluorescent stain, the time samples in the linear portion, between 30 and 240 minutes, were not analyzed. Spore outgrowth occurs at 240 minutes for unirradiated BaC and 330 minutes for irradiated BaC. This corresponds to a lag time of 90 minutes.

Figure 14 shows the fluorescence measurements for UV irradiated and unirradiated control spores (BaC). The primary interest of the graph is the steady increase in fluorescence units between two time samples, for the irradiated and

unirradiated experiments. This increase indicates the beginning of the germination phase. As explained in *Growth Phases*., the spore is transitioning out of dormancy so DNA repair can occur. The beginning of germination starts at 240 seconds for the unirradiated sample and at 330 minutes for the irradiated sample. The “triangle” that occurs between 330 and 390 seconds is enigmatic. This same unknown occurred in results by Marcum for the unirradiated sample, as seen in Figure 15, and requires further investigation [12]. The difference between the time of outgrowth for each curve denotes a lag time of 90 minutes. Choosing the 330 minute point as the beginning of germination for the irradiated sample should be a null hypothesis for this variable in future experiments, so as to clarify the true time of phase transition.

The sharp increase in fluorescence units, or burst time, signifies that the vegetative cells are now able to replicate at 2^n from the excess nutrients in the environment. The burst time for both BaC experiments starts at 400 minutes. The greater magnitude of RFUs for the unirradiated experiment signifies the greater number of cells in the system, which is expected since no intentional spore killing occurred.

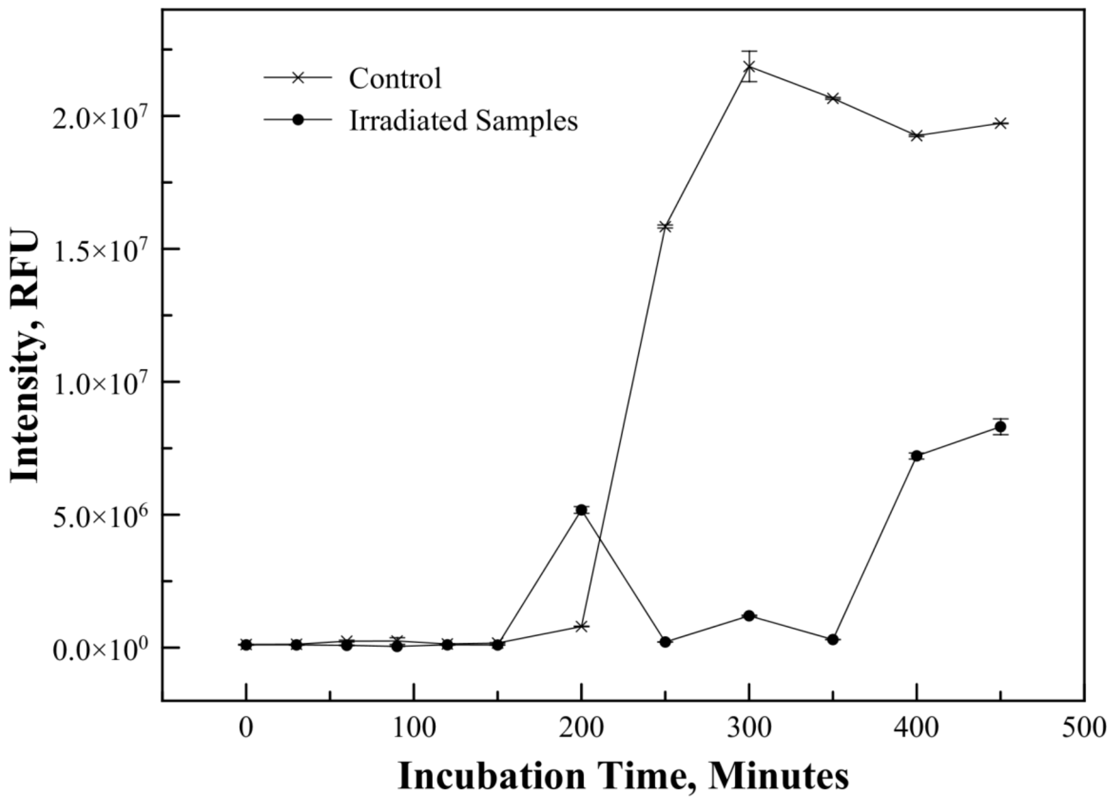

Figure 15. Fluorescence data by Marcum for *Bacillus anthracis* control spores. Three 1 mL samples were removed at 30 minute time intervals as the spores incubated in half strength minimal media. The triplicate samples were combined and 1.5 mL was stained with 5 μM SYTO 16 green fluorescent nucleic stain. Each datum was analyzed by a Horiba FluoroLog spectrofluorometer, and relative fluorescence units were recorded. The time of outgrowth for unirradiated spores and irradiated spores occurs at 200 minutes and 350 minutes, respectively. This corresponds to a lag time of 150 minutes. [12]

The fluorescence of BaDS, portrayed in Figure 16, demonstrates the same cell response to irradiation as seen in Figure 14, though at a much smaller RFU magnitude.

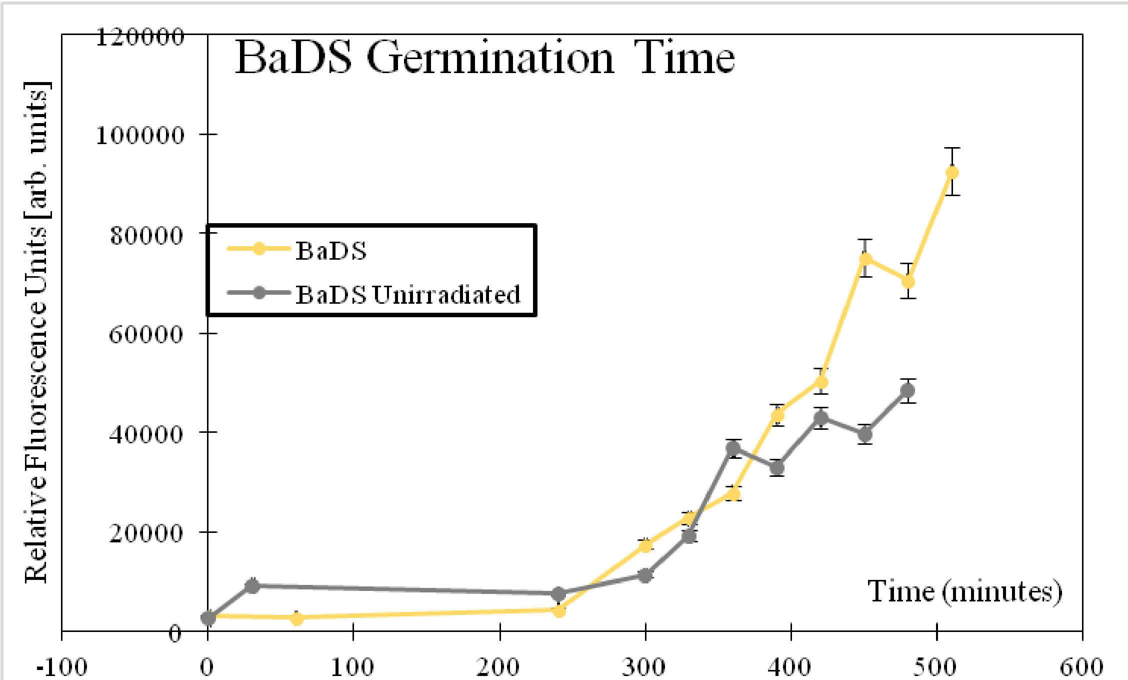

Figure 16. Fluorescence data from UV irradiated and unirradiated *Bacillus anthracis* spores supplemented with D-methionine (BaDS), average over three repetitions. Three 1 mL samples were removed at 30 minute time intervals as the spores incubated in 1X minimal media. The triplicate samples were combined and 1.5 mL was stained with 1 µM SYTO 16 green fluorescent nucleic stain. Each datum was analyzed by a Horiba FluoroLog spectrofluorometer, and relative fluorescence units were recorded. To conserve fluorescent stain, the time samples in the linear portion, between 60 and 240 minutes, were not analyzed. Spore outgrowth occurs at 240 minutes for unirradiated and 300 minutes for irradiated BaDS. This corresponds to 60 minute lag time and suggests that D-Met assisted in damage repair.

The use of 1 µM stain in lieu of 3 µM stain explains the difference in magnitude between Figure 14 and Figure 16. Higher fluorescent stain concentration guarantees enough stain to bind to all available DNA, which was discussed in *Spectrofluorometry*.. Comparing the RFU values from Figure 14 and Figure 15, it is suggested to use 3 µM stain since the magnitude of RFUs was comparable to 5 µM stain; this conserves resources while maintaining data integrity.

Unlike BaC fluorescence, there is little to no difference in outgrowth time between irradiated and unirradiated experiments in BaDS spores; which occurs at 240

minutes. This data indicates that D-methionine appears to decrease the time required for DNA to repair; it is assumed the D-Met assisted in damage repair within the spore before outgrowth began. During germination in Stage II, just before outgrowth, ABC permease transporters move methionine closer to the DNA; it is not known whether the Met is transported into the spore core. The methionine repair mechanism is not related to the prominent damage expected from UV; thymine dimers. UV can produce reactive oxygen species, but at a percentage too small to expect a sizable difference between methionine and regular spore damage repair. The reason for D-methionine repair after UV irradiation is unknown, and the true nature of methionine's effects on *anthracis* DNA repair would have to be further explored.

The larger magnitude of RFUs for irradiated BaDS beginning at 400 minutes is not expected. Greater RFUs signify more DNA exposure to the stain, which correlates to more cells. A reason for the irradiated sample containing more cells could be explained by Gould [28], who showed that germination occurred more rapidly in damaged spores than in undamaged spores. The cause of this manifestation in BaDS but not in BaC nor BaLS is unknown. Reduced cell counts could be attributed to aggregation of the spores. The initial concentration of spores should be approximately the same for all samples; each experiment was prepared the same way and from the same spore stock. Irradiation of the spore causes degradation of the spore coat. The spore will leak spore constituents such as the coat proteins and DPA, and the surface chemistry will be very different from the unirradiated sample [15]. Coat degradation could decrease probability of spore aggregation and therefore lead to shorter time before the exponential phase. When the

spores are clumped, the ability for the inner cells to receive nutrients and activate is diminished and would delay outgrowth.

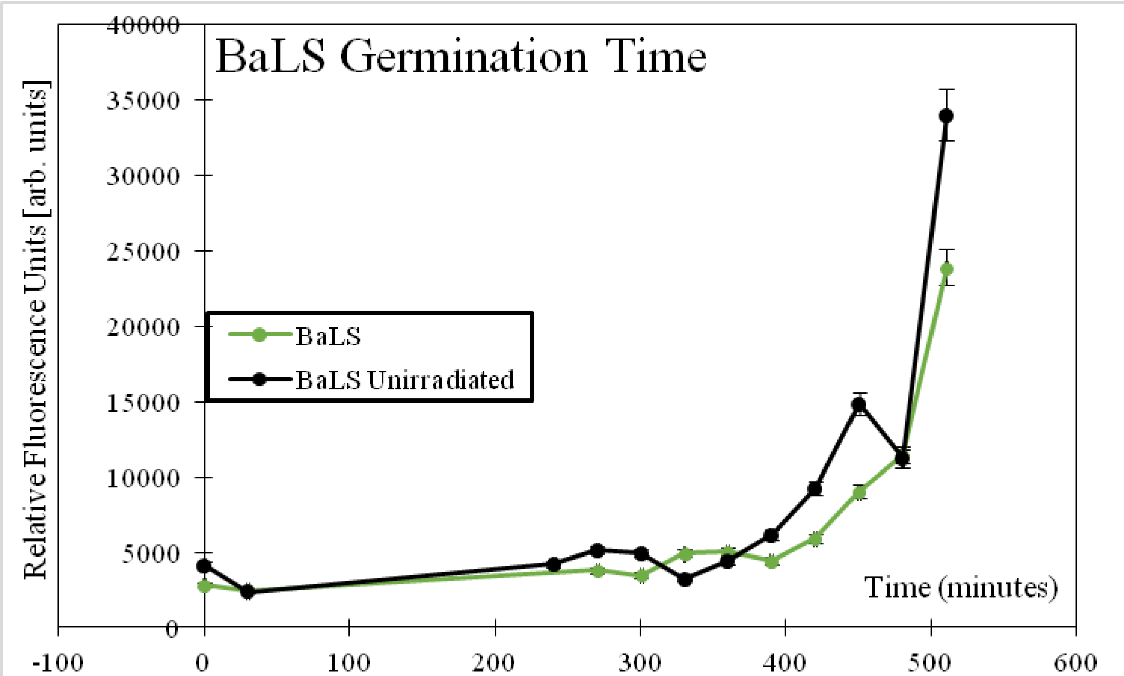

Figure 17. Fluorescence data from UV irradiated and unirradiated *Bacillus anthracis* spores supplemented with L-methionine (BaLS). Three 1 mL samples were removed at 30 minute time intervals as the spores incubated in 1X minimal media. The triplicate samples were combined and 1.5 mL was stained with 1 µM SYTO 16 green fluorescent nucleic stain. Each datum was analyzed by a Horiba FluoroLog spectrofluorometer, and relative fluorescence units were recorded. To conserve fluorescent stain, the time samples in the linear portion, between 30 and 240 minutes, were not analyzed. Spore outgrowth occurs at 330 minutes for unirradiated and 390 minutes for irradiated BaDS. This corresponds to a 60 minute lag time.

Figure 17 depicts the fluorescence data collected for irradiated and unirradiated BaLS outgrowth. These data were unique because of the delayed outgrowth time. Whereas BaC and BaDS had outgrowth starting at 240 minutes, unirradiated BaLS does not begin outgrowth until 330 minutes; a 90 minute delay. The lag time for BaLS is 60 minutes, and similar to BaC, the magnitude of unirradiated fluorescence is greater than for irradiated spores. The magnitude of RFUs is consistent with BaDS until vegetative

outgrowth. The delay in the beginning of outgrowth could be attributed to spore clumping; the proximity of spores decreases the availability of nutrients, which increases the time to activation and therefore germination. The preferential clumping from L-methionine, as described in *CD Spectrometry*, is seen again, thus adding to the assumption of L-Met aggregation.

Concentrations of 5 μM, 3 μM, and 1 μM were compared to find optimal staining. 5 μM produced saturation in the fluorolog with excitation and emission slits of 1 nm (data not shown), while the RFU values for 1 μM solution were only ten times greater than background fluorescence. The 3 μM samples produced optimal fluorescence at 0.5 nm slit wavelength for excitation and emission. As stated previously, the RFU values for 3 μM and 5 μM were of the same magnitude, thus proving that 3 μM is the preferred concentration. As mentioned, a 1 μM concentration was chosen to conserve resources for the large fluorometric matrix, at the cost of RFU resolution.

Comparison to Preceding UV Research

The survival curves produced in this research were compared against those produced by Marcum [12]. Figure 18 shows a comparison of the two data sets against the standardized corrected fluence values. The graph plots the common logarithm of total unirradiated spore count, N_o, divided by the number of counts of each sample, against the corrected fluence. Correcting the fluence accounts for any variation in the system, e.g. LED output power variation, number of LEDs, reactor design, etc.

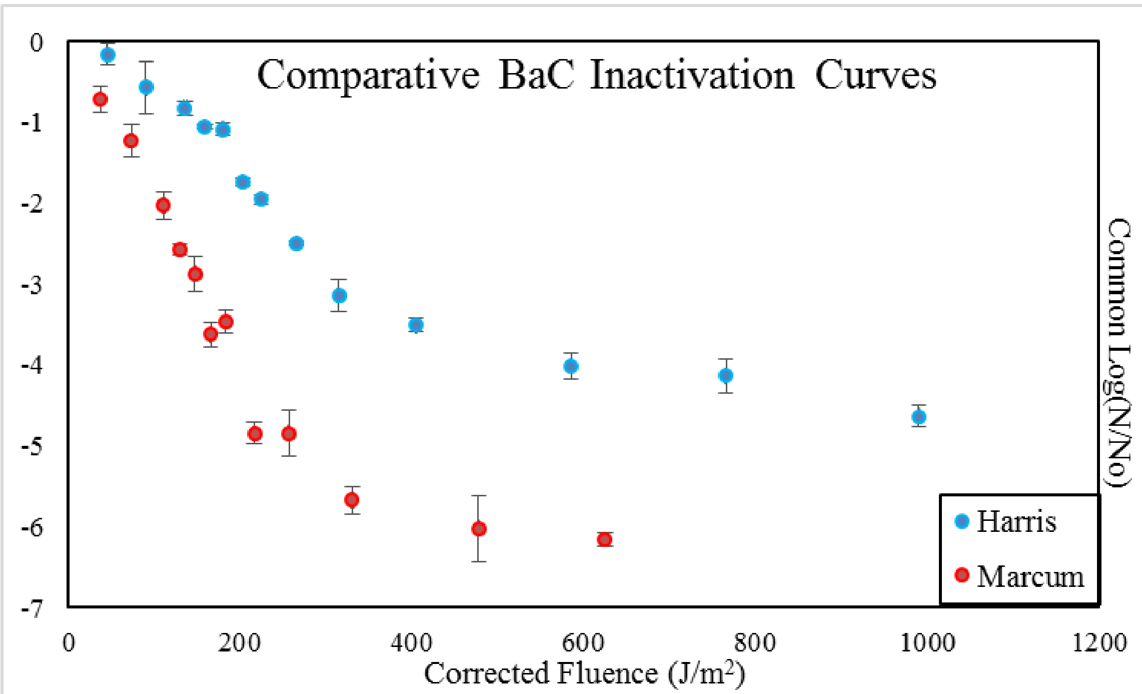

Figure 18. Comparison between inactivation curves of the Turbo RFP *anthracis* spores for the previous research and this research. The log inactivation is plotted against the corrected fluence of each system. The preceding researcher reached 6-log inactivation on a similar scale of fluence as this research achieved 4-log inactivation [12].

The correlation between the corrected fluence and the log inactivation was calculated for each of the data sets. The correlation of the previous researcher was -0.887, while the current research has a correlation of -0.915. The correlation suggests

that the spores are inactivated in a linear fashion; as dose increases, the common logarithm of CFUs is expected to decrease at the same rate, or a correlation of -1. The mean and variance of the log samples differ by 38.6% and 34%, respectively. The difference in mean and variance suggests that the distributions of the two data sets are not the same. With the fluence corrected, the distribution corresponds to the response of *anthracis* spores to UV irradiation. This response depends on the fashion in which the spores were grown and the geometry within the system, i.e. spore clumping, reactor design, fluence rate. According to the comparison, the two sets of spores respond differently.

The tailing that occurs starting at 4-$\log_{10}$ is representative of clumping of the spores [59]. Since the tailing occurs at lower log inactivation than data from Marcum, it suggests greater clumping of the spores prepared in this research. Though the procedure was completed in the exact same fashion as the procedure outlined by the previous researcher, variation is often a downfall of microbiology. The suspected source of variation between the two sets was increased clumping in this research and decrease of 13% in LED power over total operation time.

Inactivation Curves of Gamma Irradiation

The samples obtained following gamma irradiations described in *Inactivation Curves* were plated and the subsequent CFUs were counted and recorded. The primary focus of this subsection is to understand the mechanistic differences portrayed by the inactivation curves attributed to the four spore variants: BaC, BaDE, BaLE and BaDP1. The inactivation curves for each type of spore variant were averaged

over the four repetitions of the experiment. The inactivation curve for BaLE is not included due to clumping of the spores. The CFU data from the dilution series were extremely inconsistent across all experiments. The error was too great and the data could not be interpreted. The error bars for the included gamma irradiation graphs represent one standard deviation above and below the data point.

The inactivation of the control spores, BaC, acts as the basis of all comparisons. The logarithmic inactivation curve seen in Figure 19 represents BaC viability over the range of gamma doses previously discussed. The dose range originally chosen for gamma inactivation was not high enough for the inactivation of BaC. The maximum dose was 4 kGy, which was assumed to be a high estimate for 1-$\log_{10}$ inactivation according to literature for gamma irradiation of dose rates between 14 and 51 Gy/min [4] [28] [72]. The highest achieved inactivation was approximately 0.8-$\log_{10}$, thus the doses were changed to the final range of 0 to 8000 Gy.

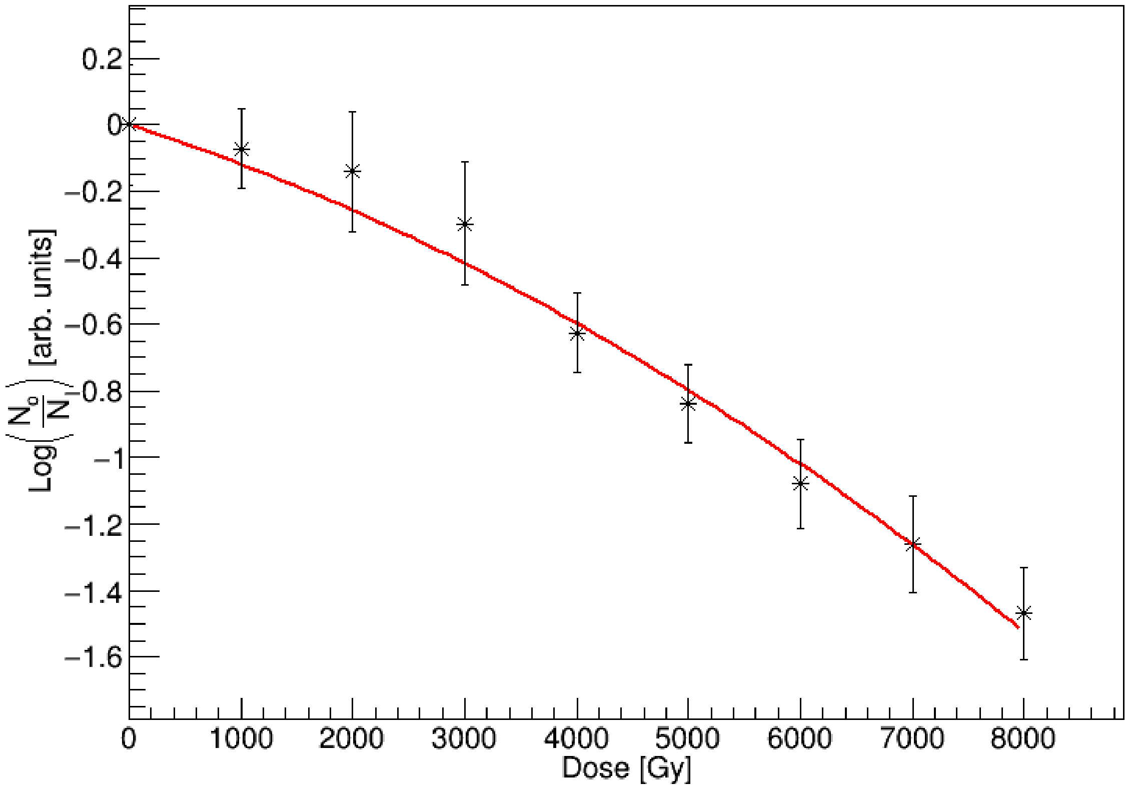

Figure 19. Gamma logarithmic inactivation curve of *Bacillus anthracis* control spores (BaC). The graph represents the response of 1.4×10^7 spores to gamma irradiation from a cesium-137 source. CFUs of triplicate plating from four repetitions of the experiment were averaged for each dose. The foremost interest of the graph is the dose corresponding to a 1-$\log_{10}$ inactivation: 5917 gray.

The curve for BaC inactivation has a shoulder for doses less than 4000 gray and is best described by a quadratic fit. Doses above 4000 gray, which includes the area of interest, the 1-$\log_{10}$ inactivation, follow a mostly linear regression. The quadratic regression for this curve, Figure 20 and Figure 21 is predicted by Equation 11, where *D* is the dose in gray.

$$\log N_o / N = \alpha D + \beta D^2 \tag{11}$$

Using this equation, the predicted dose corresponding to 1-$\log_{10}$ inactivation is 5917 Gy. The average dose for 1-$\log_{10}$ inactivation by a source with dose rate between 14 and

51Gy/min is approximately 2500 Gy. Since the dose required to inactivate the BaC spores is twice as large, it is clear that dose rate plays a major role in radiation damage [42].

The quadratic regression, described by Equation 11, has values of $-1.077\text{x}10^{-4}$ and $-1.04\text{x}10^{-8}$ for α and β, respectively, as seen in Table 5. The theory of the statistics that described the fit is the same as found in *Inactivation Curves*.

Table 5. Statistical parameters for data compiled from four repetitions of the gamma inactivation experiment for control *anthracis* spores (BaC). The terms α and β describe the quadratic regression of the data, and the following three terms represent the goodness of fit of the regression to the data.

BaC	
α	-0.00010773
β	-1.04E-08
X^2	1.54825
Reduced X^2	0.221178
R^2	0.983589

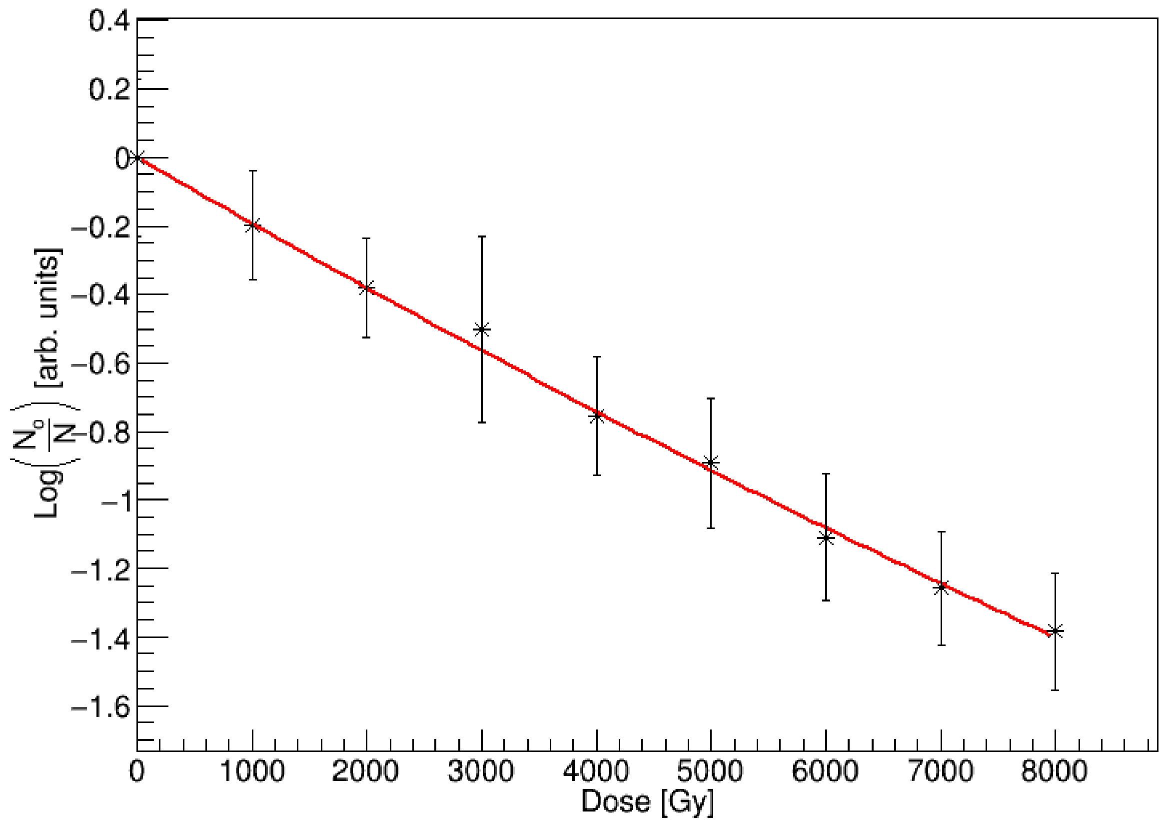

Figure 20. Gamma logarithmic inactivation curve of *Bacillus anthracis* spores in excess D-methionine (BaDE). The graph represents the response of 4.0×10^7 D-Met spores to gamma irradiation from a cesium-137 source. CFUs of triplicate plating from four repetitions of the experiment were averaged for each dose. The foremost interest of the graph is the dose corresponding to a 1-$\log_{10}$ inactivation: 5510 gray.

The curve for BaDE follows a quadratic regression, and is described by Equation 11. The values of α and β are -1.96×10^{-4} and 2.54×10^{-9}, as seen in Table 6. Unlike BaC and BaDP1, the quadratic term is positive, and can be modeled just as well by linear regression. Additionally, the quadratic regression best fits the BaDE experiments for gamma irradiation. The dose corresponding to a 1-$\log_{10}$ inactivation is 5510 Gy.

Table 6. Statistical parameters for data compiled from four repetitions of the gamma inactivation experiment for *anthracis* spores in excess of D-methionine (BaDE). The terms α and β describe the linear and quadratic coefficients for the data regression, respectively. The following three terms represent the goodness of fit of the regression to the data. The statistical descriptors suggest that the model has the best fit for gamma inactivation of BaDE spores.

BaDE	
α	-0.00019551
β	2.54E-09
X^2	0.109577
Reduced X^2	0.0156538
R^2	0.996952

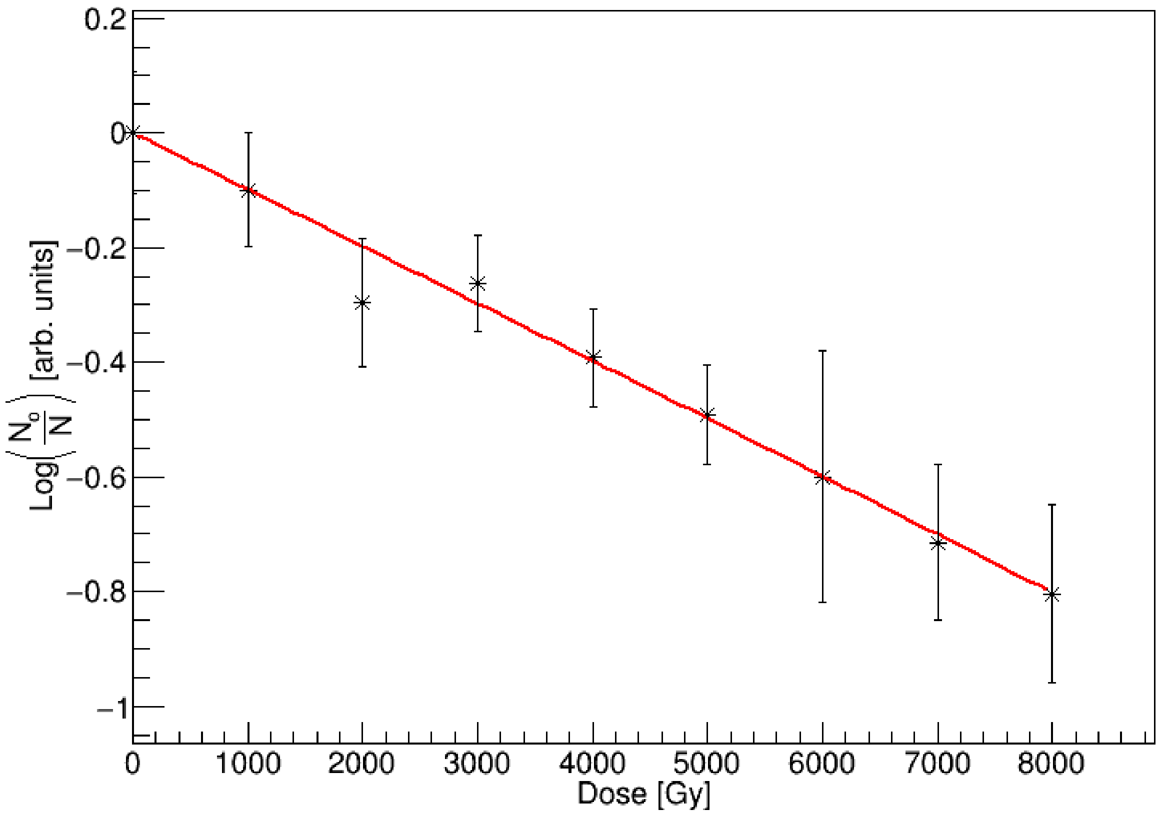

Figure 21. Gamma logarithmic inactivation curve of *Bacillus anthracis* spores supplemented with the decapeptide DP1 (BaDP1). The graph represents the response of 1.0×10^{7} DP1 spores to gamma irradiation from a cesium-137 source. CFUs of triplicate plating from four repetitions of the experiment were averaged for each dose. The foremost interest of the graph is the inability of the curve to reach a dose corresponding to a 1-$\log_{10}$ inactivation. The maximum experimental dose was not high enough to obtain a 1-$\log_{10}$ inactivation, calculated by Equation 11 to be 9940 Gy.

The curve for BaDP1 also follows the quadratic regression expressed in Equation 11. The values of α and β are -9.86×10^{-5} and -2.02×10^{-10}, as seen in Table 7. Using these values in the equation, the dose corresponding to a 1-$\log_{10}$ inactivation is 9940 Gy. This predicted value is beyond the range of irradiation completed for this experiment, as is shown by Figure 21.

Table 7. Statistical parameters for data compiled from four repetitions of the gamma inactivation experiment for *anthracis* spores in excess of the decapeptide DP1 (BaDP1). The terms α and β describe the quadratic regression of the data, and the following three terms represent the goodness of fit of the regression to the data.

BaDP1	
α	-9.86E-05
β	-2.02E-10
X^2	0.955935
Reduced X^2	0.136562
R^2	0.98146

BaDP1 and BaDE are similar in that the survival curves do not have a shoulder at low doses. The shoulder indicates an area of low dose with less cell inactivation per unit dose than at higher doses. This inactivation is related to the accumulation of damage events and/or the efficiency of enzymatic repair mechanisms. For lower inactivation: the damage events are minimal and only add up to small amounts of total damage; these few damage events can be individually repaired and the various repair mechanisms are not overwhelmed. The lack of shoulder for BaDP1 and BaDE suggests that the efficiency of repair does not diminish over time, but stays constant. The radiosensitivity of BaC changes over time, which explains the necessity of a quadratic regression.

The dose required to achieve 1-$\log_{10}$ inactivation in BaDP1 is approximately 68% larger than for BaC spores. From this fact, it is apparent that DP1 is either protecting the spore from radiation damage or aiding in damage repair, likely as an oxidative scavenger. Since methionine, which is a component of the decapeptide, has been shown to repair AP sites by scavenging reactive oxygen species and producing methionine sulfoxide [48], it is expected that the latter mechanism dominates. The efficiency of the methionine in ROS scavenging in BaDP1 over BaDE is likely attributed to the conformation of DP1.

The possible structure of DP1, viewed in Figure 7, could place methionine in an advantageous position to react with ROS that would typically react with spore DNA, in addition to histidine which reacts similarly. Additionally, the regulation of sole methionine by biological systems could decrease the effective concentration within the spore, while the methionine residual in DP1 is less likely affected by feedback regulation, as discussed in *Biological Processing*.

V. Conclusions and Recommendations

Chapter Overview

This chapter contains an overview of the previous chapters and the research as a whole. The research objectives are evaluated and reviewed given the collected data. This chapter also contains a summary of the research and future research recommendations.

Conclusions of Research

Samples containing approximately 10^7 spores of *Bacillus anthracis* (Ba) Sterne in water were irradiated with 267nm UVC light using small LEDs and, for comparison, by gammas produced from a Cs-137 source. Ba spores were supplemented with DL-methionine and a decapeptide, DP1, in different settings. L-methionine and D-methionine were introduced to Ba during sporulation and retention of the amino acid by the spore was verified using circular dichroism spectrometry.

Regular Ba spores were placed in a 3 inch diameter, stainless steel UV reactor, containing 7 LEDs. The $1x10^7$ spores in 100 mL sterile deionized water were irradiated for 80 seconds. A time of 70 seconds achieved a fluence of 152 J/m^2, which equates to a 1-$\log_{10}$ inactivation; 80 seconds was used due to an error in the original fit calculation. Following irradiation, minimal media was added and the spores were incubated for 10 hours at 37 °C. 3 samples of 0.5 mL were removed every thirty minutes from the reactor and from a parallel batch of unirradiated spores. This experiment was repeated with 1 mM L-Met and 1 mM D-Met which was added before irradiation and remained in solution through germination. Spore viability was quantified as time to outgrowth of the

spore using SYTO 16 photoluminescent dye. Fluorescence counts were compared between the parallel experiments, demonstrating a delay in outgrowth time between irradiated and unirradiated samples. The time to outgrowth for Ba spores was 240 and 330 minutes for unirradiated and irradiated spores, respectively. For D-Met spores, time to outgrowth was 240 and 300 minutes, for unirradiated and irradiated, respectively; and for L-Met 330 and 390 minutes for unirradiated and irradiated, respectively. L-Met spores aggregated which led to delayed time of outgrowth.

For gamma irradiation experiments, 36 samples of 0.5 mL solution of 10^7 spores were irradiated by a cesium-137 source with a dose rate of 6.33 Gy/min. The 36 samples were separated into 4 spore types: regular Ba spores, Ba spores sporulated in excess of D-Met (BaDE), Ba sporulated in excess of L-Met (BaLE), and Ba spores in solution with 1 mM DP1 (BaDP1). Each spore type was irradiated at doses from 0 to 8000 Gy at 1000 Gy increments. Colony forming units were collected after gamma irradiation of the 36 samples. The gamma doses corresponding to 1-$\log_{10}$ inactivation for the four types of Ba spores were: 5917 gray (Gy) for control spores; 5510 for D-methionine; 9940 Gy for DP1 spores; inconclusive for L-methionine. These values were calculated from a quadratic regression described by Equation 11. DP1 doped spores showed a significant resistance to damage, while D-Met spores showed little change in cell viability. L-Met spores clumped readily and produced unsatisfactory results. The average dose for 1-$\log_{10}$ inactivation for the control is approximately twice the value reported from literature: this research used a dose rate of 6.33 Gy/min while the literature had dose rates of 14 to 51 Gy/min. This difference in inactivation suggests the importance of dose rate in radiation effects.

Future Recommendations

This research is at the foundation of research applicable to developing radiation sensors, therapeutics to protect against radiation exposure and develop hardened materials to withstand radiation exposure. This research also presents a basis for medicinal applications such as tissue transplantation, and treating infection, ischemia and stroke. The suggestions below for prospective research continue the route towards these beneficial applications.

The procedures outlined by Welkos [26] for germination would be more conducive to this research. The small scale of the germination assays would limit cost in acquisition of DP1 and fluorescent stain. A more thorough analysis of DP1-methionine comparison would be facilitated. Additionally, the commonalities of methionine and cysteine with similar response to oxidative damage due to their sulfur containing structure, solicits a comparison of the two as radioprotectants.

The “triangle” seen in Figure 14 and Figure 17 is a baffling response of the spores that has appeared in the experiments averaged in this research, as well as research conducted by Marcum; the occurrence cannot be an anomaly. To better view this event, it would be advised to increase the data resolution around the proper time; decreasing measurement increments from 30 minutes to 10 minutes. Viewing the physical structure of the germinating cells around that time period by AFM would be beneficial.

Appendix A: Experimental Protocols

Leighton-Doi Media Recipe

The following recipe prepares 1 L of 10X sporulation media. Add the following ingredients and fill to 1 L with dH_2O. Filter sterilization is recommended. Store at 4 ^oC.

When ready to use, aseptically combine 9 parts 2X nutrient broth with 1 part 10X sporulation media.

10X Sporulation Media:

5 grams $MgSO_4 \bullet 7H_2O$
20 g KCl
10 g Glucose
2.4 g $Ca(NO_3)_2 \bullet 4H_2O$
0.2 g $MnCl_2 \bullet 7H_2O$
1 mL 0.01 M $FeSO_4 \bullet 7H_2O$ (0.28 g $FeSO_4 \bullet 7H_2O$ per 100mL H_2O)

AGFK Minimal Media Recipe

1. In 1 liter water, add 2X LB MOPS.
2. Add AGFK:
    a. 10 mM dextrose (glucose)
    b. 1 mM fructose
    c. 10 mM L-alanine
    d. 1 mM KCl (potassium chloride)
3. Double the above recipe to make double strength.
4. Heat with frequent agitation to completely dissolve solutes. Sterilize.
5. Check pH, buffer until 7.3.

Serial Dilution Procedure

Performing serial dilutions consistently and accurately is crucial for success in biological research. The following procedure was used for this experimentation.

1. Prepare 10 micro centrifuge tubes with 900 µL of water each. Label A-F, where A is 10^{-1} and G is 10^{-8}.
2. Take 100 µL of sample and place into the first tube (labeled A). This tube will be $1/10^{th}$ the concentration of your starting sample. Mix well.
3. Pipette 100 µL of that tube into the next tube ($B=10^{-2}$). Do this until all tubes have been diluted. Now, the dilution series decreases in spore concentration by $1/10^{th}$ each sequential tube.
4. Plate 100 µL of each tube in triplicate. The plates will be $1/10^{th}$ the concentration of the tube, and $1/100^{th}$ the concentration of the starting stock solution.

Gamma Irradiation Protocol

Contents:
36x 1.5mL Eppendorf tubes, 32 of which will be irradiated. Each tube closed and sealed with Parafilm.
7 tubes of each type [A-D]:

A. 10^7 spores *Bacillus anthracis* Sterne spores (BaC)
B. 10^7 spores Ba in excess of L-methionine (BaLE)
C. 10^7 spores Ba in excess of D-methionine (BaDE)
D. 10^7 spores Ba supplemented with 1mM DP1 (BaDP1)

Doses:
One of each of the four tube types [A-D] removed at doses: 1000, 2000, 3000, 4000, 5000, 6000, 7000, 8000 Gy
When I tape the tubes in pairs, it will be done according to dose. The tubes will be labeled with the respective dose at which to be pulled out. Therefore, the tube pairs will be taped by dose:

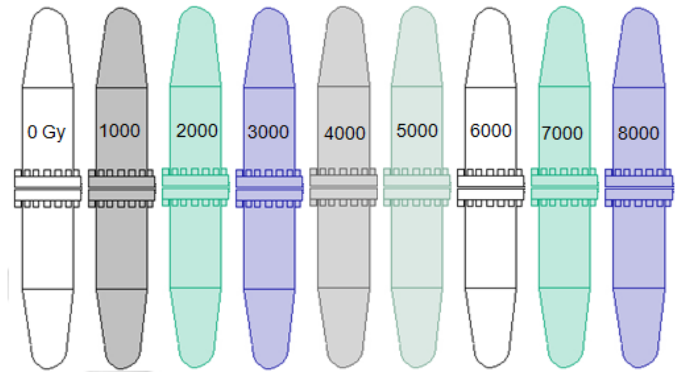

Figure A- 1. Eppendorf tube configuration for gamma irradiation. Two tubes were taped together and labeled with dose and contents.

Four tubes, one of each type [A-D], will be left out as a control and receive no irradiation.
Transport:
The 36 tubes will be held by an Eppendorf tube rack. Each tube will be sealed and labeled with a shorthand for its contents. The tubes will taped into position on the tube rack. The rack will then be wrapped with bubble wrap and labeled with a list of contents inside (with glossary of the shorthand). The bubble wrapped rack will be placed into a cardboard box with a label stating that a nonvirulent bacteria is contained within. With the box will be a letter from the company that sells the anthrax vaccine which states the safety of the bacteria. Bleach, ethanol, paper towels, biohazard garbage bags and nitrile gloves will accompany the box throughout the roundtrip.

Gamma Protocol Revision

The dose range for the initial gamma irradiation was: 0, 500, 1000, 1600, 2200, 2800, 3400, and 4000 Gy. These values did not present a 1-$\log_{10}$ inactivation and were changed for subsequent gamma irradiations. The protocol above is the final protocol used for all reported data.

Fluorescence Experiment Protocol

1. Aliquot 1.5 mL sample to Eppendorf® UVette® plastic cuvette
2. Repeat for each 30 minute time increment
3. Ensure exposure to laboratory light is minimzed
4. Add 1.5 µL SYTO 16 (for a concentration of 1 µM)
5. Incubate in dark for 30 minutes
6. Transfer to spectrofluorometer in foil covered cuvette rack

7. Sample in triplicate focusing on: 488 nm excitation; 518 nm emission
8. Dispose of spore/dye solution properly
9. Bleach cuvettes and rinse thoroughly with deionized water

Actinometry Protocol

Protocol by Rahn et al. and used for all actinometry experiments [60].

1. In volumetric flask, aseptically combine 60 mL sterile deionized water with:
    a. 0.6 M KI (9.96 g)
    b. 0.1 M KIO_3 (2.14 g)
    c. 0.01 M $Na_2B_4O_7•10H_2O$ (0.38 g)
2. Fill to 100 mL mark with deionized water and mix well
3. Only fresh solution should be used for actinometry
4. Pour solution into reactor; shaker turned on to 150 rpm
5. Turn on reactor LEDs and start timer
6. Remove initial 3 mL sample, and tightly close lid
7. Dispense sample into plastic cuvette and analyze by UV-Vis spectrophotometer at a range which includes LED wavelength and 352 nm, e.g. 200-700 nm
8. Pour contents back into reactor and close lid
9. Repeat steps 6-8 every 30 seconds for a total of ten minutes
10. For blank measurement, repeat steps 1-9, excluding step 5.

Sporulation Doping Protocol

1. From a stock culture of 10^{10} RFP spores, remove 10 μL and transfer to 250mL culture flask.
2. Aseptically add 25 mL 2X Difco Nutrient Broth to flask. [Nutrient broth solution is autoclave sterilized at the end of each day].
3. Culture flask is put in 37 °C incubator for 6-12 hours.
4. 5 mL of culture is removed from 250 mL culture flask and put into 500 mL culture flask with 50 mL Nutrient Broth. This step is repeated until original culture is all used.
5. Culture flasks are put in incubator or 6-12 hours.
6. In a 2000 mL culture flask, combine:
    a. 20 mL spore culture
    b. 20 mL sporulation supplement
    c. 180 mL 2X Nutrient Broth
    d. 1.8 mM L-methionine or D-methionine
7. Incubate at 37 °C for minimum of 2 days.
8. Check for sporulation under microscope.

Appendix B: Raw Data

Actinometry

Table A- 1. Values for the fluence calculated by Equation 8, using the power from the integrating sphere. The corrected fluence accounts for the efficiency of the system determined by the chemical actinometry experiments. The corrected fluence is the calculated fluence with a factor of efficiency and UV transmittance. The efficiency compares theoretical and experimental data and the transmittance relates the chemical solution of the actinometry experiment to the spore solution from spore irradiation experiments.

Calculated Fluence (J/m^2)	Corrected Fluence (J/m^2)
54.20092	45.98456
106.3172	90.20048
160.5181	136.185
187.6186	159.1773
212.6344	180.401
239.7349	203.3932
264.7507	224.6169
312.6976	265.2955
371.0679	314.8174
477.3851	405.0178
690.0194	585.4188
902.6538	765.8198
1167.404	990.4367

LED Characterization

The following measurements were taken at AFIT using an integrating sphere. These measurements were used for the duration of the project. Total power measurements for each LED were taken in duplicate and then averaged. The peak wavelength chosen for this research was an average of all LEDs, 267nm.

Table A- 2. LED position on reactor as compared to the designator given by SETi. The position corresponds to the LED column in Tables 1 and 2, and is written beneath the aluminum plate on the reactor.

Position	Designator
1	Y5
2	Y1
3	X9
4	I6
5	Y2
6	Y3
7	X10

UV Survival Curves

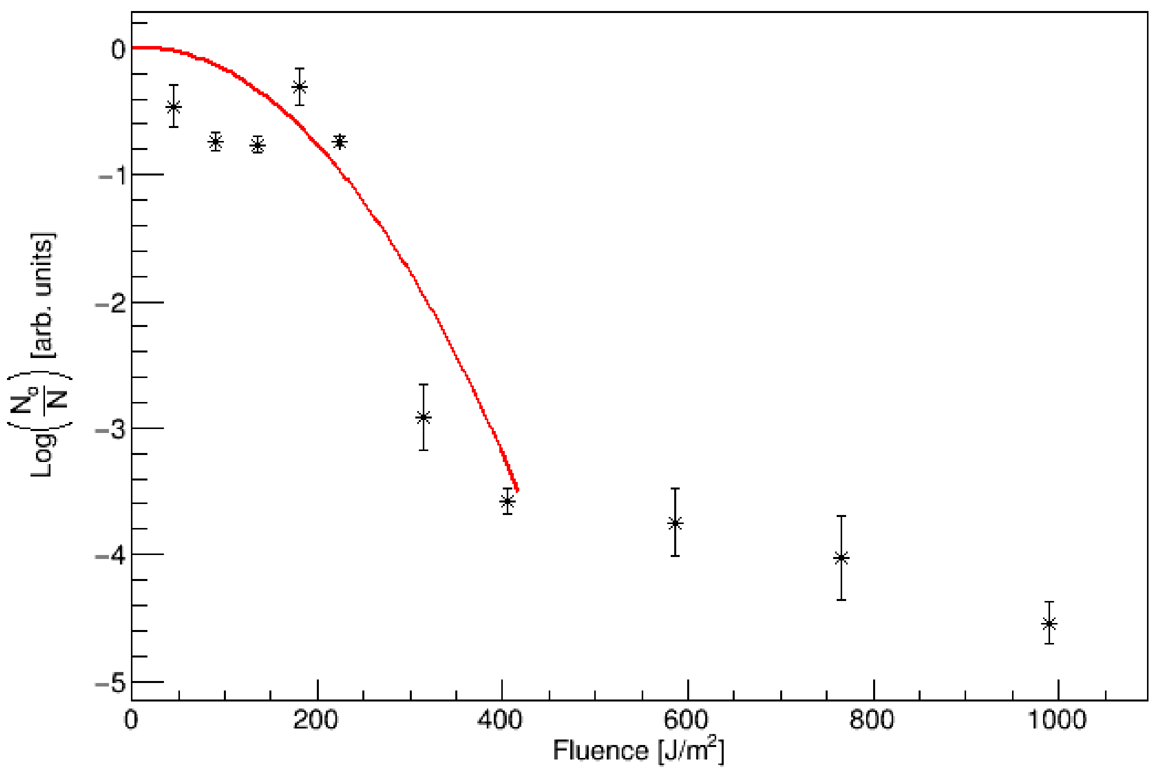

Figure A- 2. Survival curve of the first repetition of the initial UV experiments. The quadratic fit is predicted by the statistical parameters in Table A- 2. The scattered at low fluence values bring about the poor fit of the regression.

Table A- 3. Statistical parameters for the first repetition of the UV inactivation experiment. The terms α and β describe the quadratic regression of the data, and the following three terms represent the goodness of fit of the regression. This experiment had the worst fit to the regression.

Survival Curve #1	
α	0.000417848
β	-0.000021056
X^2	186.293
Reduced X^2	37.2585
R^2	0.817144

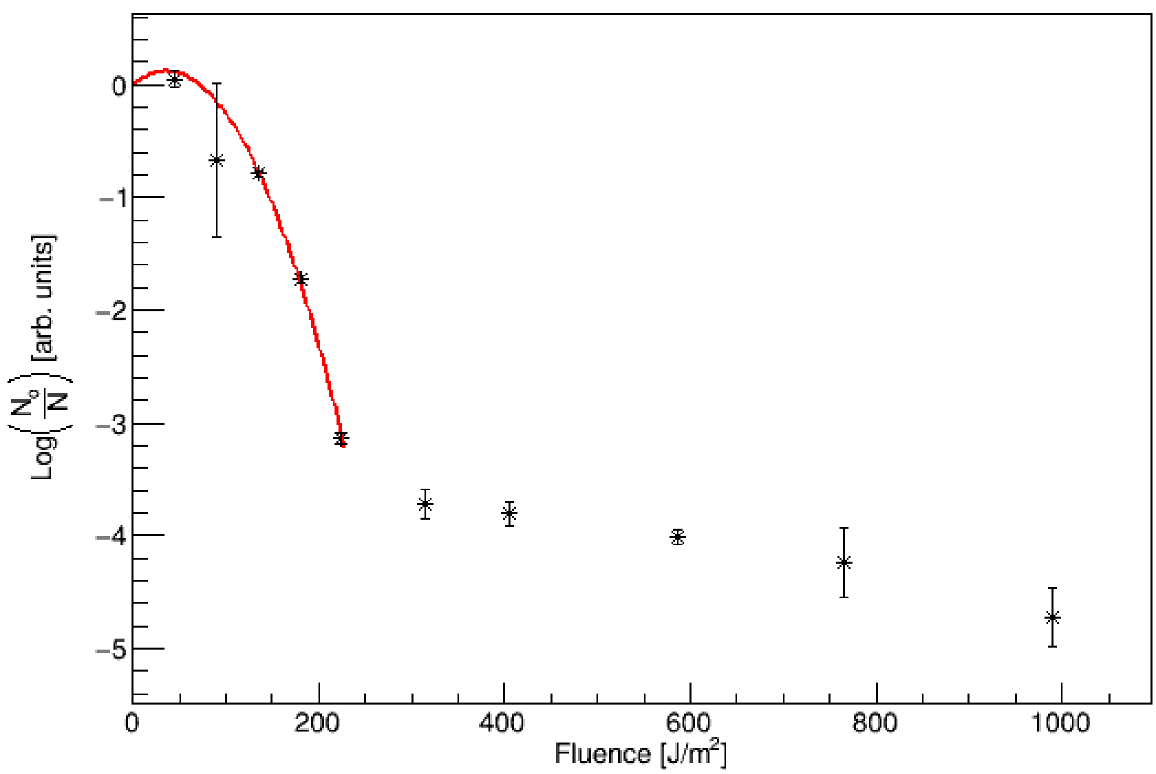

Figure A- 3. Survival curve of the second repetition of the initial UV experiments. The quadratic fit is predicted by the statistical parameters in Table A- 3.

Table A- 4. Statistical parameters for the second repetition of the UV inactivation experiment. The terms α and β describe the quadratic regression of the data, and the following three terms represent the goodness of fit of the regression.

Survival Curve #2	
α	0.00654161
β	-9.03E-05
X^2	3.71511
Reduced X^2	1.23837
R^2	0.953413

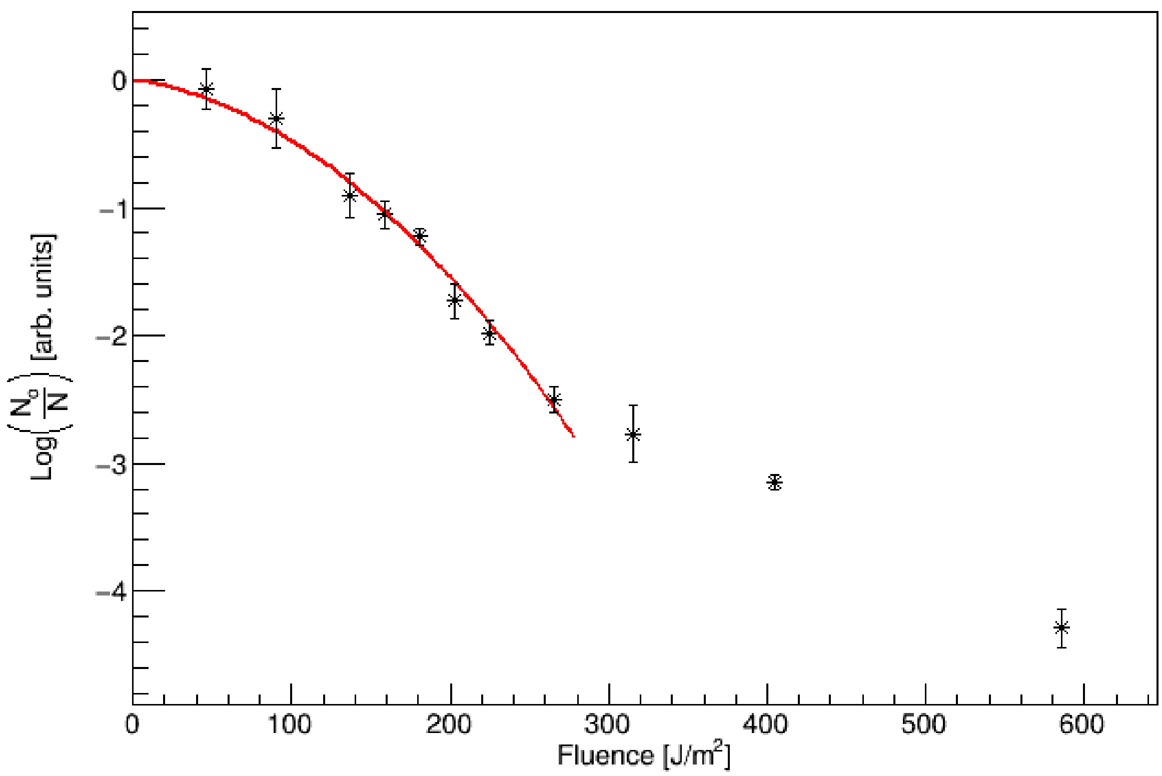

Figure A- 4. Survival curve of the third repetition of the initial UV experiments. The quadratic fit is predicted by the statistical parameters in Table A- 4. Tailing occurs at lower log inactivation than the other experiments, but the regression best fits this data.

Table A- 5. Statistical parameters for the third and final repetition of the UV inactivation experiment. The terms α and β describe the quadratic regression of the data, and the following three terms represent the goodness of fit of the regression. This experiment had the best fit to the regression.

Survival Curve #3	
α	-0.00178376
β	-2.97E-05
X^2	4.18909
Reduced X^2	0.698182
R^2	0.986755

Appendix C: Vendor Provided Fact Sheets

Plasmid Fact Sheet

The following information can be obtained on ATCC's website. This is a snapshot of the information provided by ATCC for the plasmid pRB373 used in this project [73].

ATCC

Product Sheet

pRB373 (ATCC® 77373™)

Please read this FIRST

Biosafety Level
1

Intended Use

This product is intended for research use only. It is not intended for any animal or human therapeutic or diagnostic use.

Citation of Strain

If use of this culture results in a scientific publication, it should be cited in that manuscript in the following manner: pRB373 (ATCC® 77373™)

Description

Designation: pRB373
Media:
ATCC® Medium 1227: LB Medium (ATCC medium 1065) with 50 mcg/ml ampicillin

Conditions

Temperature: 37.0°C

Vector Information

Size (kb): 5.8000001907348630
Vector: pRB373 (plasmid)
Construction: pUB110, pBR322
Marker(s):ampR,bleR,neoR
Construct size (kb): 5.800000190734863
Features: marker(s): ampR, neoR, bleR
replicon: pUB110, pMB1
terminator: rrnB, to phage lambd

References

References and other information relating to this product are available online at www.atcc.org.

Biosafety Level: 1

Appropriate safety procedures should always be used with this material. Laboratory safety is discussed in the current publication of the *Biosafety in Microbiological and Biomedical Laboratories* from the U.S. Department of Health and Human Services Centers for Disease Control and Prevention and National Institutes for Health.

Figure A- 5. ATCC pRB373 plasmid information. The pRB373 plasmid is best grown in LB medium with 50 µg/mL of ampicillin at 37 °C. The sheet also provides information about the size of the plasmid and its vector and construction.

SETi LED Fact Sheets

The following three sheets were provided from the company SETi [66]. They provide manufacturer specifications for the LEDs purchased including voltage, current, and peak wavelength. These specifications were not explicitly used in data analysis, as an integrating sphere was used to more accurately determine peak wavelength and power output of the LEDs.

QC Inspection Report

SYSTEM 1	Customer	AFIT WP AFB		Date	3/31/2014	PO #	033114PM
	Part #	UVTOP	260	TO39	FW	Box #	0
SN: 03102007	Tested	JM3				Item #	0

#	Voltage*, V	Current, mA	Power*, W	Peak Wave*, nm	HB, nm	PSV*, W / nm		Date / Time
I6	5.354887	19.99	8.50E-04	268.4	10.9	6.24E-05		3/31/14 13:00
I7	5.372759	19.99	8.61E-04	268.4	10.9	6.30E-05		3/31/14 13:00
3								
4								
5								
6								
7								
8								
9								
10								
11								
12								
13								
14								
15								
16								
17								
18								
19								
20								
21								
22								
23								
24								
25								
26								
27								
28								
29								
30								
MIN	5.354887	19.99	8.50E-04	268.4	10.9	6.24E-05		
MAX	5.372759	19.99	8.61E-04	268.4	10.9	6.30E-05		
AVG	5.363823	19.99	8.56E-04	268.4	10.9	6.27E-05		

TESTED BY	JM3	*Peak wavelength measurement tolerance is +/- 2 nm *Optical power output measurement tolerance is +/- 10% *Forward voltage measurement tolerance is +/- 2%
QC INSPECTOR	FJ	

Figure A- 6. SETi manufacturer specifications for purchased LEDs. The LED of concern is I6, the other LED burned out in a previous research effort.

SETi Sensor Electronic Technology, Inc.		QC Inspection Report						
SYSTEM 2	Customer	AFIT WP AFB			Date	4/24/2014	PO #	042114PB
	Part #	UVTOP	260	TO39	FW		Box #	0
SN: 06206032	Tested	CWG					Item #	0
#	Voltage*, V	Current, mA	Power*, W	Peak Wave*, nm	HB, nm	PSV*, W / nm		Date / Time
X9	5.344748	20.00	1.10E-03	268.8	10.5	8.26E-05		4/24/14 8:26
Y2	5.332419	20.00	1.11E-03	268.8	10.5	8.32E-05		4/24/14 8:26
Y3	5.337442	20.00	1.10E-03	268.8	10.5	8.22E-05		4/24/14 8:27
Y4	5.340143	20.00	1.11E-03	268.8	10.5	8.30E-05		4/24/14 8:27
Y6	5.357629	20.00	1.12E-03	268.8	10.5	8.44E-05		4/24/14 8:28
6								
7								
8								
9								
10								
11								
12								
13								
14								
15								
16								
17								
18								
19								
20								
21								
22								
23								
24								
25								
26								
27								
28								
29								
30								
MIN	5.332419	20.00	1.10E-03	268.8	10.5	8.22E-05		
MAX	5.357629	20.00	1.12E-03	268.8	10.5	8.44E-05		
AVG	5.3424762	20.00	1.11E-03	268.8	10.5	8.31E-05		
TESTED BY		CWG	*Peak wavelength measurement tolerance is +/- 2 nm *Optical power output measurement tolerance is +/- 10% *Forward voltage measurement tolerance is +/- 2%					
QC INSPECTOR		FJ						

Figure A- 7. SETi manufacturer specifications for purchased LEDs. The LEDs of concern are X9, Y2, and Y3; the other LEDs burned out in a previous research effort.

SETi SENSOR ELECTRONIC TECHNOLOGY, INC.	QC Inspection Report							
	Customer	AFIT WP AFB			*Date*	6/2/2014	*PO #*	053014PB
	Part #	UVTOP	260	TO39	FW		*Box #*	0
	Tested	CWG					*Item #*	0
#	Voltage*, V	Current, mA	Power*, W	Peak Wave*, nm	HB, nm	PSV*, W / nm		Date / Time
X10	5.349346	20.00	1.08E-03	268.8	10.5	8.10E-05		6/2/14 8:49
Y1	5.368031	20.00	1.02E-03	268.8	10.5	7.65E-05		6/2/14 8:50
Y5	5.356182	20.00	1.04E-03	268.8	10.5	7.82E-05		6/2/14 8:50
4								
5								
6								
7								
8								
9								
10								
11								
12								
13								
14								
15								
16								
17								
18								
19								
20								
21								
22								
23								
24								
25								
26								
27								
28								
29								
30								
MIN	5.349346	20.00	1.02E-03	268.8	10.5	7.65E-05		
MAX	5.368031	20.00	1.08E-03	268.8	10.5	8.10E-05		
AVG	5.357853	20.00	1.05E-03	268.8	10.5	7.85E-05		
TESTED BY			CWG	*Peak wavelength measurement tolerance is +/- 2 nm *Optical power output measurement tolerance is +/- 10% *Forward voltage measurement tolerance is +/- 2%				
QC INSPECTOR			FJ					

Figure A- 8. SETi manufacturer specifications for purchased LEDs. The three LEDs listed were all used in this research effort.

Appendix D: Regression Code

The code used for Figures 10 and 19-21 was written by Dr. Anthony Kelly and amended by Cameron Harris to fit the data of the UV and IR inactivation curves. The code is run in ROOT, a free source program developed by CERN.

```
#include <fstream> // File management
#include <string>  // Communication with the user
#include <sstream> // More communication manipulation
#include <ctime>   // Make a time stamp

#include "TGraph.h"  // Graphing from ROOT
#include "TGraphErrors.h"   // Graphing with ERRORS from ROOT
#include "TStyle.h" // Pretty plots
#include "TF1.h" // 1-D functions with ROOT
#include "TMath.h"
#include "TROOT.h"

int CameronsUVCode() {

  gROOT->SetStyle("BABAR");

  char InputFileName[100] = "C:/Users/Cameron Harris/Documents/_RESEARCH/Codes/UV/UVExp3.txt";        // THIS IS
IMPORTANT
  const int NumberOfUnknowns = 6;
  Double_t unknowns[NumberOfUnknowns] = { 1, 2, 3, 4, 5, 6 };
         const int SIZE = 11;

  ifstream InputFile(InputFileName);

  cout << string( 100, '\n');

         cout << InputFileName << endl;

  string ReadLine("");

  if (InputFile.is_open()) {
    while (!InputFile.eof()) {
      getline(InputFile,ReadLine);
      ++NumberOfLines;
    }
  }
  else {
    cout << "Hello!!  Error Code 100." << endl;
    cout << "I am sorry, um, but, there seems to be a problem." << endl;
    cout << "Please check that the input file name is correct." << endl;
    cout << "Most likely... you forgot to add the file extension .txt" << endl;
    return 100;
  }
  InputFile.close();*/

  // Make the Data Arrays

 Double_t time_vals[SIZE];
 Double_t fluence_vals[SIZE];
 Double_t control_vals[SIZE];
 Double_t experiment_vals[SIZE];
 Double_t normalized_vals[SIZE];
 Double_t xerrors_vals[SIZE];
```

```
  Double_t error_vals[SIZE];

    Double_t fractionallogs[SIZE];

    Double_t Minx = 99999;
    Double_t Maxx = -99999;
    Double_t Miny = 99999;
    Double_t Maxy = -99999;

  // Open the text file and start filling the data arrays
    //  InputFile.open(InputFileName);

    for (int i = 0; i < SIZE; ++i) {
      InputFile >> time_vals[i];        // Time Column
      InputFile >> fluence_vals[i];     // Fluence Column
      InputFile >> control_vals[i];     // Control Column
      InputFile >> experiment_vals[i];   // Experimental Column
      InputFile >> normalized_vals[i];  // Normalized AVERAGE Column
      InputFile >> error_vals[i];         // Error Values Column

                xerrors_vals[i] = 0.0;
     // cout << time_vals[i] << "\n";
                cout << i << "\t" << fluence_vals[i] << endl;

                if (normalized_vals[i] > Maxy) Maxy = normalized_vals[i]; // Pretty plots
      if (normalized_vals[i] < Miny) Miny = normalized_vals[i]; // Pretty plots
      if (fluence_vals[i] > Maxx) Maxx = fluence_vals[i];       // Pretty plots
      if (fluence_vals[i] < Minx) Minx = fluence_vals[i];       // Pretty plots
    }
  InputFile.close();

  // All that follows is to make the graph and make it pretty
  //gROOT->SetStyle("BABAR"); // See rootlogon.C if you REALLY want to go there

    TCanvas *c1 = new TCanvas("c1","",10,10,800,600);
    //c1->SetLogx();
    //c1->SetLogy();

//              TGraph *myG = new TGraph(SIZE, fluence_vals, normalized_vals); //THIS is what made the graph
  TGraphErrors *myG = new TGraphErrors(SIZE,fluence_vals,normalized_vals,xerrors_vals,error_vals); //THIS is what made
the graph//

    myG->GetYaxis()->SetTitle("Log#left(#frac{N_{o}}{N}#right) [arb. units]"); // LaTex in ROOT uses "#" sign \left(
\right)
    myG->GetXaxis()->SetTitle("Fluence [J/m^{2}]");
    myG->GetXaxis()->CenterTitle();
    myG->GetYaxis()->CenterTitle();
    myG->GetYaxis()->SetTitleOffset(1.3);
    myG->GetXaxis()->SetRangeUser(0.0,Maxx*10.0);
    //myG->GetYaxis()->SetRangeUser(normalized_vals[1]/10.0,normalized_vals*10.0);
    myG->SetMarkerSize(1.0); // Graph Point Font Size (Dots)

  myG->Draw("ap*"); // Is what actually creates the graphic

  // Here comes the fitting
    TF1 *myFit = new TF1("myFit", "([0]*x+[1]*x*x)", 0.0, 280);
//TF1 *myFit = new TF1("myFit", "([0]*x+[1]*x*x)", 0.0, Maxx);

    if (normalized_vals[0] < normalized_vals[SIZE-1]) {
        myFit->SetParameter(0,Miny);
        myFit->SetParameter(1,0.0003);
        //myFit->SetParameter(2,fluence_vals[SIZE/2]);
        //myFit->SetParameter(3,Maxy);
        myFit->SetParName(0,"Min Asymptote");
```

```
    myFit->SetParName(1,"Slope Factor");
    //myFit->SetParName(2,"Inflection Point");
    //myFit->SetParName(3,"Max Asymptote");
 }
 else {
    myFit->SetParameter(0,0.04);
    myFit->SetParameter(1,0.00);
    //myFit->SetParameter(2,3.0);
    //myFit->SetParameter(3,Miny);
    myFit->SetParName(0,"Max Asymptote");
    myFit->SetParName(1,"Slope Factor");
    //myFit->SetParName(2,"Inflection Point");
    //myFit->SetParName(3,"Min Asymptote");
 }

 cout << string( 60, '*');
 cout << "\n*\n";
 cout << "* Hello!\n* Thank you for using this fitting package\n";
 time_t now = time(0);
 char* currentime = ctime(&now);
 cout << "* This software was lasted used:\t" << currentime << "*\n";
 cout << string( 60, '*');
 cout << "\n";


 myG->Fit(myFit,"RE"); // Money line

   // Here come the blue lines

/* TF1 *ReverseEngineer = new TF1("ReverseEngineer","[2]*TMath::Power( (([0]-[3])/(x-[3]))-1.0 , 1.0/[1])",0,Maxx);
 ReverseEngineer->SetParameter(0,myFit->GetParameter(0));
 ReverseEngineer->SetParameter(1,myFit->GetParameter(1));
 //ReverseEngineer->SetParameter(2,myFit->GetParameter(2));
 //ReverseEngineer->SetParameter(3,myFit->GetParameter(3));

 double OutPutValues[NumberOfUnknowns];

 for (int i = 0; i < NumberOfUnknowns; ++i) {
    OutPutValues[i] = ReverseEngineer->Eval(unknowns[i]);
 }

 // Write out fitting results into a file called FittingResults_<YOUR INPUT FILE NAME>.txt
/*
std::stringstream OutputFileNameStream;
 string TempString = InputFileName;
 OutputFileNameStream << "FittingResults_";
 OutputFileNameStream << TempString.c_str();
 ofstream OutputFile(OutputFileNameStream.str().c_str());
          */
 cout << "Parameter 1:\t" << myFit->GetParameter(0) << "\n";
 cout << "Parameter 2:\t" << myFit->GetParameter(1) << "\n";
// cout << "Parameter 3:\t" << myFit->GetParameter(2) << "\n";
 //cout << "Parameter 4:\t" << myFit->GetParameter(3) << "\n";
          cout << "Chi-square:\t" << myFit->GetChisquare() << "\n";
          cout << "Fit looks like:\t(" << myFit->GetParameter(0) << "-" << myFit->GetParameter(3);
          cout << ")/(1+(x/" << myFit->GetParameter(2) << ")^" << myFit->GetParameter(1);
          cout << ") + " << myFit->GetParameter(3) << "\n";

    // Begin the calculation of the Coefficient of Determination (R2 = 1 - SSres/SStot)

 double MeanOfObservedData = 0.0;
 for (int i = 0; i < SIZE; ++i) {
    MeanOfObservedData += normalized_vals[i];
 }
```

```
  MeanOfObservedData /= (SIZE*1.0);

  double TotalSumOfSquares = 0.0;
  for (int i = 0; i < SIZE; ++i) {
    TotalSumOfSquares += TMath::Power(normalized_vals[i]-MeanOfObservedData,2.0);
  }

  double ResidualSumOfSquares = 0.0;
  for (int i = 0; i < SIZE; ++i) {
    ResidualSumOfSquares += TMath::Power(normalized_vals[i]-myFit->Eval(fluence_vals[i]),2.0);
  }

  double CoefficientOfDetermination = 1.0 - ResidualSumOfSquares/TotalSumOfSquares;

  //OutputFile << "R2 value:\t" << CoefficientOfDetermination << "\n";
  std::cout << "R2 value:\t" << CoefficientOfDetermination << "\n";

        /*
  // Backout the Unknowns
  OutputFile << "<*><*><*> UNKNOWNS <*><*><*>\n";
  OutputFile << "\n\n\tConcentration\tO.D.\n";
  for (int i = 0; i < NumberOfUnknowns; ++i) {
    OutputFile << "\t" << OutPutValues[i] << "\t\t" << unknowns[i] << "\n";
  }
  */
  std::cout << "\n\n";
  std::cout << "<*><*><*> UNKNOWNS <*><*><*>\n";
  cout << "\tFluences\tLog Normalized\n";

  // Plot the Unknown Unto the Graph in Blue
  TLine *myVerticalLines[NumberOfUnknowns];
  for (int i = 0; i < NumberOfUnknowns; ++i) {
    myVerticalLines[i] = new TLine(OutPutValues[i],0.0,OutPutValues[i],unknowns[i]);
    myVerticalLines[i]->SetLineWidth(4.0);
    myVerticalLines[i]->SetLineColor(kBlue);
    myVerticalLines[i]->SetLineStyle(2);
    myVerticalLines[i]->Draw("l");
  }

  TLine *myHorizontalLines[NumberOfUnknowns];
  for (int i = 0; i < NumberOfUnknowns; ++i) {
    myHorizontalLines[i] = new TLine(OutPutValues[i],unknowns[i],0.0,unknowns[i]);
    myHorizontalLines[i]->SetLineWidth(4.0);
    myHorizontalLines[i]->SetLineColor(kBlue);
    myHorizontalLines[i]->SetLineStyle(2);
    myHorizontalLines[i]->Draw("l");
  }
   // c1->Print(OutputFileNameStream.str().c_str());

  cout << "\n\n\n" << endl;

 // Updates the Logbook with the stuff
  ofstream WriteOutLogBook("Logbook.txt",std::ofstream::app);
  WriteOutLogBook << InputFileName << "\t" << NumberOfUnknowns << "\t";
  for (int i = 0; i < NumberOfUnknowns; ++i) {
    WriteOutLogBook << unknowns[i] << "\t";
  }
  WriteOutLogBook << CoefficientOfDetermination << "\t";
  WriteOutLogBook << currentime;
  WriteOutLogBook << "\n";
  WriteOutLogBook.close();

}
```

Bibliography

[1] B. S. Berlett and R. L. Levine, "Designing Antioxidant Peptides," *Redox Report,* vol. 19, no. 2, pp. 80-86, 2014.

[2] M. J. Daly, "Death by Protein Damage in Irradiated Cells," *DNA Repair,* vol. 11, no. 1, pp. 12-21, 2012.

[3] E. J. Wulfsberg, "Radiation Damage Effect Mitigation of Beta-Galactosidase from Peptides," Unpublished.

[4] E. R. Blatchley, A. Meeusen, A. I. Aronson and L. Brewster, "Inactivation of *Bacillus* Spores by Ultraviolet or Gamma Radiation," *Journal of Environmental Engineering,* vol. 131, no. 9, pp. 1245-1252, 2005.

[5] P. Setlow, "Spores of *Bacillus subtilis*: Their Resistance to and Killing by Radiation, Heat, and Chemicals," *Journal of Applied Microbiology,* vol. 101, pp. 514-525, 2005.

[6] S. B. Vuyyuri, D. A. Hamstra and D. Khanna, "Evaluation of D-Methionine as a Novel Oral Radiation Protector for Prevention of Mucositis," *Clinical Cancer Research,* vol. 14, no. 7, pp. 2161-2170, 2008.

[7] W. L. Nicholson, N. Munakata, G. Horneck, H. J. Melosh and P. Setlow, "Resistance of *Bacillus* Endospores to Extreme Terrestrial and Extraterrestrial Environments," *Microbiology and Molecular Biology Reviews,* vol. 64, no. 3, p. 548–572, 2000.

[8] P. A. Vaishampayan, E. Rabbow, G. Horneck and K. J. Venkateswaran, "Survival of *Bacillus pumilus* Spores for a Prolonged Period of Time in Real Space Conditions," *Astrobiology,* vol. 12, no. 5, pp. 487-497, 2012.

[9] E. A. Knight, "Modeling Thermal Inactivation of Bacillus Spores," M.S. Thesis, Air Force Institute of Technology, Wright Patterson AFB, 2009.

[10] T. N. Tran, "Comparison of Continuous Versus Pulsed Ultraviolet Light Emitting Diode Use in Water Disinfection on *Bacillus globigii* Spores," Unpublished.

[11] M. Spencer, "Design Considerations for a Water Treatment System Utilizing Ultra-Violet Light Emitting Diodes," M.S. Thesis, Air Force Institute of Technology, Wright Patterson AFB, 2014.

[12] C. C. Marcum, "Measurements of DNA Damage and Repair in *Bacillus anthracis* Sterne Spores by UV Radiation," M.S. Thesis, Air Force Institute of Technology, Wright Patterson AFB, 2014.

[13] J. Rivera, A. Morgenstern, F. Bruchertseifer, J. F. Kearney, C. L. Turnbough, E. Dadachova and A. Casadevall, "Microbicidal Power of Alpha Radiation in Sterilizing Germinating *Bacillus anthracis* Spores," *Antimicrobial Agents and Chemotherapy,* vol. 58, no. 3, p. 1813–1815, 2014.

[14] R. Moeller, P. Setlow, G. Horneck, T. Berger, G. Reitz, P. Rettberg, A. J. Doherty, R. Okayasu and W. L. Nicholson, "Roles of Major, Small, Acid-Soluble Spore Proteins and Spore-Specific and Universal DNA Repair Mechanisms in Resistance of *Bacillus subtilis* Spores to Ionizing Radiation from X Rays and High-Energy Charged-Particle Bombardment," *Journal of Bacteriology,* vol. 190, no. 3, pp. 1134-1140, 2008.

[15] Y. Xing, A. Li, D. L. Felker and L. W. Burggraf, "Nanoscale Structural and Mechanical Analysis of *Bacillus anthracis* Spores Inactivated with Rapid Dry Heating," *Applied and Environmental Microbiology,* vol. 80, no. 5, pp. 1739-1749, 2014.

[16] A. Benjdia, K. Heil, T. R. M. Barends, T. Carell and I. Schlichting, "Structural Insights into Recognition and Repair of UV-DNA Damage by Spore Photoproduct Lyase, a Radical SAM Enzyme," *Nucleic Acids Research,* vol. 40, no. 18, p. 9308–9318, 2012.

[17] M. T. Iannotti and R. Pisani Jr., "Inactivation of *Bacillus atrophaeus* Spores in Healthcare Waste by UV Light Coupled with H2O2," *Brazilian Journal of Chemical Engineering,* vol. 30, no. 03, pp. 507-519, 2013.

[18] P. C. Turnbull, "Introduction: Anthrax History, Disease and Ecology," *Current Topics Microbiology and Immunology,* vol. 271, pp. 1-19, 2002.

[19] N. H. Bergman, E. C. Anderson, E. E. Swenson, M. M. Niemeyer, A. D. Miyoshi and P. C. Hanna, "Transcriptional Profiling of the *Bacillus anthracis* Life Cycle In Vitro and an Implied Model for Regulation of Spore Formation," *Journal of*

Bacteriology, vol. 188, no. 17, pp. 6092-6100, 2006.

[20] M. Martchenko, S. I. Candille, H. Tang and S. N. Cohen, "Human Genetic Variation Altering Anthrax Toxin Sensitivity," *Proceedings of the National Academy of Sciences*, vol. 109, no. 8, pp. 2972-2977, 2012.

[21] S. D. Zink and D. L. Burns, "Importance of SrtA and SrtB for Growth of *Bacillus anthracis* in Macrophages," *Infection and Immunity*, vol. 73, no. 8, p. 5222–5228, 2005.

[22] P. J. Piggot and D. W. Hilbert, "Sporulation of *Bacillus subtilis*," *Current Opinion in Microbiology*, vol. 7, no. 6, pp. 579-586, 2004.

[23] T. M. Koehler, "*Bacillus anthracis* Physiology and Genetics," *Molecular Aspects of Medicine*, vol. 30, no. 6, pp. 386-396, 2009.

[24] R. Pandey, A. T. Beek, N. O. Vischer, J. P. Smelt and S. Brul, "Live Cell Imaging of Germination and Outgrowth of Individual *Bacillus subtilis* Spores; The Effect of Heat Stress Quantitatively Analyzed with SporeTracker," *PLOS One*, vol. 8, no. 3, pp. 1-10, March 2013.

[25] J. A. Hoch, "*Bacillus subtilis* and Other Gram-Positive Bacteria: Biochemistry, Physiology, and Molecular Genetics," Washington, D.C., American Society for Microbiology, 1993, pp. 113-124.

[26] S. L. Welkos, C. K. Cote, K. M. Rea and P. H. Gibbs, "A Microtiter Fluorometric Assay to Detect the Germination of *Bacillus anthracis* Spores and the Germination Inhibitory Effects of Antibodies," *Journal of Microbiological Methods*, vol. 56, p. 253– 265, 2003.

[27] P. Setlow, "Germination of Spores of *Bacillus* Species: What We Know and Do Not Know," *Journal of Bacteriology*, vol. 196, no. 7, p. 1297–1305, 2014.

[28] G. W. Gould and Z. J. Ordal, "Activation of Spores of *Bacillus cereus* by γ-Radiation," *Journal of General Microbiology*, vol. 50, pp. 77-84, 1967.

[29] X. Yi and P. Setlow, "Studies of the Commitment Step in the Germination of Spores of *Bacillus* Species," *Journal of Bacteriology,* vol. 192, no. 13, p. 3424–3433, 2010.

[30] V. I. Klichko, J. Miller, A. Wu, S. G. Popov and K. Alibek, "Anaerobic Induction of *Bacillus anthracis* Hemolytic Activity," *Biochemical and Biophysical Research Communications,* vol. 303, no. 3, pp. 855-862, 2003.

[31] R. Moeller, M. Raguse, G. Reitz, R. Okayasu, Z. Li, S. Klein, P. Setlow and W. L. Nicholson, "Resistance of *Bacillus subtilis* Spore DNA to Lethal Ionizing Radiation Damage Relies Primarily on Spore Core Components and DNA Repair, with Minor Effects of Oxygen Radical Detoxification," *Applied and Environmental Microbiology,* vol. 80, no. 1, p. 104–109, 2014.

[32] D. A. Ball, R. Taylor, S. J. Todd, C. Redmond, E. Couture-Tosi, P. Sylvestre, A. Moir and P. A. Bullough, "Structure of the Exosporium and Sublayers of Spores of the *Bacillus cereus* Family Revealed by Electron Crystallography," *Molecular Microbiology,* vol. 68, no. 4, p. 947–958, 2008.

[33] M. G. Stabin, Radiation Protection and Dosimetry: An Introduction to Health Physics, New York: Springer, 2007.

[34] J. G. Calvert and J. N. Pitts, Photochemistry, 2nd ed., John Wiley and Sons, 1967.

[35] R. P. Sinha and D.-P. Häder, "UV-Induced DNA Damage and Repair: A Review," *The Royal Society of Chemistry and Owner Societies,* vol. 1, no. 4, p. 225–236, 2002.

[36] L. Yang and L. Li, "The Enzyme-Mediated Direct Reversal of a Dithymine Photoproduct in Germinating Endospores," *International Journal of Molecular Sciences,* vol. 14, no. 7, pp. 13137-13153, June 2013.

[37] C. G. Elles, I. A. Shkrob and R. A. Crowell, "Excited State Dynamics of Liquid Water: Insight from the Dissociation Reaction Following Two-Photon Excitation," *Journal of Chemical Physics,* vol. 126, no. 16, pp. 164503:1-8, 2007.

[38] A. Chandor-Proust, O. Berteau, T. Douki, D. Gasparutto, S. Ollagnier-de-Choudens, M. Fontecave and M. Atta, "DNA Repair and Free Radicals, New Insights into the Mechanism of Spore Photoproduct Lyase Revealed by Single

Amino Acid Substitution," *Journal of Biological Chemistry,* vol. 283, no. 52, p. 36361–36368, 2008.

[39] J. B. Broderick, B. R. Duffus, K. S. Duschene and E. M. Shepard, "Radical S-Adenosylmethionine Enzymes: A Chemical Review," *American Chemical Society,* vol. 114, no. 8, p. 4229−4317, 2014.

[40] L. Yang, G. Lin, D. Liu, K. J. Dria, J. Tesler and L. Li, "Probing the Reaction Mechanism of Spore Photoproduct Lyase (SPL) via Diastereoselectivity Labeled Dinucleotide SP TpT Substrates," *Journal of The American Chemical Society,* vol. 133, no. 27, pp. 10434-10447, June 2011.

[41] C. Kisker, "Prokaryotic Nucleotide Excision Repair," *Cold Spring Harbor Perspectives in Biology,* vol. 5, no. 3, pp. 1-18, March 2013.

[42] E. L. Alpen, Radiation Biophysics, San Diego: Academic Press, 1998.

[43] L. M. Dorfman and G. E. Adams, "Reactivity of the Hydroxyl Radical in Aqueous Solutions," *National Standard Reference Data System,* vol. 1, pp. 1-59, 1973.

[44] R. Moeller, E. Stackebrandt, G. Reitz, T. Berger and P. Rettberg, "Role of DNA Repair by Nonhomologous-End Joining in *Bacillus subtilis* Spore Resistance to Extreme Dryness, Mono- and Polychromatic UV, and Ionizing Radiation," *Journal of Bacteriology,* vol. 189, no. 8, p. 3306–3311, 2007.

[45] J. Kopoldová, J. Liebster and E. Gross, "Radiation Chemical Reactions in Aqueous Solutions of Methionine and Its Peptides," *Radiation Research,* vol. 30, no. 2, pp. 261-274, 1967.

[46] A. Ohara, "On the Radiolysis of Methionine in Aqueous Solution by Gamma Irradiation," *Journal of Radiation Research,* vol. 7, no. 1, pp. 18-28, 1966.

[47] F. Shimazu, U. S. Kumta and A. L. Tappel, "Radiation Damage to Methionine and Its Derivatives," *Radiation Research,* vol. 22, no. 2, pp. 276-287, 1964.

[48] C. You, "Spx Mediates Oxidative Stress Regulation of the Methionine Sulfoxide Reductases Operon in *Bacillus subtilis,*" *BMC Microbiology,* vol. 8, no. 128, pp. 1-13, 2008.

[49] B. A. Murphy, F. J. Grundy and T. M. Henkin, "Prediction of Gene Function in Methylthioadenosine Recycling from Regulatory Signals," *Journal of Bacteriology,* vol. 184, p. 2314–2318, 2002.

[50] M.-F. Hullo, S. Auger, E. Dassa, A. Danchin and I. Martin-Verstraete, "The MetNPQ Operon of *Bacillus subtilis* Encodes an ABC Permease Transporting Methionine Sulfoxide, D- and L-Methionine," *Research in Microbiology,* vol. 155, p. 80–86, 2004.

[51] A. Krisko and M. Radman, "Biology of Extreme Radiation Resistance: The Way of *Deinococcus radiodurans,*" *Cold Spring Harbor Perspectives in Biology,* vol. 5, no. 7, pp. 1-12, 2013.

[52] D. Slade and M. Radman, "Oxidative Stress Resistance in *Deinococcus radiodurans*," *Microbiology and Molecular Biology Reviews,* vol. 75, no. 1, p. 133–191, 2011.

[53] M. J. Daly, E. K. Gaidamakova, V. Y. Matrosova, J. G. Kiang, R. Fukumoto, D.-Y. Lee, N. B. Wehr, G. A. Viteri, B. S. Berlett and R. L. Levine, "Small-Molecule Antioxidant Proteome-Shields in *Deinococcus radiodurans*," *PLoS ONE,* vol. 5, no. 9, pp. 1-15, 2010.

[54] R. O. Rahn, M. I. Stefan, J. R. Bolton, E. Goren, P.-S. Shaw and K. R. Lykke, "Quantum Yield of the Iodide-Iodate Chemical Actinometer: Dependence on Wavelength and Concentration," *Photochemistry and Photobiology,* vol. 78, no. 2, pp. 146-152, 2003.

[55] S. Goldstein and J. Rabani, "The Ferrioxalate and Iodide-Iodate Actinometers in the UV Region," *Journal of Photochemistry and Photobiology A: Chemistry,* vol. 193, no. 1, pp. 50-55, 2008.

[56] H. J. Kuhn, S. E. Braslavsky and R. Schmidt, "Chemical Actinometry," IUPAC, London, 2004.

[57] R. O. Rahn, "Potassium Iodide as a Chemical Actinometer for 254nm Radiation: Use of Iodate as an Electron Scavenger," *Photochemistry and Photobiology,* vol. 66, no. 4, pp. 450-455, 1197.

[58] J. R. Bolton, M. I. Stefan, P.-S. Shaw and K. R. Lykke, "Determination of the Quantum Yields of the Potassium Ferrioxalate and Potassium Iodide-Iodate

Actinometers and a Method for the Calibration of Radiometer Detectors," *Journal of Photochemistry and Photobiology A: Chemistry*, vol. 222, no. 1, pp. 166-169, 2011.

[59] M. A. Wurtele, T. Kolbe, M. Lipsz, A. Kulberg, M. Weyers, M. Kneissl and M. Jekel, "Application of GaN-Based Ultraviolet-C Light Emitting Diodes-UV LEDs for Water Disinfection," *Water Research*, vol. 45, no. 3, pp. 1481-1489, 2011.

[60] R. O. Rahn, J. Bolton and M. I. Stepan, "The Iodide/Iodate Actinometer in UV Disinfection: Determination of the Fluence Rate Distribution in UV Reactors," *Photochemistry and Photobiology*, vol. 82, no. 1, pp. 611-615, 2006.

[61] J. M. Slocik, A. O. Govorov and R. R. Naik, "Plasmonic Circular Dichroism of Peptide-Functionalized Gold Nanoparticles," *American Chemical Society*, vol. 11, no. 2, pp. 701-705, 2011.

[62] S. M. Kelly, T. J. Jess and N. C. Price, "How to Study Proteins by Circular Dichroism," *Biochimica et Biophysica Acta*, vol. 1751, no. 2, pp. 119-139, 2005.

[63] J. R. Lakowicz, Principles of Fluorescence Spectroscopy, New York: Springer, 2011.

[64] T. Leighton and R. Doi, "The Stability of Messenger Ribonucleic Acid During Sporulation in *Bacillus subtilis*," *The Journal of Biological Chemistry*, vol. 246, no. 10, pp. 3189-95, May 1971.

[65] United States Environmental Protection Agency, "Biological Sample Preparation Project: Detection of *Bacillus anthracis* Spores in Soil," January 2011.

[66] Sensor Electronics Technology, Inc, 2011. "LED Specifications of TO39 with Flat Window LEDs" [Online]. Available: http://www.s-et.com/spec-sheets/TO39.pdf.

[67] W. L. Nicholson and B. Galeano, "UV Resistance of *Bacillus anthracis* Spores Revisited: Validation of *Bacillus subtilis* Spores as UV Surrogates for Spores of *Bacillus anthracis* Sterne," *Applied and Environmental Microbiology*, vol. 69, no. 2, pp. 1327-1330, 2003.

[68] Y.-J. Wei, C.-G. Liu and L.-P. Mo, "Ultraviolet Absorption Spectra of Iodine, Iodide Ion and Triiodide Ion," *Spectroscopy and Spectral Analysis,* vol. 25, no. 1, pp. 86-88, 2005.

[69] A. J. Hayter, Probability and Statistics for Engineers and Scientists, Belmont: Thomson Brooks/Cole, 2007.

[70] O. D. Monera, T. J. Sereda, N. E. Zhou, C. M. Kay and R. S. Hodges, "Relationship of Sidechain Hydrophobicity and Alpha-Helical Propensity on the Stability of the Single-Stranded Amphipathic Alpha-Helix," *Journal of Peptide Science,* vol. 1, pp. 319-329, 1995.

[71] H. Mamane-Gravetz and K. G. Linden, "Relationship Between Physiochemical Properties, Aggregation and UV Inactivation of Isolated Indigenous Spores in Water," *Journal of Applied Microbiology,* vol. 98, pp. 351-363, 2005.

[72] A. A. Hammad and S. A. Abo El-Nour, "Destruction of *Bacillus cereus* Spores as Surrogate for Anthrax Spores by Gamma Radiation," *Arab Journal of Nuclear Science and Applications,* vol. 46, no. 4, pp. 237-244, 2013.

[73] American Type Culture Collection, February 2006. [Online]. Available: www.ATCC.com.

[74] A. C. Eischeid, J. N. Meyer and K. G. Linden, "UV Disinfection of Adenoviruses: Molecular Indications of DNA Damage Efficiency," *Applied and Environmental Microbiology,* vol. 75, no. 1, pp. 23-28, Januaey 2009.

[75] Y. Xue and W. L. Nicholson, "The Two Major Spore DNA Repair Pathways, Nucleotide Excision Repair and Spore Photoproduct Lyase, Are Sufficient for the Resistance of *Bacillus subtillis* Spores to Artificial UV-C and UV-B but Not to Solar Radiation," *Applied and Environmental Microbiology* , vol. 62, no. 7, pp. 2221-2227, July 1996.

[76] R. Moeller, T. Douki, J. Cadet, E. Stackebrandt, W. L. Nicholson, P. Rettberg, G. Reitz and G. Horneck, "UV Radiation Induced Formation of DNA Bipurimidine Photoproducts in *Bacillus subtillis* Endospores and Their Repair During Germination," *International Microbiology,* vol. 10, pp. 39-46, January 2007.

[77] F. H. Ramirez-Guadiana, M. Barraza-Salas, N. Ramirez-Ramired, M. Ortiz-Cortes, P. Setlow and M. Pedraza-Reyes, "Alternative Excision Repair of Ultraviolet B and C-Induced DNA Damage in Dormant and Developing Spores of *Bacillus subtilis*," *Journal of Bacteriology,* vol. 194, no. 22, pp. 6096-6104, September 2012.

[78] V. A. Luna, D. King, C. Davis, T. Rycerz, M. Ewert, A. Cannons, P. Amuso and J. Cattani, "Novel Sample Preparation Method for Safe and Rapid Detection of *Bacillus anthracis* Spores in Environmental Powders and Nasal Swabs," *Journal of Clinical Microbiology,* vol. 41, no. 3, pp. 1252-1255, November 2003.

[79] J. Sub, S. Volz, U. Obst and T. Schwartz, "Application of a Molecular Biology Concept for the Detection of DNA Damage and Repair During UV Disinfection," *Water Research,* vol. 43, pp. 3705-3716, June 2009.

[80] P. J. Riesenman and W. L. Nicholson, "Role of the Spore Coat Layers in *Bacillus subtilis* Spore Resistance to Hydrogen Peroxide, Artificial UV-C, UV-B, and Solar Radiation," *Applied and Environmental Microbiology,* vol. 66, no. 2, pp. 620-626, November 2000.

[81] T. Douki, B. Setlow and P. Setlow, "Photosensitization of DNA by Dipicolinic Acid, a Major Component of Spores of *Bacillus* Species," *Photochemistry and Photobiology Sciences,* vol. 4, pp. 591-597, June 2005.

[82] B. Setlow and P. Setlow, "Role of DNA Repair in *Bacillus subtilis* Spore Resistance," *Journal of Bacteriology,* vol. 178, no. 12, pp. 3486-3495, 1996.

[83] J. A. Sikorsky, D. A. Primerano, T. W. Fenger and J. Denvir, "Effect of DNA Damage on PCR Amplication Efficiency with the Relative Threshold Cycle Method," *Biochemical and Biophysical Research Communications,* vol. 323, pp. 823-830, 2004.

[84] P. Setlow, "Spore Germination," *Current Opinion in Microbiology,* vol. 6, pp. 550-556, 2003.

[85] S. A. Bustin, V. Benes, J. A. Garson, J. Hellemans, J. Huggett, M. Kubista, R. Mueller, T. Nolan, T. Nolan, M. W. Pfaffl, G. L. Shipley, J. Vandesompele and

C. T. Wittwer, "The MIQE Guidelines: Minimum Information for Publication of Quantitative Real-Time PCR Experiments," *Clinical Chemistry,* vol. 55, no. 4, pp. 611-622, 2009.

[86] CDC, "Anthrax Sterne Strain (34F2) of *Bacillus anthracis*," August 2009. [Online]. Available: http://www.cdc.gov/nczved/divisions/dfbmd/diseases/anthrax_sterne/.

[87] G. B. Knudson, "Photoreactivation of Ultraviolet-Irradiated, Plasmid-Bearing, and Plasmid-Free Strains of *Bacillus anthracis*," *Applied and Environmental Microbiology*, vol. 52, no. 3, pp. 444-449, September 1986.

[88] L. J. Rose and H. O'Connell, "UV Light Inactivation of Bacterial Biothreat Agents," *Applied and Environmental Microbiology* , vol. 75, no. 9, pp. 2987-2990, 2009.

[89] D. F. Zygmunt, "Anthrax," in *Medical Aspects of Biological Warfare*, Washington D.C., Walter Reed Army Medical Center, 2007, pp. 69-90.

[90] J. Miller, W. J. Broad, W. Broad and S. Engelberg, Germs: Biological Weapons and America's Secret War, New York : Touchstone, 2002.

[91] Norton, "DASYLab Data Acquisition, Control and Analysis Software," Maine 2012. [Online]. Available: http://www.mccdaq.com/products/dasylab.htm.

[92] Bio-Rad, "CFX96 Touch, CFX96 Touch Deep Well, CFX Connect, and CFX384 Touch Real-Time PCR Detection Systems," 2013. [Online]. Available: http://www.bio-rad.com/webroot/web/pdf/lsr/literature/10021337.pdf. [Accessed 1 August 2014].

[93] IUPAC, "Compendium of Chemical Terminology, The Gold Book," Oxford, 1997. [Online]. Available: http://goldbook.iupac.org/Q04991.html.

[94] R. Goodacre, B. Shann, R. J. Gilbert, E. M. Timmins, A. C. McGovern, B. K. Alsberg, D. B. Kell and N. A. Logan, "Detection of the Dipicolonic Acid Biomarker in *Bacillus* Spores using Curie-Point Pyrolysis Mass Spectrometry and Fourier Transform Infrared Spectroscopy," *Journal of Analytical Chemistry*, vol. 72, no. 1, pp. 119-127, January 2000.

[95] University of Alabama in Huntsville, "Virtual Laboratories in Probability and Statistics: Central Limit Theorem," 2014. [Online]. Available: http://www.math.uah.edu/stat/sample/CLT.html.

[96] Wageningen UR, "Wageningen Bioinformatics Webportal: Primer3Plus DNA Sequencer," July 2014. [Online]. Available: http://www.bioinformatics.nl/cgi-bin/primer3plus/primer3plus.cgi.

[97] Qiagen, "EndoFree Plasmid Purification Handbook," 2012. [Online]. Available: http://www.qiagen.com/resources/resourcedetail?id=f8ed5bab-15c3-4211 -bfa8-4fbe207aad74&lang=en.

[98] Laerd Statistics, "Pearson Product-Moment Correlation," 2013. [Online]. Available: https://statistics.laerd.com/statistical-guides/pearson-correlation-coefficient-statistical-guide.php.

[99] U.S. Environmental Protection Agency, "Ultraviolet (UV) Light Emitting Diode (LED) Use in Advanced Oxidation Process (AOP)," Wright Patterson AFB, 2012.

[100] Qiagen, "IT 1-2-3 QGlow DNA Sample Purification Kit," 2015. [Online]. Available: http://biofiredefense.com/sample-purification/. [Accessed 2015].

[101] MRSEC Education Group, "Structure of DNA," University of Wisconsin-Madison, January 2014. [Online]. Available: http://www.education.mrsec.wisc.edu/132.htm.

[102] World Health Organization, " UV Radiation Frequently Asked Questions," 2014. [Online]. Available: http://www.who.int/uv/faq/whatisuv/en/index2.html.

[103] R. J. Saldanha, "Rapid Targeted Gene Disruption in *Bacillus anthracis*," *BMC Biotechnology*, vol. 13, no. 72, pp. 1-8, 2013.

[104] C. Aouadhi, H. Simonin, A. Maaroufi and S. Mejri, "Optimization of Nutrient-Induced Germination of *Bacillus sporothermodurans* Spores Using Response Surface Methodology," *Food Microbiology*, vol. 36, pp. 320-326, 2013.

[105] W. A. Baum, "Attenuation of Ultraviolet Light by the Lower Atmosphere," Ph.D. Dissertation, California Institute of Technology, Pasadena, 1950.

[106] B. J. Berger, S. English, G. Chan and M. H. Knodel, "Methionine Regeneration and Aminotransferases in *Bacillus subtilis*, *Bacillus cereus*, and *Bacillus anthracis*," *Journal of Bacteriology,* vol. 185, no. 8, p. 2418–2431, 2003.

[107] E. G. Biesta-Peters, M. W. Reij, H. Joosten, L. G. M. Gorris and M. H. Zwietering, "Comparison of Two Optical-Density-Based Methods and a Plate Count Method for Estimation of Growth Parameters of *Bacillus cereus*," *Applied and Environmental Microbiology,* vol. 76, no. 5, p. 1399–1405, 2010.

[108] N. Chondrogianni, I. Petropoulos, S. Grimm, K. Georgila, B. Catalgol, B. Friguet, T. Grune and E. S. Gonos, "Protein Damage, Repair and Proteolysis: A Review," *Molecular Aspects of Medicine,* vol. 35, pp. 1-71, 2014.

[109] J. B. Dalton and C. L. A. Schmidt, "The Solubilities of Certain Amino Acids and Related Compounds in Water, the Densities of Their Solutions at Twenty-Five Degrees, and the Calculated Heats of Solution and Partial Molar Volumes," *The Journal of Biological Chemistry,* vol. 109, pp. 241-248, 1935.

[110] M. J. Daly, E. K. Gaidamakova, V. Y. Matrosova, A. Vasilenko, M. Zhai, R. D. Leapman, B. Lai, S.-M. W. Li, K. M. Kemner and J. K. Fredrickson, "Protein Oxidation Implicated as the Primary Determinant of Bacterial Radioresistance," *PLoS Biology,* vol. 5, no. 4, pp. 769-779, 2007.

[111] L. A. Dauphin, B. R. Newton, M. V. Rasmussen, R. F. Meyer and M. D. Bowen, "Gamma Irradiation Can Be Used To Inactivate *Bacillus anthracis* Spores without Compromising the Sensitivity of Diagnostic Assays," *Applied and Environmental Microbiology,* vol. 74, no. 14, p. 4427–4433, 2008.

[112] M. Dizdaroglu, P. Jaruga, M. Birincolglu and H. Rodriguez, "Free Radical-Induced Damage to DNA: Mechanisms and Measurement," *Free Radical Biology and Medicine,* vol. 32, no. 11, pp. 1102-1115, March 2002.

[113] A. Driks, "*Bacillus subtilis* Spore Coat," *Journal of Microbiology and Molecular Biology,* vol. 63, no. 1, pp. 1-20, March 1999.

[114] R. E. Hilsen, B. Kournikakis and B. Ford, "Inactivation of Microorganisms by Gamma Irradiation: *Bacillus atropheus* Spores and *Erwinia herbicola*," Defense Research and Development Canada, 2005.

[115] L. J. Hoffman, "Thermogravimetric Analysis of *Bacillus anthracis* Spores of DNA by Spectroscopy and Chromatography of Pyrolysis Products," M.S. Thesis, Air Force Institute of Technology, Wright Patterson AFB, OH, 2013.

[116] A. X. Hurst, "Modeling of *Bacillus Spores*: Inactivation and Outgrowth," M.S. Thesis, Air Force Institute of Technology, Wright Patterson AFB, OH, 2011.

[117] L. Kong, P. Zhang, J. Yu, P. Setlow and Y.-q. Li, "Monitoring the Kinetics of Uptake of a Nucleic Acid Dye during the Germination of Single Spores of *Bacillus* Species," *Journal of Analytical Chemistry,* vol. 82, pp. 8717-8724, 2010.

[118] R. Kort, A. C. O'Brien, I. H. M. van Stokkum, S. J. C. M. Oomes, W. Crielaard, K. J. Hellingwerf and S. Brul, "Assessment of Heat Resistance of Bacterial Spores from Food Product Isolates by Fluorescence Monitoring of Dipicolinic Acid Release," *Applied and Environmental Microbiology,* vol. 71, no. 7, p. 3556–3564, 2005.

[119] A. G. Li, Y. Xing and L. W. Burggraf, "Thermal Effects on Surface Structures and Properties of *Bacillus anthracis* Spores on Nanometer Scales," *Langmuir,* vol. 29, pp. 8343-8354, 2013.

[120] J. M. Mason and P. Setlow, "Essential Rold of Small, Acid-Soluble Spore Proteins in Resistance of *Bacillus subtilis* Spores to UV Light," *Journal of Bacteriology,* vol. 167, no. 1, pp. 174-178, 1986.

[121] J.-L. Ravanat, T. Douki and J. Cadet, "Direct and Indirect Effects of UV Radiation on DNA and Its Components," *Journal of Photochemistry and Photobiology B: Biology,* vol. 63, pp. 88-102, August 2001.

[122] K. Rudi, B. C. Johnsrud, G. Skjefstad, I. Tryland and I. Hagen, "Different Length (DL) qPCR for Quantification of Cell Killing by UV-induced DNA Damage," *International Journal of Environmental Research and Public Health*, vol. 7, pp. 3376-3381, 2010.

[123] S. Sarasanandarajah, J. Kunnil, B. V. Bronk and L. Reinisch, "Two-Dimensional Multiwavelength Fluorescence Spectra of Dipicolinic Acid and Calcium Dipicolinate," *Journal of Applied Optics,* vol. 44, no. 7, pp. 1182-1187, March 2005.

[124] T. Douki, B. Setlow and P. Setlow, "Effects of the Binding of Alpha/Beta-Type Small, Acid-Soluble Spore Proteins on the Photochemistry of DNA in Spores of *Bacillus subtilis* and In Vitro," *Photochemistry and Photobiology,* vol. 81, pp. 163-169, 2005.

[125] L. del Carmen Huesca Espitia, C. Caley, I. Bagyan and P. Setlow, "Base-Change Mutations Induced by Various Treatments of *Bacillus subtillis* Spores with and without DNA Protective Small, Acid-Soluble Proteins," *Mutation Research,* vol. 503, pp. 77-84, April 2002.

[126] W. S. Klug and S. R. Cummings, Concepts of Genetics, 5 ed., Prentice-Hall, Inc, 1997.

[127] T. M. Koehler, Z. Dai and M. Kaufman-Yarbray, "Regulation of the *Bacillus anthracis* Protective Antigen Gene: CO2 and a Trans-Acting Element Activate Transcription from One of Two Promoters," *Journal of Bacteriology,* vol. 176, no. 3, pp. 586-595, February 1994.

[128] S. Kominami, "A Radical Cation Produced in a γ-Irradiated Single Crystal of L-Methionine as Studied by Electron Spin Resonance and Optical Absorption Spectroscopy," *The Journal of Physical Chemistry*, vol. 78, no. 12, pp. 1729-1733, 1971.

[129] S. Leuko, B. A. Neilan, B. P. Burns, M. R. Walter and L. J. Rothschild, "Molecular Assessment of UVC Radiation-Induced DNA Damage Repair in the Stromatolitic Halophilic Archaeon, *Halococcus hamelinensis*," *Journal of Photochemistry and Photobiology B: Biology,* vol. 102, pp. 140-145, October 2011.

[130] B. Setlow, S. Atluri, R. Kitchel, K. Koziol-Dube and P. Setlow, "Role of Dipicolinic Acid in Resistance and Stability of Spores of *Bacillus subtilis* with or without DNA-Protective Alpha/Beta-Type Small, Acid-Soluble Proteins," *Journal of Bacteriology,* vol. 188, no. 11, pp. 3740-3747, June 2006.

[131] John Wiley & Sons Publishing, "Interactive Concepts in Biochemistry: Anthrax," 2002. [Online]. Available: http://www.wiley.com/college/boyer/0470003790/cutting_edge/anthrax/ anthrax.htm.

[132] D. R. Koehler, J. Courcelle and P. C. Hanawalt, "Kinetics of Pyrimidine(6-4)Pyrimidone Photoproduct Repair in *E. coli*," *Journal of Bacteriology*, vol. 178, no. 5, pp. 1347-1350, March 1996.

REPORT DOCUMENTATION PAGE	*Form Approved* *OMB No. 0704–0188*

1. REPORT DATE (DD–MM–YYYY)	2. REPORT TYPE	3. DATES COVERED (*From — To*)
26-03-2015	Master's Thesis	June 2013 – March 2015

4. TITLE AND SUBTITLE The Efficiency of Methionine as a Radioprotectant of *Bacillus anthracis* for Cell Viability and Outgrowth Time after UVC and Gamma Irradiation	5a. CONTRACT NUMBER 5b. GRANT NUMBER 5c. PROGRAM ELEMENT NUMBER
6. AUTHOR(S) Harris, Cameron N, 2Lt, USAF	5d. PROJECT NUMBER F2KTAS2142G001 5e. TASK NUMBER 5f. WORK UNIT NUMBER
7. PERFORMING ORGANIZATION NAME(S) AND ADDRESS(ES) Air Force Institute of Technology Graduate School of Engineering and Management (AFIT/EN) 2950 Hobson Way WPAFB OH 45433-7765	8. PERFORMING ORGANIZATION REPORT NUMBER AFIT-ENP-MS-15-M-105
9. SPONSORING / MONITORING AGENCY NAME(S) AND ADDRESS(ES) 711th Human Performance Wing, AFRL 2610 Seventh Street, Bldg. 441 Wright-Patterson AFB, Ohio 45433 AFNWC/NCA 8601 Frost Avenue Kirtland, AFB NM mark.suriano@us.af.mil	10. SPONSOR/MONITOR'S ACRONYM(S) 711 HPW, AFRL/RHXBC; AFNWC/NCA 11. SPONSOR/MONITOR'S REPORT NUMBER(S)

12. DISTRIBUTION / AVAILABILITY STATEMENT
Distribution Statement A. Approved for Public Release; Distribution Unlimited

13. SUPPLEMENTARY NOTES

14. ABSTRACT
Samples containing 10^7 spores of *Bacillus anthracis* (Ba) Sterne in water were irradiated with 267nm UVC using small LEDs and, for comparison, Cs-137 gammas. Before irradiation, 1mM L-Met and D-Met were added to solution and remained through germination. Following UV irradiation, minimal media was added and the spores were incubated for various times. Spore viability was quantified as lag time of the spore using SYTO 16 photoluminescence. Fluorescence was compared between irradiated and unirradiated experiments, demonstrating a delay in outgrowth for irradiated samples. D-Met samples showed increased damage repair, while L-Met spores expressed delayed outgrowth for unirradiated and irradiated spores. L-methionine and D-methionine were introduced to Ba during sporulation and adherence was verified using CD spectrometry. 1mM DP1 was added to Ba before irradiation. CFUs were collected after gamma irradiation for 1000Gy increments for 0-8000Gy. The gamma doses corresponding to 1-$\log_{10}$ inactivation for the four spore types were: ~5000Gy for control and D-methionine; >8000Gy for DP1 spores; inconclusive for L-methionine. DP1 spores showed a significant resistance to damage, while D-Met spores showed minimal change in survival. L-Met spores clumped readily and produced unsatisfactory results. The gamma dose rate used doubled the dose expected to inactivate 90% of Ba spores.

15. SUBJECT TERMS
Anthracis, methionine, gamma, 267nm UVC, spectrofluorometry, circular dichroism

16. SECURITY CLASSIFICATION OF:			17. LIMITATION OF ABSTRACT	18. NUMBER OF PAGES	19a. NAME OF RESPONSIBLE PERSON Dr. Larry W. Burggraf, AFIT/ENP
a. REPORT U	b. ABSTRACT U	c. THIS PAGE U	UU	125	19b. TELEPHONE NUMBER (Include Area Code) (937) 785-3636 x4507 Larry.Burggraf@afit.edu

Standard Form 298 (Rev. 8–98)
Prescribed by ANSI Std. Z39.18